N63-18488

LIQUID ROCKET PLANT

HIGH CHAMBER PRESSURE
OPERATING FOR LAUNCH
VEHICLE ENGINES

Contract NAS 8-4008

Report No. 4008-F-1 | 15 April 1963

[redacted]

AEROJET
GENERAL TIRE
GENERAL

AEROJET-GENERAL CORPORATION
SACRAMENTO, CALIFORNIA

0628

Copy No. 10

Date: 15 April 1963

High Chamber Pressure Operation for Launch Vehicle Engines

Prepared By

AEROJET-GENERAL CORPORATION
Liquid Rocket Plant
Sacramento 9, California

Final Report

4008-F-1

Contract NAS 8-4008

Prepared For

PROPULSION AND VEHICLE ENGINEERING DIVISION
GEORGE C. MARSHALL SPACE FLIGHT CENTER
Huntsville, Alabama

FOREWORD

This final report presents a summary of all technical progress and accomplishments in the course of fulfilling Contract NAS 8-4008, "High Chamber Pressure Operation for Launch Vehicle Engines".

TABLE OF CONTENTS

Table of Contents (Cont.)

Table of Contents (Cont.)

FIGURE LIST

FIGURE LIST (Cont.)

FIGURE NO.

FIGURE LIST (Cont.)

FIGURE LIST (Cont.)

FIGURE NO.

FIGURE LIST (Cont.)

LIST OF TABLES

I. INTRODUCTION

The purpose of this investigation was to study the suitability of high chamber pressures for launch vehicle engines. Appropriate missions, and the effects of high chamber pressure on thermodynamic performance and combustion stability have been determined.

II. SUMMARY

An analysis of the most appropriate applications of high pressure launch vehicles has been made. An optimum chamber pressure has been developed for various applications, and the effect of chamber pressure on vehicle performance has been determined. Both LO_2/LH_2 and LO_2/RP-1 systems were considered.

The effect of non-ideal gas criteria on thermodynamic performance has been compared with ideal gas criteria for pressures up to 10,000 psia, and for simple and complex exhaust gas compositions.

The effect of high pressure on combustion stability has been studied theoretically and experimentally. A survey of existing theories of combustion stability has been made. The Princeton University Theory of sensitive time lag *vs* interaction index was selected for evaluation of experimental results. A bibliography of pertinent publications in the field of combustion stability is included.

Recommendations of future work in combustion stability and engine performance at high chamber pressures have been made.

III. APPLICATION ANALYSIS

A. SUMMARY

The objective of the application analysis was to determine the best applications for engines using high thrust chamber pressure in launch vehicles. For each application, the best value of thrust chamber pressure was determined, and the effect of chamber pressure on vehicle performance has been established. To accomplish the objectives, the application analysis was divided into five major tasks:

1. An engine weight study,
2. a cycle analysis,
3. a mixture ratio selection,
4. an area ratio selection,
5. a vehicle performance study.

Each of the tasks was accomplished for both LOX/LH_2 and LOX/RP-1 propellants. A detailed discussion of each is found in the following paragraphs.

B. ENGINE WEIGHT

A method of determining engine weight has been derived. Using the derived method, engine weight can be determined from nozzle throat area, nozzle area ratio, chamber pressure, nozzle type (deLaval or forced-deflection), mixture ratio, and oxidizer and fuel turbopump flow rates.

The engine was divided into two major components to perform the weight analysis:

1. The turbopump assembly (TPA)
2. and the engine-less-the-TPA weights.

The basic independent variables selected for the TPA weight were the propellant flow rate and the pump discharge pressure. TPA weights are shown in Figure III-1 The method of analysis is discussed in Section III,A,1 below.

Engine-less-the-TPA weights are presented in Figure III-2 Thrust chamber throat area and pressure were chosen as the independent variables. The weight curves were developed for a constant nozzle exit area. Nozzle weight - area ratio variation was calculated and plotted for deLaval and forced-deflection nozzles (see Figures III-3 and III-4). The method and assumptions used to determine these weights are discussed in Section III,A,2 below.

1. Turbopump Assembly Weight

Turbopump assembly weight as a function of pump discharge pressure and flow rate is shown in Figure III-1. This figure is based on weight estimates from actual TPA designs. The TPA weight data covers various pump discharge pressures and weight flow rates. The term $\rho^{0.8}$ in the expression $\dot{W}/\rho^{0.8}$ (the abscissa in Figure III-1) is based upon analytical studies. Data for pressure levels not covered by design data were obtained by extrapolation of existing designs.

Various TPA designs are incorporated in this figure with the actual weights shown as the numbered end of the vertical line. The design corresponding to the numbers is shown on the table attached to the figure. TPA weights were obtained from Figure III-1 in the following manner:

a. Weights for integrated pumping systems, (fuel and oxidizer pump run by the same turbine, such as the Titan turbopumps) were determined by taking the summation of the oxidizer and fuel weight flows divided by their respective densities to the 0.8 power, (i.e., $\dot{W}ox/\rho^{0.8}$ + $\dot{W}/\rho^{0.8}$), and reading the corresponding total turbopump assembly weight. Weights for integrated turbopump systems are determined in this manner because of the difficulty in determining the portion of weight of the common turbine which is chargeable to each pump.

Total weight for an integrated pumping system having different oxidizer and fuel pump discharge pressures can be obtained by assuming an average pump discharge pressure.

b. Total turbopump system weights for engines (such as the M-1) having distinct oxidizer and fuel turbopumps can be determined by obtaining the weight of each individual pump using its corresponding flow rate and fluid density, and summing the two individual pump weights.

2. Engine-Less-the-TPA Weight

Engine-less-the-TPA weights (Figure III-2)were based upon two assumptions:

(1) Cooling tube wall thickness is constant;

(2) weight differences of the gas generators, combustion chambers, injectors and manifolds are insignificant (at the same flow rate) with changes in chamber pressure.

The assumption of constant tube wall thickness was based on previous heat transfer studies indicating that a minimum tube wall thickness is desirable regardless of chamber pressure. Minimum tube wall thickness is obtained by reducing tube diameter as pressure is increased.

Using the assumptions discussed above, the engine-less-the-TPA weight for engines of fixed thrust level does not vary with thrust chamber pressure provided that the nozzle exit area is held constant, and that the nozzle throat area is proportional to chamber pressure. The nozzle exit area maintained in the weight study was that obtained with a nozzle area ratio of 30, and a chamber pressure of 1000 psia. For this exit area, the area ratios at chamber pressures of 2000, 3000, 4000, and 5000 psia are 60, 90, 120, and 150, respectively. For these nozzle area ratios, the engine-less-TPA weight difference between deLaval and forced-deflection nozzles is negligible.

To determine engine weights at area ratios other than assumed in the engine-less-the-TPA weight study, a nozzle weight - area ratio relationship was established. Figures III-3 and III-4 present the change in nozzle weight divided by chamber pressure and throat area as a function of area ratio change. This curve is based on a 1000 psia chamber pressure. Using the equation shown on Figures III-3 & III-4 , the curve can be used for other chamber pressures. Nozzle weights are based upon contours which produce an average exit velocity vector angle of 8^o. This selection was based on past studies which indicated that the payloads of 8^o nozzles are 1 to 1½% greater than 10^o nozzles. Thus 8^o nozzles were used as the basis for nozzle weight studies in this study.

Because Figure III-2 was constructed for 10^o nozzles, it should be noted that Figures III-3 & III-4 also incorporate the correction for the nozzle weight differences between 10^o and 8^o nozzles.

3. <u>Air Frame Weight</u>

Stage air frame weight (stage inert weight excluding the engine) is calculated from inert weight parameters (K_T, K_{AF}) which were established in past weight studies (Aerojet-General Contract NAS 5-1025). The inert weight parameters of O_2/H_2 and O_2/RP-1 are:

		Single Stages	First Stages	Upper Stages
K_T	O_2/H_2	0.00788	0.00918	0.00751
	O_2/RP-1	0.00700	0.00846	-
K_{SF}	O_2/H_2	0.626	0.617	0.677
	O_2/RP-1	0.813	0.813	-

Using these weight parameters, stage air frame inert weight can be calculated by the following formula,

$$M_{(inert)} = (KT)\ (FV) + (KAF)\ (VPT)$$

where:

KT	=	Thrust dependent inert weight factor (excluding the engine)
FV	=	Vacuum thrust, lbf
KAF	=	Volume dependent inert weight factor, lb/ft^3
VPT	=	Total propellant tank volume, ft^3

C. CYCLE ANALYSIS

The purpose of the cycle analysis was to determine performance degradation, pressure drops, and engine mixture ratios for gas generator and staged-combustion cycle engine systems. Performance degradation is defined here as the difference between thrust chamber specific impulse and overall engine specific impulse. Engine system pressure drop determinations yield the relationship of pump discharge pressure to thrust chamber pressure. Engine mixture ratio is defined as the ratio of engine oxidizer flow to engine fuel flow. Specific impulse data used in this analysis were based on ideal gas thermochemical data (assuming shifting equilibrium flow) because non-ideal gas effects have been shown to be insignificant.

The following is a list of cycle analysis symbols:

A_2	Exit area of nozzle - in^2
A_t	Nozzle throat area - in^2
C_F	Thrust coefficient
C_p	Specific heat at constant pressure - Btu/lb °R
C*	Characteristic velocity - ft/sec
g	Gravity constant - ft/sec^2

III, C, Cycle Analysis (cont.)

Δh	Enthalpy drop across nozzle - ft - lb/lb
$d(\Delta h)$	Increase in enthalpy resulting from pump work - ft lb/lb
H	Pump head rise - ft
I_{spE}	Overall engine specific impulse - sec
$d\ I_{spPW}$	Specific impulse resulting from pump work - sec
I_{spTMC}	Thrust chamber specific impulse obtained from thermochemical data - sec
I_{spTC}	Effective thrust chamber specific impulse = $I_{spTMC} + I_{spPW}$
I_{spD}	Specific impulse degradation - sec
I_{spTE}	Specific impulse of the turbine exhaust products - sec
J	778 ft - lb/Btu
K	Ratio of specific heats
K_1, K_2, K_3, K_{ind}	Constants
MR_E	Overall engine mixture ratio
MR_{GG}	Gas generator mixture ratio
MR_{TC}	Thrust chamber mixture ratio
η_f	Fuel pump efficiency
η_o	Oxidizer pump efficiency
η_t	Turbine efficiency
P_c	Combustion pressure - psia
P_D	Pump discharge pressure - psia
P_1	Turbine exit pressure - psia
P_2	Nozzle exit pressure - psia
P_3	Ambient pressure - psia
R	Gas constant $\frac{\text{ft - lb}}{\text{lb mole } ^{o}R}$
ΔT	Temperature drop across the turbine - ^{o}R

V_e	Effective exhaust velocity - ft/sec
$\dot{W}_{fGG}$	Gas generator fuel flow rate - lb/sec
$\dot{W}_{oGG}$	Gas generator oxidizer flow rate - lb/sec
$\dot{W}_{fTC}$	Thrust chamber fuel flow rate - lb/sec
$\dot{W}_{oTC}$	Thrust chamber oxidizer flow rate - lb/sec
$\dot{W}_{GG}$	Total gas generator flow rate ($\dot{W}_{oGG} + \dot{W}_{fGG}$) - lb/sec
$\dot{W}_{TC}$	Total thrust chamber flow rate ($\dot{W}_{oTC} + \dot{W}_{fTC}$) - lb/sec
λ	Divergence coefficient

1. Performance Degradation

a. Gas Generator Cycle

A schematic of a gas generator cycle engine is shown in Figure III-5. The oxidizer and fuel turbopump assembly are driven by a single bipropellant gas generator. The gas generator propellants are tapped from the main pump discharge lines, injected into the generator, and burned. After passing through the turbine, the gases are expanded through a nozzle, providing additional thrust. Performance degradation of the gas generator cycle is a result of the low specific impulse associated with these turbine exhaust products. Figures III-6 & III-7 are plots of performance degradation versus thrust chamber specific impulse for O_2/H_2 and O_2/RP-1 gas generator cycle engines. The following analysis shows the development of the curve:

I_{sp} degradation is given by

$$I_{sp_D} = I_{sp_{TC}} - I_{sp_E} \qquad \text{Equation (1)}$$

I_{sp_E} is given by

$$I_{sp_E} = \frac{(\dot{W}_{oTC} + \dot{W}_{fTC}) I_{sp_{TC}} + (\dot{W}_{oGG} + \dot{W}_{fGG}) I_{sp_{TE}}}{(\dot{W}_{oTC} + \dot{W}_{fTC}) + (\dot{W}_{oGG} + \dot{W}_{fGG})} \qquad \text{Equation (2)}$$

Substituting equation (2) into (1)

$$I_{spD} = I_{spTC} - \frac{(\dot{W}_{oTC} + \dot{W}_{fTC})\ I_{spTC} + (\dot{W}_{oGG} + \dot{W}_{fGG})\ I_{spTE}}{(\dot{W}_{oTC} + \dot{W}_{fTC}) + (\dot{W}_{oGG} + \dot{W}_{fGG})} \quad \text{Equation (3)}$$

Putting the right hand side of the equation over a common denominator, algebraically rearranging, and simplifying,

$$I_{spD} = \frac{I_{spTC} - I_{spTE}}{\frac{\dot{W}_{TC}}{\dot{W}_{GG}} + 1}$$

For reasons which will become evident further in the analysis, $\frac{\dot{W}_{TC}}{\dot{W}_{GG}}$ is changed to the form

$$\frac{\dot{W}_{TC}}{\dot{W}_{GG}} = \frac{\dot{W}_{fTC}\ (1 + MRTC)}{\dot{W}_{fGG}\ (1 + MRGG)}$$

I_{sp} degradation is now given by

$$I_{spD} = \frac{I_{spTC} - I_{spTE}}{(\dot{W}_{fTC}/\dot{W}_{fGG})\left[(1 + MRTC)/(1 + MRGG)\right] + 1} \quad \text{Equation (4)}$$

The three unknowns in this expression are $I_{sp}TC$, $I_{sp}TE$ and $\frac{\dot{W}_{fTC}}{\dot{W}_{fGG}}$

(1) Determination of $\frac{\dot{W}_{fTC}}{\dot{W}_{fGG}}$

The relation of gas generator flow to thrust chamber flow is found by equating pump horsepower requirements to turbine power output. The pump horsepower requirements are:

$$SHP_o = \frac{H_o\ (\dot{W}_{oTC} + \dot{W}_{oGG})\ Kind}{550\,\eta_o}$$

$$SHP_f = \frac{H_f\ (\dot{W}_{fTC} + \dot{W}_{fGG})\ Kind}{550\,\eta_f}$$

The K_{ind} is an assumed value which provides for the additional horsepower requirements of a hydraulic, turbine-driven inducer.

Turbine power output is expressed by

$$(\dot{W}_{oGG} + \dot{W}_{fGG})\ (C_p \Delta T \eta_t \frac{J}{550})$$

Equating pump requirements to turbine output gives

$$\frac{H_o\ (\dot{W}_{oTC} + \dot{W}_{oGG})\ K_{ind}}{550\,\eta_o} + \frac{H_f\ (\dot{W}_{fTC} + \dot{W}_{fGG})\ K_{ind}}{550\,\eta_f} = \qquad \text{Equation (5)}$$

$$(\dot{W}_{oGG} + \dot{W}_{fgg})\ \frac{C_p \Delta T \eta_t J}{550}$$

$$\frac{H_o\ K_{oind}}{550\,\eta_o} = \text{Constant} = K_1$$

$$\frac{H_f\ K_{find}}{550\,\eta_f} = \text{Constant} = K_2$$

For a given gas generator and turbine system (gas generator mixture ratio and turbine pressure ratio)

$$\frac{C_p \Delta T \eta_t}{550} = \text{Constant} = K_3$$

Substituting into Equation (5) the above constants

$$K_1(\dot{W}_{oTC} + \dot{W}_{oGG}) + K_2(\dot{W}_{fTC} + \dot{W}_{fGG}) = K_3(\dot{W}_{oGG} + \dot{W}_{fGG})$$

Combining terms

$$\dot{W}_{oGG}(K_3 - K_1) + \dot{W}_{fGG}(K_3 - K_2) = \dot{W}_{oTC}\ (K_1) + \dot{W}_{fTC}(K_2) \qquad \text{Equation (6)}$$

From a definition of mixture ratio

$$\dot{W}_{oGG} = \dot{W}_{fGG}\ MRGG$$

$$\dot{W}_{oTC} = \dot{W}_{fTC}\ MRTC$$

Substituting these two relationships into Equation (6) gives

$$\dot{W}_{fGG}\left[MR_{GG}\,(K_3-K_1) + (K_3-K_2)\right] = \dot{W}_{fTC}\,(MR_{TC}\,K_1 + K_2)$$

and finally

$$\frac{\dot{W}_{fTC}}{\dot{W}_{fGG}} = \frac{MR_{GG}\,(K_3 - K_1) + (K_3 - K_2}{MR_{TC}\,(K_1) + K_2}$$

(2) Determination of I_{spTC}

Thrust chamber I_{sp} values were obtained from computer calculations based upon shifting equilibrium flow of the combustion products (Figures III-8 & III-9). The thrust chamber I_{sp} obtained from this curve represents a thermochemical energy level of the combustion products and does not include energy put into the propellants by the pumps. Consequently, the actual energy level (or I_{sp}) of the combustion products is somewhat higher than the computer thermochemical data predicts. The correction is calculated as follows:

By applying a momentum equation it can be shown that

$$I_{sp} = \frac{\lambda V_e}{g} \qquad \text{Equation (7)}$$

From an energy equation for flow through a nozzle

$$V_e = \sqrt{2g\Delta h} \qquad \text{Equation (8)}$$

Substituting Equation (8) into (7)

$$I_{sp} = \frac{\lambda}{g}\sqrt{2g\Delta h} \qquad \text{Equation (9)}$$

The change in I_{sp} for a change in Δh can be found by taking the first derivative of Equation (9) with respect to Δh.

$$\frac{d\,I_{sp}}{d(\Delta h)} = \lambda\sqrt{\frac{2}{g}}\left(\frac{1}{2}\right)(\Delta h)^{-\frac{1}{2}}$$

and

$$d\,I_{sp\,PW} = \frac{\lambda}{\sqrt{2g}}\;\frac{d(\Delta h)}{(\Delta h)^{1/2}} \qquad \text{Equation (10)}$$

The change in I_{sp} due to pump energy can be found by assuming d (Δh) as the pump energy and Δh as the enthalpy drop across the nozzle before pump work is added. Actually, the Δh in the denominator of Equation (10) is an intermediate point between the energy level before pumping work is added, and the energy level after pumping work is added. However, because d(Δh) is small compared to Δh, the end result of using an intermediate Δh does not warrant the mathamatical complications. With the above assumptions, we may then substitute for $(\Delta h)^{\frac{1}{2}}$ in Equation (10),

$$(\Delta h)^{\frac{1}{2}} = \frac{g}{\lambda} \frac{I_{spTMC}}{\sqrt{2g}} \qquad \text{Equation (11)}$$

This gives $d(I_{spPW}) = \frac{\lambda}{\sqrt{2g}} \frac{d(\Delta h)}{(g/\lambda)\left(I_{spYMC}/\sqrt{2g}\right)}$

$$dI_{spPW} = \frac{\lambda^2}{g} \frac{d(\Delta h)}{I_{spTMC}} \qquad \text{Equation (12)}$$

d(Δh) is the energy per pound of propellant added by the pumps, or,

$$d(\Delta h) = \left[\frac{H_f \dot{W}_{fTC}}{\eta f} + \frac{H_o \dot{W}_{oTC}}{\eta o}\right] \frac{1}{\dot{W}_{TC}} \qquad \text{Equation (13)}$$

also

$$\dot{W}_{fTC} + \dot{W}_{oTC} = \dot{W}_{TC} = \dot{W}_{fTC} \quad (1 + MRTC)$$

and

$$\dot{W}_{oTC}/\dot{W}_{fTC} = MRTC$$

$$\dot{W}_{fTC}/\dot{W}_{TC} = \frac{1}{1 + MR_{TC}} \quad \text{and} \quad \frac{\dot{W}_{oTC}}{\dot{W}_{TC}} = \frac{MR_{TC}}{1 + MR_{TC}}$$

Substituting these relationships into Equations (13) gives

$$d(\Delta h) = \left[\frac{H_f}{\eta f} + \frac{H_o}{\eta o} \cdot MR_{TC}\right] \frac{1}{1 + MR_{TC}} \qquad \text{Equation (14)}$$

Finally, substituting Equation (14) into Equation (12) gives

$$d\, I_{sp_{PW}} = \frac{\lambda^2}{g}\left[\frac{\left(H_f/\eta_f\right) + \left(H_o/\eta_o\right) M_{RTC}}{I_{sp_{TMC}}\,(1 + M_{RTC})}\right] \qquad \text{Equation (15)}$$

Therefore, the $I_{sp}TC$ that is used in Equation (4) is the thermochemical $I_{sp_{TMC}}$ obtained from Figures III-8 and III-9 plus the d $I_{sp_{PW}}$ calculated using Equation (15). A plot of d $I_{sp_{PW}}$ versus $I_{sp_{TMC}}$ for various thrust chamber pressures is shown in Figures III-10 and III-11.

(3) Determination of $I_{sp_{TE}}$

From the definition of I_{sp} it can be shown that

$$I_{sp} = \frac{C_F\, C^*}{g} \qquad \text{Equation (16)}$$

where C* (characteristic velocity) is given by

$$C^* = \frac{(K g R T)^{\frac{1}{2}}}{K\left[\left(\frac{2}{K+1}\right)^{\frac{K+1}{K-1}}\right]^{1/2}} \qquad \text{Equation (17)}$$

For turbine thrust the K, R, and T are all at turbine exit conditions.

C_F, (thrust coefficient) is given by

$$C_F = \sqrt{\frac{2K^2}{K-1}\left(\frac{2}{K+1}\right)^{\frac{K+1}{K-1}}\left[1 - (P_2/P_1)^{\frac{K-1}{K}}\right]} + \frac{P_2 - P_3}{P_1} \cdot \frac{A_2}{A_t} \qquad \text{Equation (18)}$$

The pressure ratio $\frac{P_2}{P_1}$ is the nozzle exit pressure divided by turbine exit pressure. For this analysis the nozzle was assumed to be optimum expansion at sea level so that P_2 equals

P_3. Therefore $C_{F_{opt}}$ is given by

$$C_{F_{opt}} = \sqrt{\frac{2K^2}{K-1}\left(\frac{2}{K+1}\right)^{\frac{K+1}{K-1}}\left[1-\left(\frac{P_2}{P_1}\right)^{\frac{K-1}{K}}\right]}$$

Vacuum thrust coefficient is related to $C_{F_{opt}}$ by

$$C_{FVAC} = C_{F_{opt}} + \frac{A_2}{A_t}\left(\frac{P_2}{P_1}\right)$$

Values of $C_{F_{vac}}$ and $C_{F_{opt}}$ as functions of $\frac{P_2}{P_1}$ and K have been published and are available. Therefore, the I_{sp} of the turbine exhaust is determined by calculating C*, obtaining a value of C_F, and substituting these two into Equation (16). It is noted that the I_{spTE} is calculated assuming frozen equilibrium conditions. At the comparatively low turbine exhaust temperature, it has been shown that the assumption is reasonable.

(4) Procedure for Calculating Engine Specific Impulse

All required expressions for the calculation of engine I_{sp} degradation using Equation (4) have now been derived. Optimum sea-level engine I_{sp} for the gas generator cycle can now be determined as follows:

(a) At the given P_c and MR, obtain $I_{sp_{TMC}}$ from Figures III-8 or III-9.

(b) With the $I_{sp_{TMC}}$ obtain in step (a) determine d $I_{sp_{PW}}$ pump work using Figure III-10 or III-11.

(c) Add the d $I_{sp_{PW}}$ to the $I_{sp_{TMC}}$. Using this number and the given P_c, the I_{sp} degradation can be determined from Figure III-6 or III-7.

(d) The engine I_{sp_E} is given by

$$I_{sp_E} = I_{sp_{TMC}} + d\, I_{sp_{PW}} - I_{sp_D}.$$

Plots of engine I_{sp_E} at optimum sea-level expansion versus chamber pressure for various thrust chamber mixture ratios are shown in Figures III-12 and III-13. These curves are developed by following the above procedure for several thrust chamber mixture ratios and chamber pressures.

(e) Staged-Combustion Cycle

The staged-combustion cycle (shown schematically in Figure III-14) consists of a gas generator-driven turbine with the turbine exhaust injected into the thrust chamber. Because the turbine exhaust is expanded through the main thrust chamber, the staged-combustion cycle engine specific impulse is equal to the thrust chamber specific impulse. Also, there is no effect of pump work upon specific impulse, because whatever energy is input in the system by the pumps is thus removed by the turbine. Therefore, staged-combustion cycle engine specific impulse is equal to thermochemical specific impulse as predicted by the computer. It is recognized that there is an entropy increase in this system because of the irreversible processes resulting from pump and turbine inefficiencies and line losses. However, the entropy increase is reflected in the pressure drop between the pump discharge and the main combustor.

2. Pressure Drops

a. Gas Generator Cycle

Pump discharge pressure as a function of chamber pressure is shown in Figure III-15 for the gas generator cycle. The tabulated pressure drops and their variation with chamber pressure are presented with the curves. The curves shown in this figure are independent of thrust level.

The fuel pressure drop through the coolant jacket, approximately 200 psi, was based upon the LR87-AJ-5 engine. To scale this pressure drop to other chamber pressures, it was estimated that 50% of the 200 psi drop results from coolant tube "turn arounds", tube splits, and the "straight line" skirt section tubes. Pressure drop will remain approximately constant at all chamber pressures. The remaining 100 psi drop is produced by the coolant tubes in the throat and combustion chamber section. With increasing chamber pressure at constant thrust, combustion chamber size will decrease, and heat transfer coefficients will increase. Coolant velocity must therefore be increased. As a result, the pressure drop in these areas is increased with increases in chamber pressure. For scaling purposes, the pressure drop was assumed to be directly proportional to chamber pressure.

$$P_{\text{Coolant Jacket}} = 100 + 100 \left(\frac{P_c}{P_c} \right)_{\text{Titan}}$$

b. Staged-Combustion Cycle

The main factor affecting a staged-combustion cycle pressure schedule is turbine pressure ratio. Increased thrust chamber pressure can be provided only at the expense of the turbine pressure ratio. Figures III-16 & III-17 show the relationship of chamber pressure to pump discharge pressure for O_2/H_2 and O_2/RP-1 staged-combustion engines. It should be noted that the maximum chamber pressure attainable with a staged combustion cycle is limited. This "peaking" of the chamber pressure results because an incremental change in pump discharge pressure at this point is more than overcome by the increased turbine pressure ratio required to develop the additional pump discharge pressure. Higher chamber pressures can be reached only by increasing the turbine inlet temperature, i.e., changing the gas generator mixture ratio, thus increasing the energy per pound of driven gas.

The derivation of the analytical expression used in determining the turbine pressure ratio is presented below.

Turbine pressure ratio, P_r, is defined by

$$P_r = P_1/P_2$$

where

P_1 is the turbine nozzle inlet pressure

P_2 the static exit pressure of isentropic expansion.

Pressure ratio is related to temperature ratio by

$$P_1/P_2 = (T_1/T_2)^{\frac{k}{k-1}}$$

The temperature drop across the turbine, ΔT, the difference between T_1 and T_2, is calculated through the use of the isentropic spouting velocity $- C_o$ relationship. This velocity corresponds to the complete transformation of turbine inlet energy into kinetic energy, and is related to ΔT as follows:

$$C_p \ \Delta T = \frac{C_o^2}{2g}$$

The isentropic spouting velocity is also related to the amount of kinetic energy required to deliver the necessary shaft horsepower as follows:

$$\dot{W}_{oG} \ \frac{C_o^2}{2g} = \frac{SHP \times 550}{\eta_t}$$

The total shaft horsepower, SPH, is given by the sum of the pump horsepowers:

$$SHP = \frac{\dot{W}_o \; H_o \; K_{oind}}{550\eta_o} + \frac{\dot{W}_f \; H_f \; K_{find}}{550\eta_f}$$

K_{ind} accounts for the additional power requirements of the hydraulically driven inducer.

Using the above equations, the turbine pressure ratio can now be determined. Shaft horsepower is computed first, followed by compiling the spouting velocity, the turbine temperature drop, and finally the turbine pressure ratio. Using this pressure ratio and established engine pressure drops, the thrust chamber pressure can be determined.

3. Engine Mixture Ratio

a. Gas Generator Cycle

Engine mixture ratio is defined as engine oxidizer flow divided by engine fuel flow:

$$MR_E = \frac{\dot{W}_{oTC} + \dot{W}_{oGG}}{\dot{W}_{fTL} + \dot{W}_{fGG}}$$

$$MR = \left[\frac{\frac{\dot{W}_{fTC}}{\dot{W}_{fGG}} \quad \frac{MR_{TC}}{MR_{GG}} + 1}{\frac{\dot{W}_{fTC}}{\dot{W}_{fGG}} + 1} \right] MR_{GG}$$

An expression for $\frac{\dot{W}_{FTC}}{\dot{W}_{FGG}}$ has already been derived (see Section III-6-1) . Using the above expressions, the relationship of MR_E vs MR_{TC} for O_2/H_2 and O_2/RP-1 gas generator cycle has been established (Figures III-18 and III-19).

b. Staged-Combustion Cycle

For the staged-combustion cycle, engine mixture ratio is equal to thrust chamber mixture ratio.

D. MIXTURE RATIO SELECTION

The best basis for selecting engine mixture is maximum vehicle performance. In this way the trade-off between specific impulse and propellant bulk density can be evaluated accurately. The process is quite cumbersome and time consuming. Evaluations of this nature have shown that the effect on optimum chamber pressure resulting from use of slightly off optimum mixture ratios is insignificant. Furthermore, film cooling requirements affect the best mixture ratio, and these effects are extremely difficult to predict accurately in a preliminary analysis such as this. Experience has shown that for propellants of approximately equal density, the best thrust chamber mixture ratio is very close to that yielding maximum nozzle effective exhaust velocity. This criterion has been used in selecting mixture ratio for O_2/RP-1 propellants. A plot of effective exhaust velocity as a function of thrust chamber mixture ratio and thrust chamber pressure for O_2/RP-1 propellants is shown in Figure III-20 . The line of maximum effective exhaust velocity for the mixture ratio selection is also shown on this figure. The mixture ratios which yield maximum effective exhaust velocity are plotted on Figure III-21 as a function of thrust chamber pressure. This mixture ratio variation with chamber pressure has been used in the application analysis of O_2/RP-1 propellants.

For O_2/H_2 propellants, the propellant bulk density varies widely with mixture ratio. Therefore, the maximum effective exhaust velocity criterion applied to O_2/RP-1 propellants is inadequate. The mixture ratio for O_2/H_2 propellants must be selected for maximum velocity performance. This was accomplished in a previous study (Aerojet-General Contract NAS 5-1025).

The results of this study show that the optimum thrust chamber mixture ratio for O_2/H_2 propellants varies linearly with thrust chamber pressure from 6 at 1000 psia to 7 at 5000 psia (Figure III-22). This thrust chamber mixture ratio variation has been used for further application analysis effort for O_2/H_2 propellants.

E. AREA RATIO SELECTION

Nozzle area ratios were selected on the basis of maximum vehicle performance for first and upper stages of multistage vehicles, and for single-stage vehicles.

The vehicles were analyzed for the following cases:

1. First-stages for velocity increments of 10,000 and 20,000 ft/sec using both O_2/H_2 and O_2/RP-1 propellants;

2. single-stage vehicles for a 300 nm orbit, using both propellants;

3. and upper stages for velocity increments of 10,000, 15,000, and 20,000 ft/sec using O_2/H_2 only; both deLaval and forced-deflection engines were considered for the boosters and single-stage vehicles; only deLaval nozzles were considered for upper-stage vehicles.

Stage payload was used as the basis for selecting optimum area ratios; for each stage, nozzle, and mission, the variation in payload was calculated considering each of the following:

1. Thrust chamber specific impulse variations with chamber pressure and area ratio;

2. a range of area ratios for each chamber pressure;

3. variation of turbopump weight with propellant flow rates;

4. change in nozzle skirt weight with area ratio;

5. change of ideal velocity increment with area ratio;

6. mixture ratio variation with chamber pressure.

(See Mixture Ratio Selection Section III-D).

Nozzle surface friction and heat transfer losses were neglected. Therefore, the best area ratio will be slightly smaller than indicated by the peak payload points. Area ratios 1% off the peak paylaod points were selected as optimum. The net effect is that of decreasing the nozzle length and surface area to account for the heat transfer and frictional effects. The results of this study are shown in Figures III-23 through III-27.

The optimum area ratio for upper-stage vehicles includes the effect of the required additional interstage structure with increases in area ratio. The method of this analysis is discussed briefly in the following paragraphs.

At an instant prior to the upper stage light-off, the total load on the interstage structure is equal to the light-off weight of the upper stage times the burn-out g's of the booster. The weight of the interstage structure, for a conical or cylindrical configuration, is proportional to the load on the structure, and to the length of the structure. The thrust of the upper-stage engine is proportional to the throat area and to the chamber pressure. It can be shown that the engine diameter, and hence, its length, is directly proportional to the square root of the thrust per engine and to the area ratio, and inversely proportional to the square root of the chamber pressure.

This analysis can be summarized as follows:

a. $W_{iss} \propto PL$

b. $P = W_{Lo} (a/g)_{Bo}$

c. $$F_t = C_f \, P_c \, A_t$$
$$= C_f \, P_c \, A_e/A_t$$
$$= C_f \, P_c \, \pi D_e^2/4\epsilon$$

$$D_e = \sqrt{4 \, F_i \epsilon / \pi \, C_f \, P_c}$$

d. $$L_e = K_1 \sqrt{\frac{4 \, F_i \, \epsilon}{\pi \, C_f \, P_c}}$$

where:

W_{iss}	-	Weight of interstage structure, lb
P	-	Load on structure, lb
L	-	Length of structure, ft
W_{lo}	-	Light-off weight of upper stage, lb
a/g	-	Burn out g's of lower stage
F_i	-	Vacuum thrust per engine, lb_f
C_f	-	Vacuum thrust coefficient
P_c	-	Chamber pressure, psia
A_t	-	Throat area, in^2
A_e	-	Exit area, in^2
ϵ	-	Nozzle area ratio, A_e/A_t
D_e	-	Exit diameter, in.
L_e	-	Engine length, in.
K_1	-	Engine length - diameter proportionality constant

Also, because the length of the interstage structure will be dependent upon the length of the engine, the result can be written by substituting (b.) and (d.) into (a) and rearranging.

$$\frac{W_{iss}}{W_{lo}} = (a/g)_{Bo} K_2 \sqrt{\frac{F_i \epsilon}{P_c}}$$

where K_2 is equal to 3×10^{-7} in^{-1}.

The factor K_2 was determined on the basis of interstage structure weights for existing vehicles.

The variation of interstage structure weight with area ratio and chamber pressure, as expressed by the above equation, was used in determinating the optimum area ratio for upper stages. The results of the upper stage area ratio analysis are shown on Figure III-27.

F. VEHICLE PERFORMANCE

Using the engine and stage weight data, engine performance, mixture ratios, and area ratios discussed in the previous paragraphs, vehicle payloads were calculated as a function of thrust chamber pressure for various missions. The results of these calculations are shown on Figures III-28 through III-36. These figures show relative payload as a function of thrust chamber pressure for the engine cycles and nozzle types investigated.

The relative payload shows percentage payload increases attainable with advanced concepts as compared with those obtained with a conventional engines. The conventional engine is defined as an engine using a gas generator cycle, a deLaval nozzle, and operating at a 1000 psia thrust chamber pressure. The vehicle payload to lightoff weight ratio is shown on the performance figures for the conventional engine.

The plot of single-stage-to-orbit performance for LOX/LH_2 propellants is shown on Figure III-28. The maximum payload capability for this vehicle is realized by incorporating all advanced concepts (staged-combustion cycle, forced-deflection nozzle, and high thrust chamber pressure). The combination results in a 48% payload gain over the conventional engine. The payload gains are proportionately smaller for engine configurations using only some of the advanced concepts. It is significant that for each configuration, the payload capability is increased by increasing the thrust chamber pressure. For intermediate missions (i.e., first stages of multi-stage vehicles) the percentage gains are somewhat less than for single-stage-to-orbit missions. The maximum values are 17% at an approximate ideal velocity of 20,000 ft/sec and 6% at 10,000 ft/sec. (Figures III-29 and III-30).

It should be noted that at an ideal velocity increment of 10,000 ft/sec, the variation in payload capability over a wide range of thrust chamber pressures is relatively insignificant for each combination of nozzle and cycle.

Figures III-31 through III-33 show the performance variation with thrust chamber pressure for first stages of vehicles using LOX/RP-1 propellants. These figures show the same general relationships between the various engine configurations as for LOX/LH_2. The relative gains for any configuration over the conventional at each mission, however, are significantly greater than for LOX/LH_2. These gains for the engine using all advanced concepts are 138% for a single-stage-to-300 n.m.-orbit mission, 36% for an approximate ideal velocity increment of 20,000 ft/sec, and 13.5% at 10,000 ft/sec.

A comparison of the LOX/LH_2 and LOX/RP-1 single-stage-to-orbit vehicles indicates that the relative gain in capability with the staged-combustion cycle is much greater for LOX/RP-1 than it is for LOX/LH_2. The gain can be attributed to the much lower performance of a conventional LOX/RP-1 engine.

Figures III-34 through III-36 show the relative payloads of upper-stage LOX/LH_2 vehicles for three missions. Calculations were performed for engine configurations using the gas generator cycle and the staged-combustion cycle, with the deLaval nozzles. The relative gains in capability for these vehicles over the conventional are much smaller than for stages operating in the atmosphere. The maximum gains are 9%, 5½%, and 3% for ideal velocity requirements of 20,000, 15,000, and 10,000 ft/sec, respectively.

A tabulation of the optimum thrust chamber pressures based upon vehicle performance for each engine configuration and mission investigated follows below:

FIRST- AND SINGLE-STAGE VEHICLES

LOX/LH_2

Nozzle	Cycle	OPTIMUM PRESSURE V_i = 10,000 ft/sec	V_i = 20,000 ft/sec	Single Stage
DL	GG	5000 psia	4200 psia	4000 psia
DL	S-C	4000	4250*	4100
F-D	GG	2600	2700	3300
F-D	S-C	3800	3600	3600

LOX/RP-1

Nozzle	Cycle	V_i = 10,000 ft/sec	V_i = 20,000 ft/sec	Single Stage
DL	GG	3000 psia	2800 psia	2800 psia
DL	S-C	3500*	3500	3200
F-D	GG	2700	2600	2600
F-D	S-C	3500*	3500*	3500*

UPPER-STAGE VEHICLES

LOX/LH_2 - DELAVAL NOZZLE

Cycle	OPTIMUM PRESSURE V_i = 10,000 ft/sec	V_i = 15,000 ft/sec	V_i = 20,000 ft/sec
GG	3100 psia	4000 psia	3400 psia
S-C	4250*	4250*	4250*

* Values of chamber pressure that are the maximum attainable with the staged-combustion cycle (see Figures III-16 and III-17).

In all cases where the peak payload occurs near the maximum attainable chamber pressures for the staged-combustion, careful consideration must be given to turbopump discharge pressure when selecting the optimum operating chamber pressure. A cursory examination of the plots of pump-discharge pressure <u>vs</u> thrust chamber pressure reveals that discrete pump discharge pressures are required at the maximum thrust chamber pressure values. However, actual design practice would dictate the selection of a chamber pressure slightly below the maximum value. From this point, adjustments could be made to the pump discharge pressure to compensate for performance irregulatities, (i.e., non-ideal gas behavior, fabrication nonconformance), giving assurance of more fully meeting design goals.

G. INJECTION DENSITY EFFECTS

An evaluation of the effect of chamber pressure on injection density was performed on O_2/RP-1 and O_2/H_2 propellants for contraction ratios of 2, 4, and 6. The contraction ratio, (A_c/A_t) is defined as the ratio of the chamber cross-sectional area to the throat area. The injection density is defined as the ratio of the cross-sectional area of the chamber to the total area of the orifices in the injector.

The results of this study are shown in Figures III-37 through III-42. Based upon a lower practical limit of injection density for conventional injectors (12 to 14), these figures show the maximum chamber pressure attainable with conventional injectors for each propellant combination at various contraction ratios.

Conventional injectors for thrust chambers and gas generators use a great many, very small holes. The amount of propellant which can be injected through these injectors is limited by both the allowable pressure drop, and the ratio of the area of the injector to the area of the orifice, i.e., injection density. In a conventional injector, a substantial fraction of injector face area is unavailable for injection because of the presence of the many manifold rings separating the two propellants behind the injector. Therefore, conventional injectors are severely limited with respect to the attainable injection density. Thus, if the conventional injector is applied to a high chamber pressure engine, very large contraction ratios must be used.

Figures III-37 through III-42 also show that if fewer but larger injection orifices (large element injectors) are used, the injection density is decreased and hence, improved. Thus, the maximum chamber pressure attainable (without large pressure drops across the injector or high contraction ratios) increases. Increases in the injector pressure drop are undesirable because pump discharge pressure requirements and therefore, pumping system weight, would increase. Large contraction ratios also result in high combustion chamber and injector weights. Thus, weight can be saved by incorporating large element injectors in high pressure engines.

Figures III-37 through III-42 were constructed by use of the following relationship:

$$A_{orf} = C_D \frac{\dot{W}}{\sqrt{\rho\, 2g\ \Delta P_i}}$$

where,

A_{orf}	=	Area of the orifice
$\dot{W}$	=	Propellant flow rate
ρ	=	Propellant density
P_i	=	Pressure drop across the injector face
C_D	=	Orifice discharge coefficient

A discharge coefficient of 0.85 was assumed for RP-1 and O_2, and 0.90 for H_2.

B

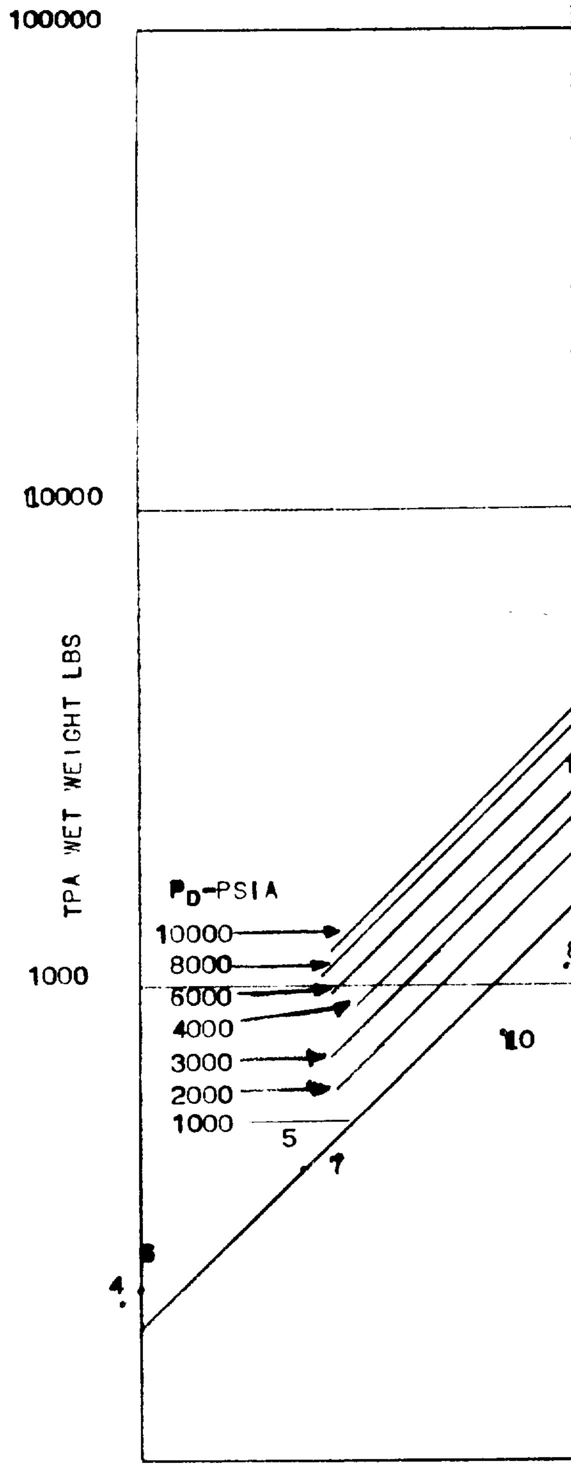

3OPUMP ASSEMBLY WET WEIGHTS

OPELLANT	PUMP DISCHARGE PRESSURE PSI	TPA WEIGHT-LB
)$_4$/A-50	4000	3000
)$_4$/A-50	4000	17,500
$_2$/LH$_2$	4000	10,620
$_2$/RP-1	1000	223
$_2$/RP-1	1000	402
)$_4$/A-50	1000	238
)$_4$/A-50	1000	470
?	1300	1100
$_2$/LH$_2$	4000	126,000
/RP-1	1200	800
	1500	2800
	1500	2900

FIGURE III-1

A

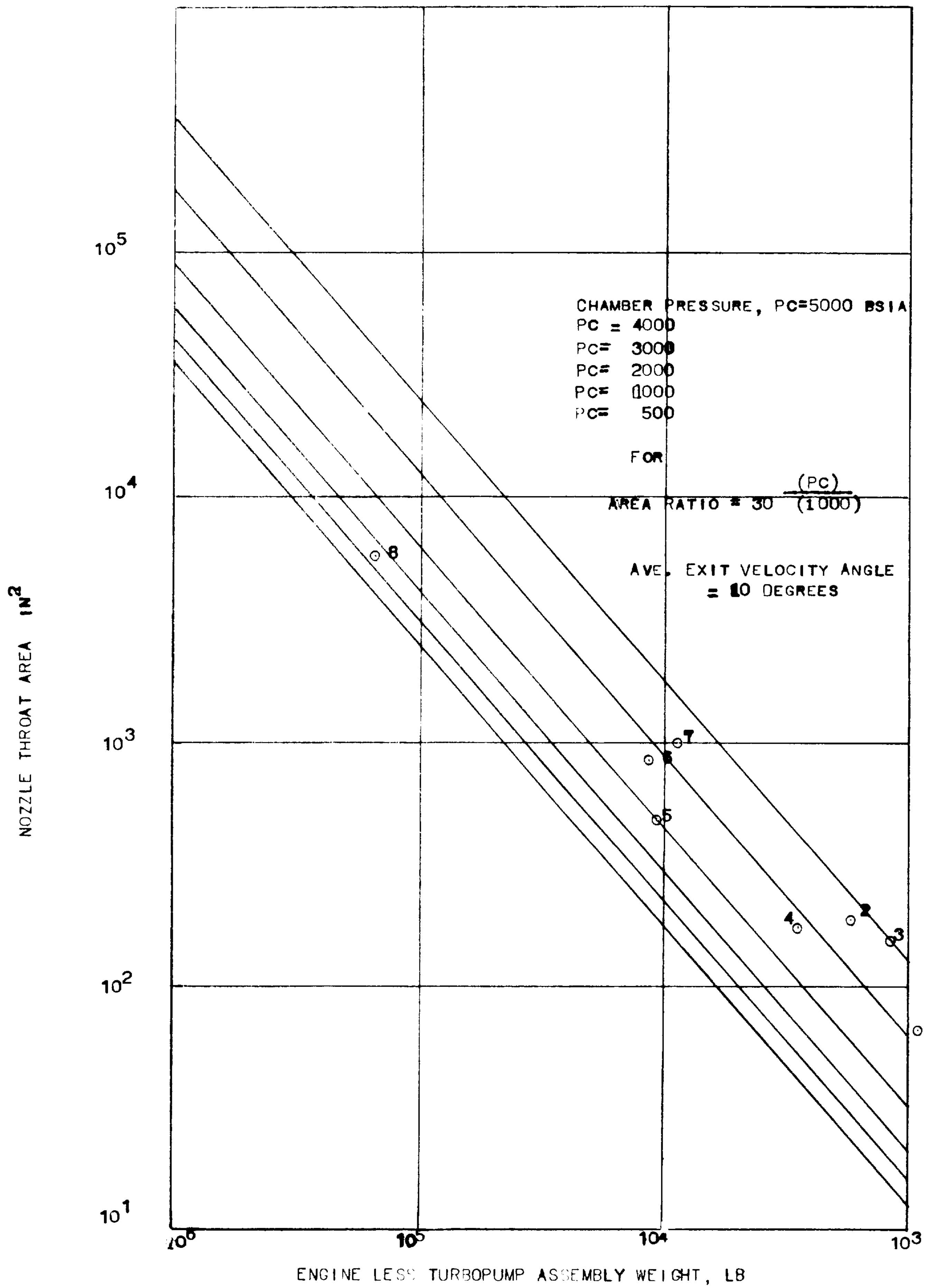

CHAMBER PRESSURE, PC=5000 PSIA
PC = 4000
PC= 3000
PC= 2000
PC= 1000
PC= 500
FOR
AREA RATIO = 30 (PC)/(1000)
AVE. EXIT VELOCITY ANGLE = 10 DEGREES
NOZZLE THROAT AREA IN²
ENGINE LESS TURBOPUMP ASSEMBLY WEIGHT, LB

B

ENGINE-LESS-TURBOPUMP WEIGHT
MP WEIGHT

LISTED BELOW ARE THE ENGINES USED TO CORRELATE THE ANALYTICAL WEIGHT STUDY
TO CORRELATE THE ANALYTICAL WEIGHT STUDY

KEY	PRODUCTION ENGINES	PC, PSIA
1	LR91-AJ-5 (TITAN II 2ND STAGE)	819
2	LR87-AJ-5 (TITAN II 1ST STAGE)	766
	ENGINE WEIGHT STUDIES	
3	200K (O_2/H_2)	700
4	800K (N_2O_4/A-50)	2770
5	HS-10 (1.5 $\bar{M}$ O_2/RP-1)	1000
6	M-1 (1 $\bar{M}$ O_2/H_2)	1000
7	2 $\bar{M}$	2500
8	2 4 $\bar{M}$	2500

PC, PSIA

Figure III-2

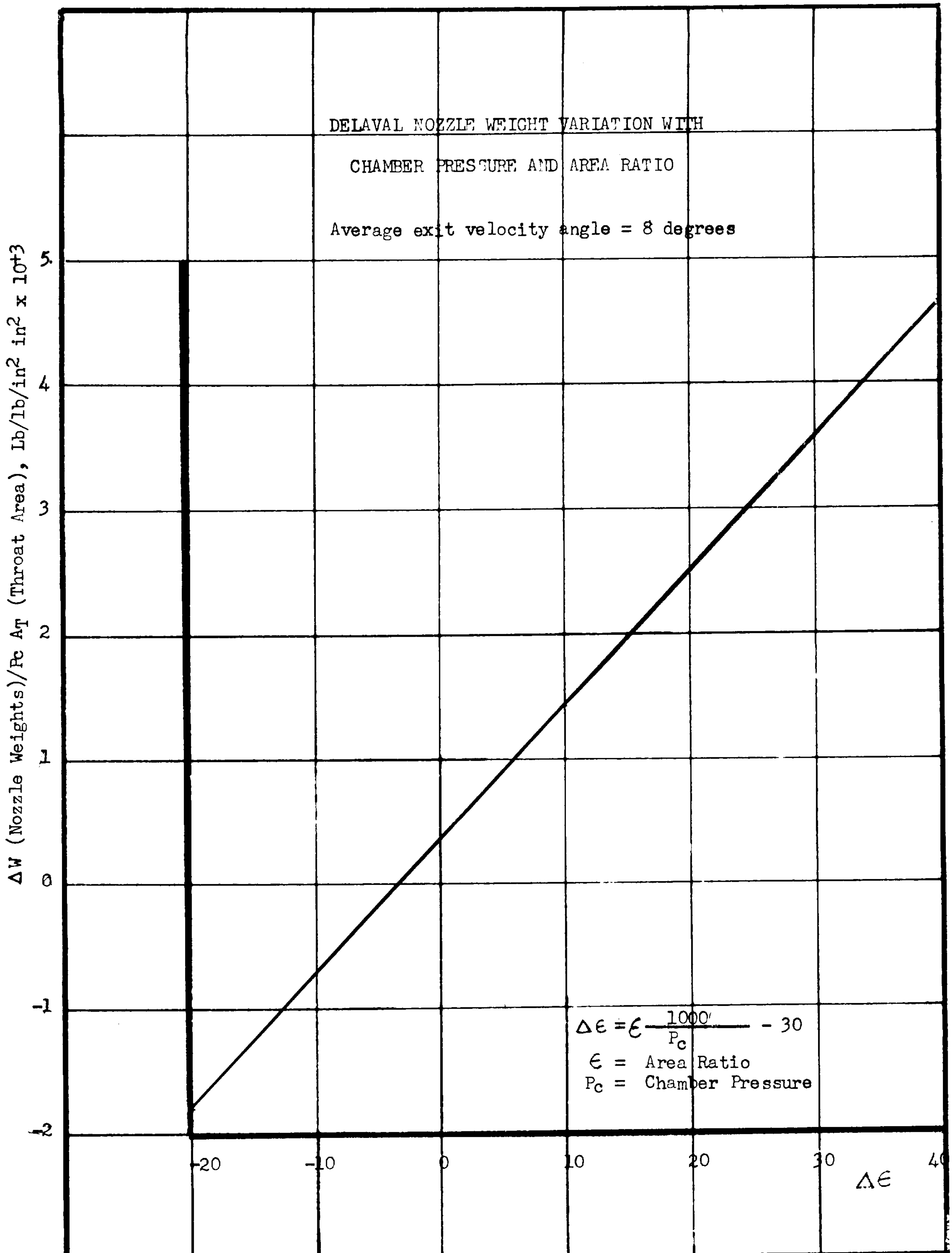

DELAVAL NOZZLE WEIGHT VARIATION WITH
CHAMBER PRESSURE AND AREA RATIO
Average exit velocity angle = 8 degrees
ΔW (Nozzle Weights)/Pc AT (Throat Area), Lb/lb/in2 in2 x 10+3
5
4
3
2
1
0
-1
-2
-20
-10
0
10
20
30
40
Δε
Δε = ε 1000/Pc - 30
ε = Area Ratio
Pc = Chamber Pressure

Figure III-3

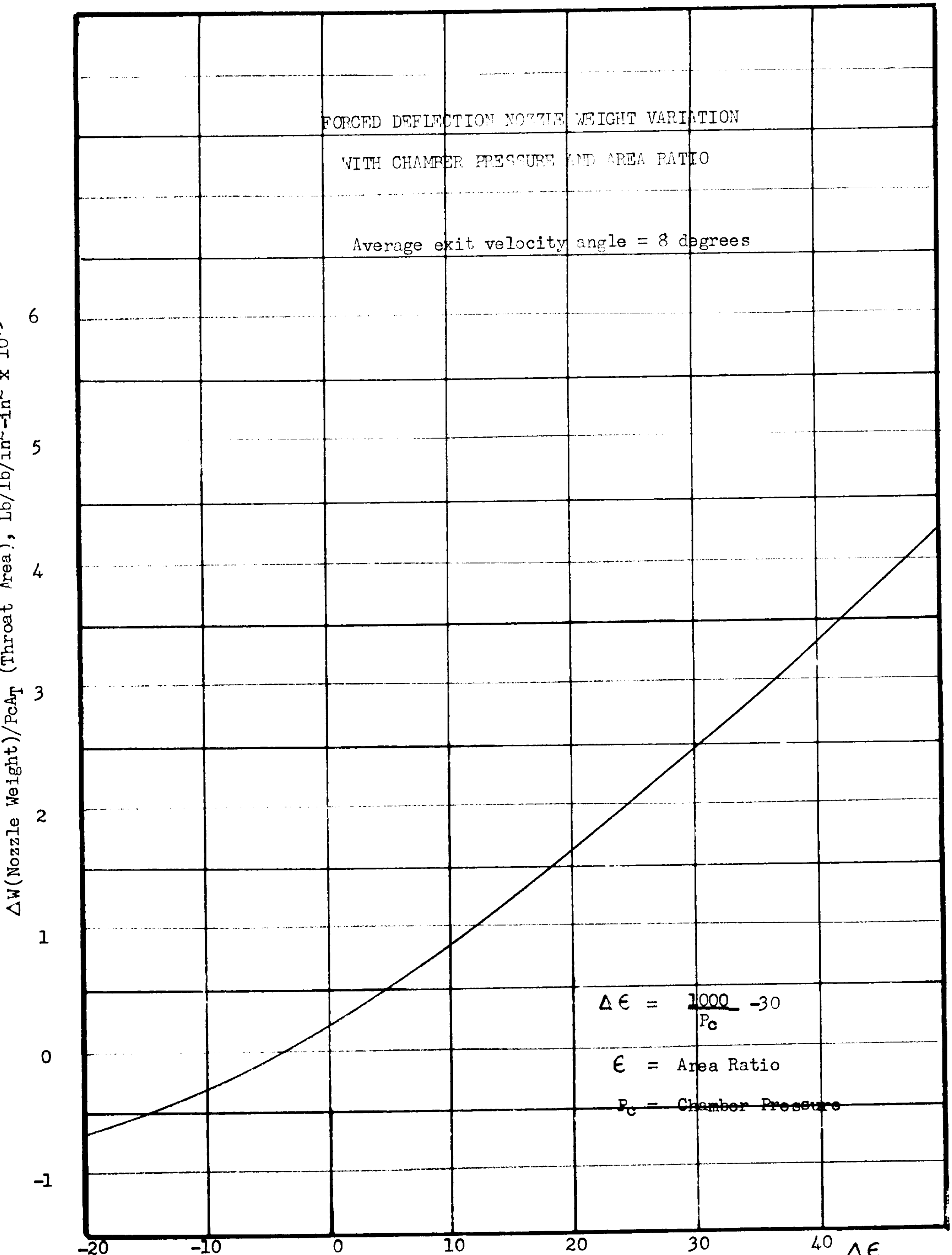
FORCED DEFLECTION NOZZLE WEIGHT VARIATION
WITH CHAMBER PRESSURE AND AREA RATIO
Average exit velocity angle = 8 degrees
ΔW(Nozzle Weight)/P_cA_T (Throat Area), Lb/lb/in^2-in^2 x 10^{+3}
6
5
4
3
2
1
0
-1
$\Delta \epsilon = \frac{1000}{P_c} - 30$
ϵ = Area Ratio
P_c = Chamber Pressure
-20
-10
0
10
20
30
40
$\Delta \epsilon$

Figure III-4

GAS GENERATOR CYCLE

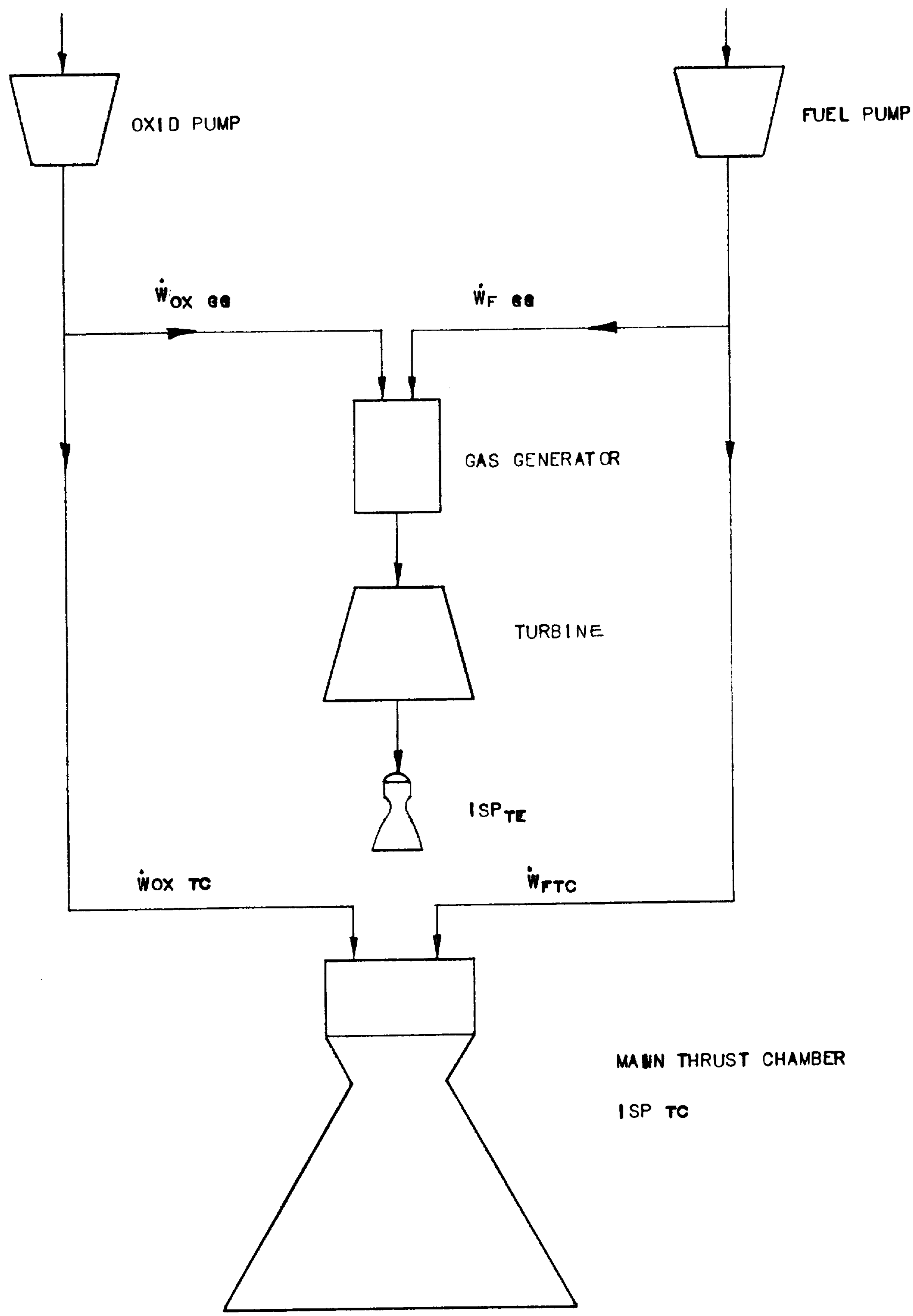

FIGURE III #5

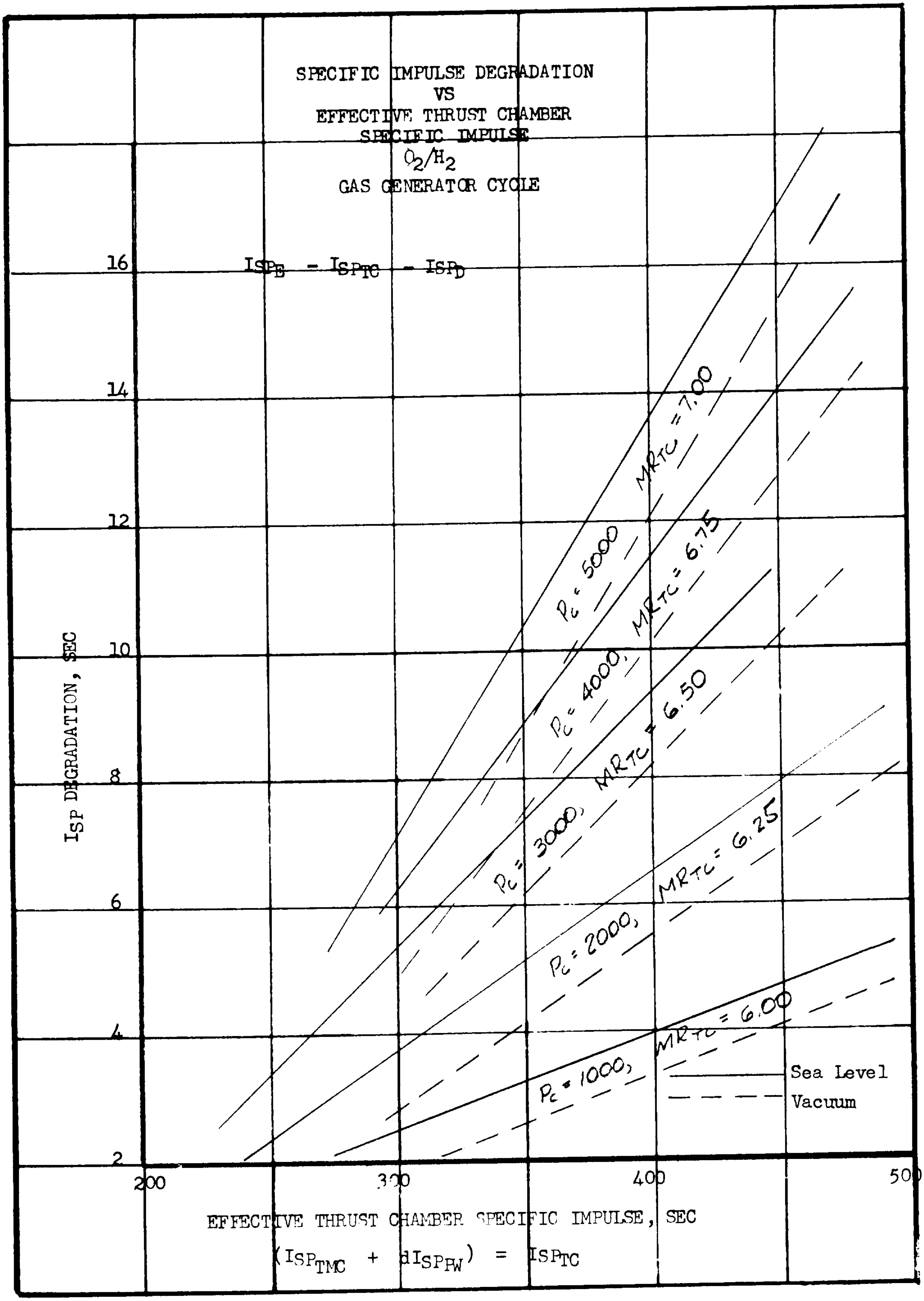
SPECIFIC IMPULSE DEGRADATION
VS
EFFECTIVE THRUST CHAMBER
SPECIFIC IMPULSE
O_2/H_2
GAS GENERATOR CYCLE
$Isp_E - Isp_{TC} - Isp_D$
16
14
12
10
8
6
4
2
I_{SP} DEGRADATION, SEC
200
300
400
500
EFFECTIVE THRUST CHAMBER SPECIFIC IMPULSE, SEC
$(Isp_{TMC} + dIsp_{FW}) = Isp_{TC}$
$P_c = 5000$, $MR_{TC} = 7.00$
$P_c = 4000$, $MR_{TC} = 6.75$
$P_c = 3000$, $MR_{TC} = 6.50$
$P_c = 2000$, $MR_{TC} = 6.25$
$P_c = 1000$, $MR_{TC} = 6.00$
Sea Level
Vacuum

Figure III-6

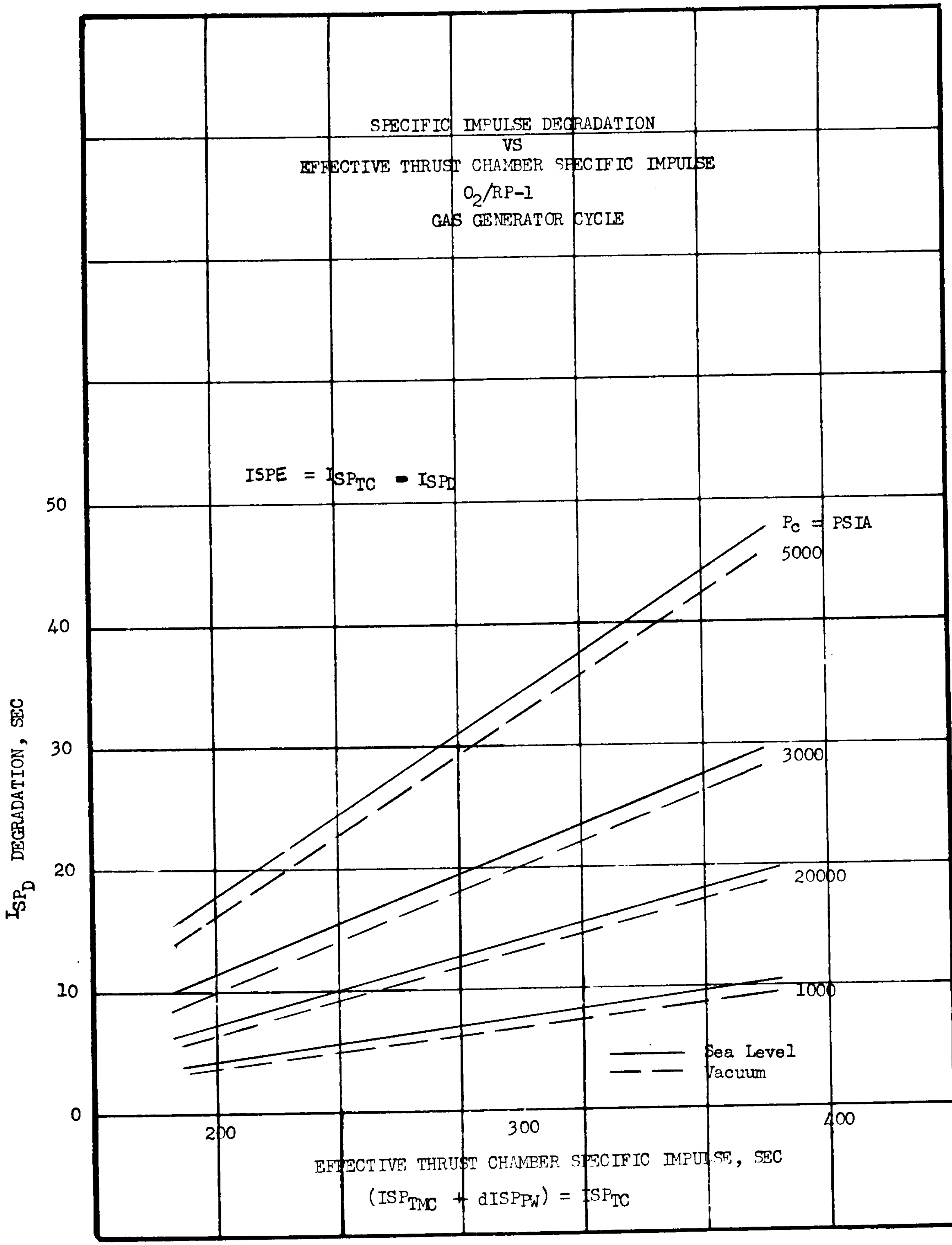
SPECIFIC IMPULSE DEGRADATION
VS
EFFECTIVE THRUST CHAMBER SPECIFIC IMPULSE
O_2/RP-1
GAS GENERATOR CYCLE
ISPE = $I_{SP_{TC}}$ - I_{SP_D}
P_c = PSIA
5000
3000
20000
1000
Sea Level
Vacuum
I_{SP_D} DEGRADATION, SEC
50
40
30
20
10
0
200
300
400
EFFECTIVE THRUST CHAMBER SPECIFIC IMPULSE, SEC
(ISP_{TMC} + $dISP_{PW}$) = ISP_{TC}

Figure III-7

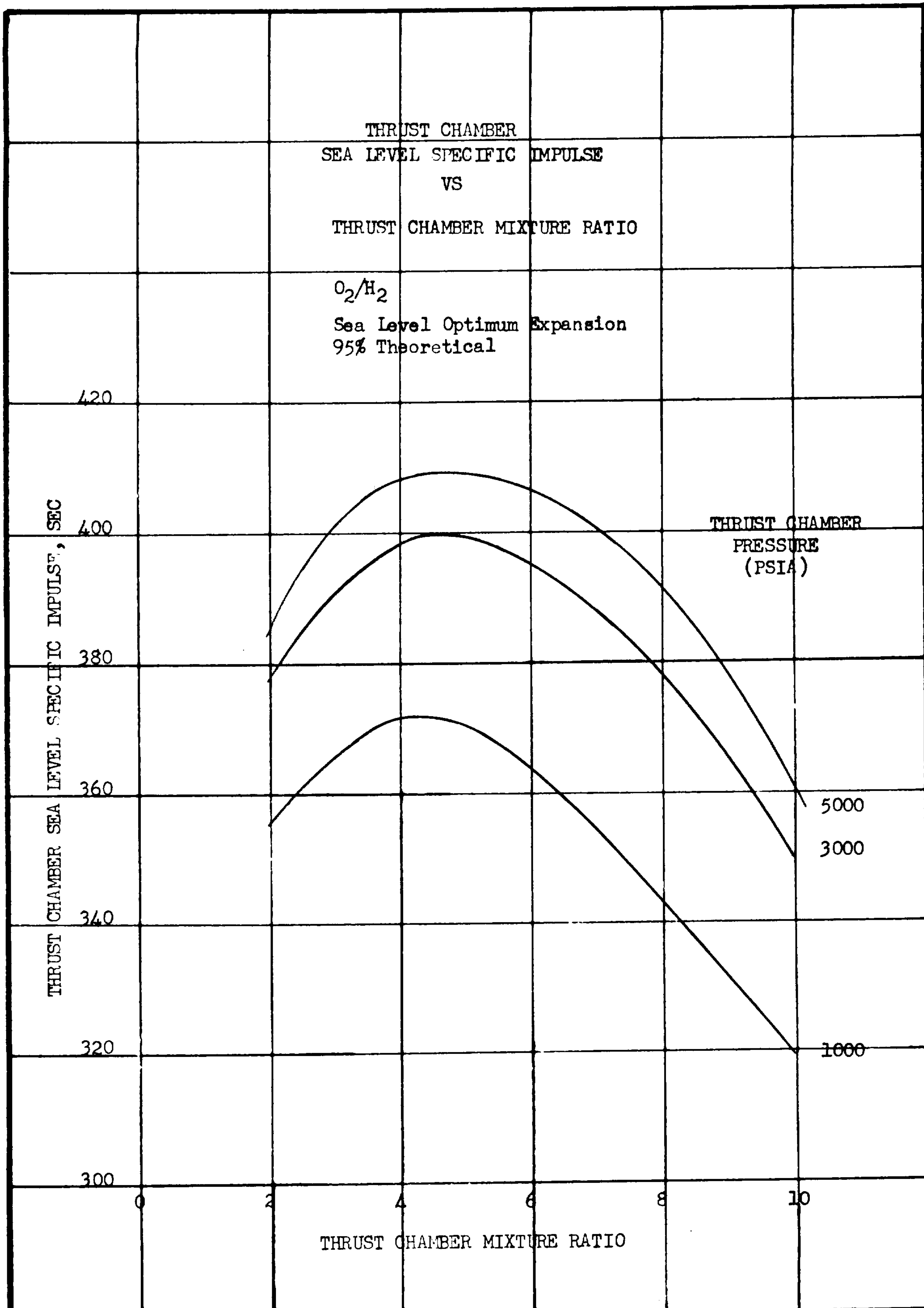
THRUST CHAMBER
SEA LEVEL SPECIFIC IMPULSE
VS
THRUST CHAMBER MIXTURE RATIO
O_2/H_2
Sea Level Optimum Expansion
95% Theoretical
THRUST CHAMBER PRESSURE (PSIA)
5000
3000
1000
420
400
380
360
340
320
300
0
2
4
6
8
10
THRUST CHAMBER SEA LEVEL SPECIFIC IMPULSE, SEC
THRUST CHAMBER MIXTURE RATIO

Figure III-8

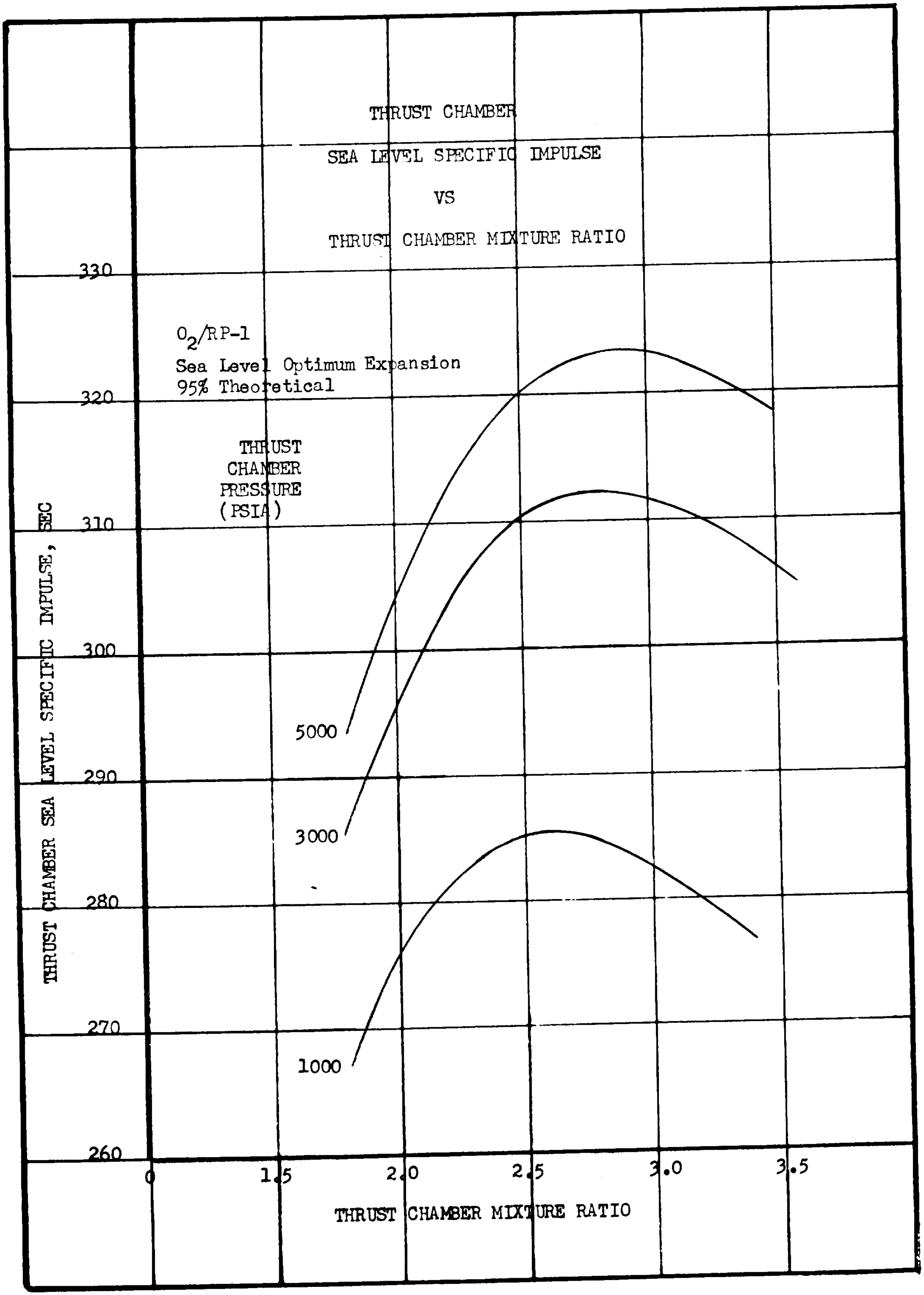
THRUST CHAMBER
SEA LEVEL SPECIFIC IMPULSE
VS
THRUST CHAMBER MIXTURE RATIO
O_2/RP-1
Sea Level Optimum Expansion
95% Theoretical
THRUST
CHAMBER
PRESSURE
(PSIA)
5000
3000
1000
330
320
310
300
290
280
270
260
THRUST CHAMBER SEA LEVEL SPECIFIC IMPULSE, SEC
0
1.5
2.0
2.5
3.0
3.5
THRUST CHAMBER MIXTURE RATIO

Figure III-9

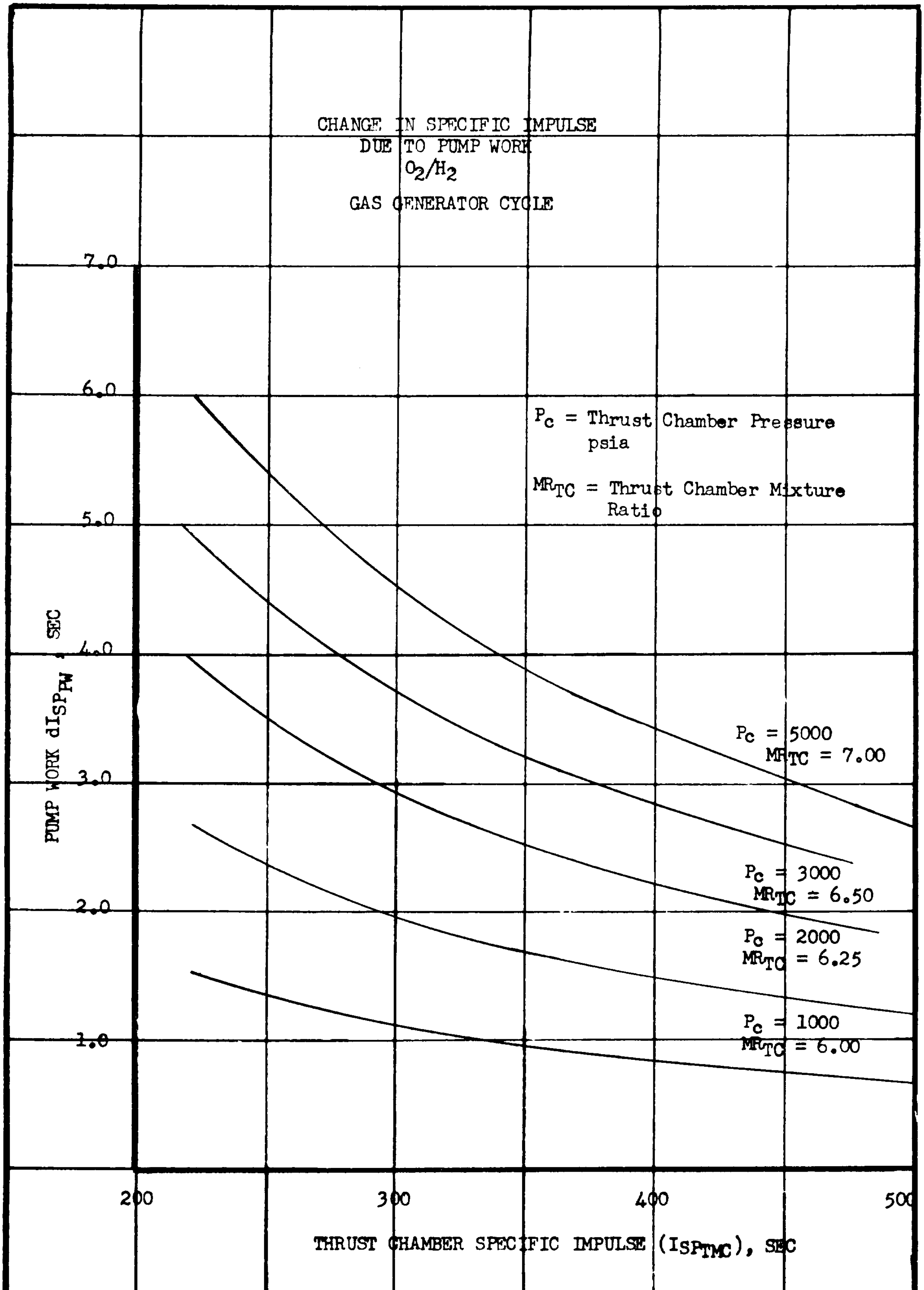

Figure III-10

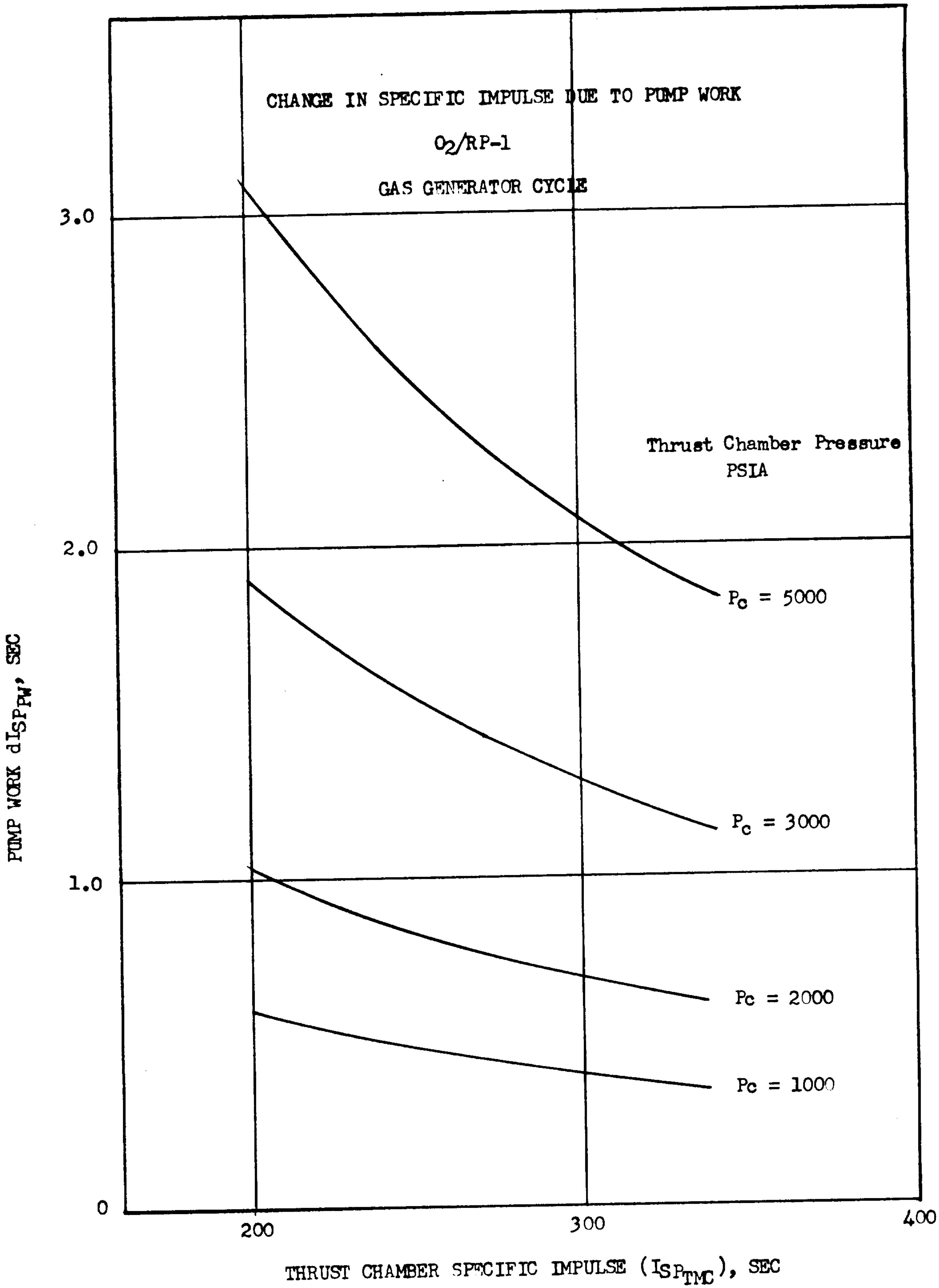

Figure III-11

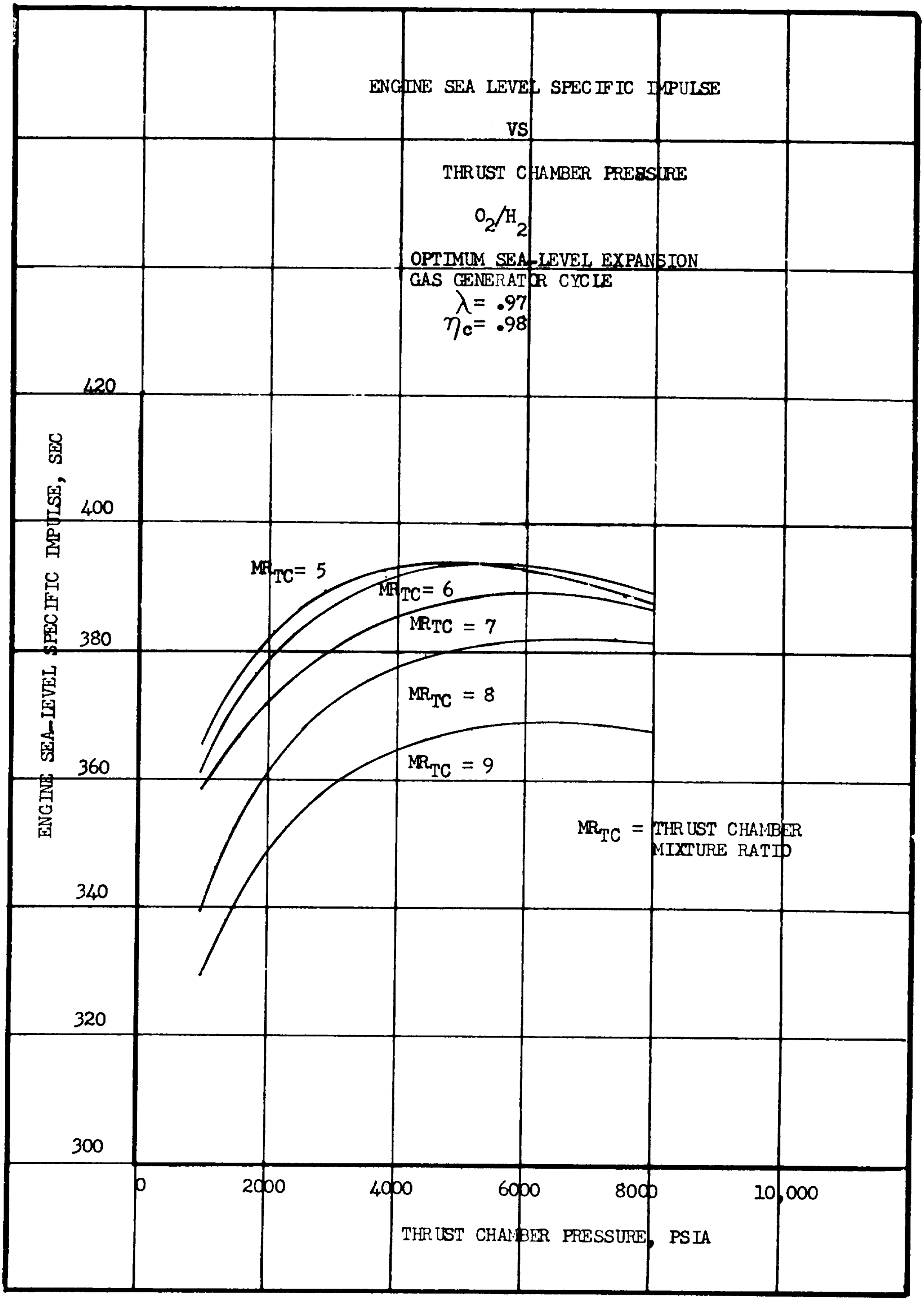

Figure III-12

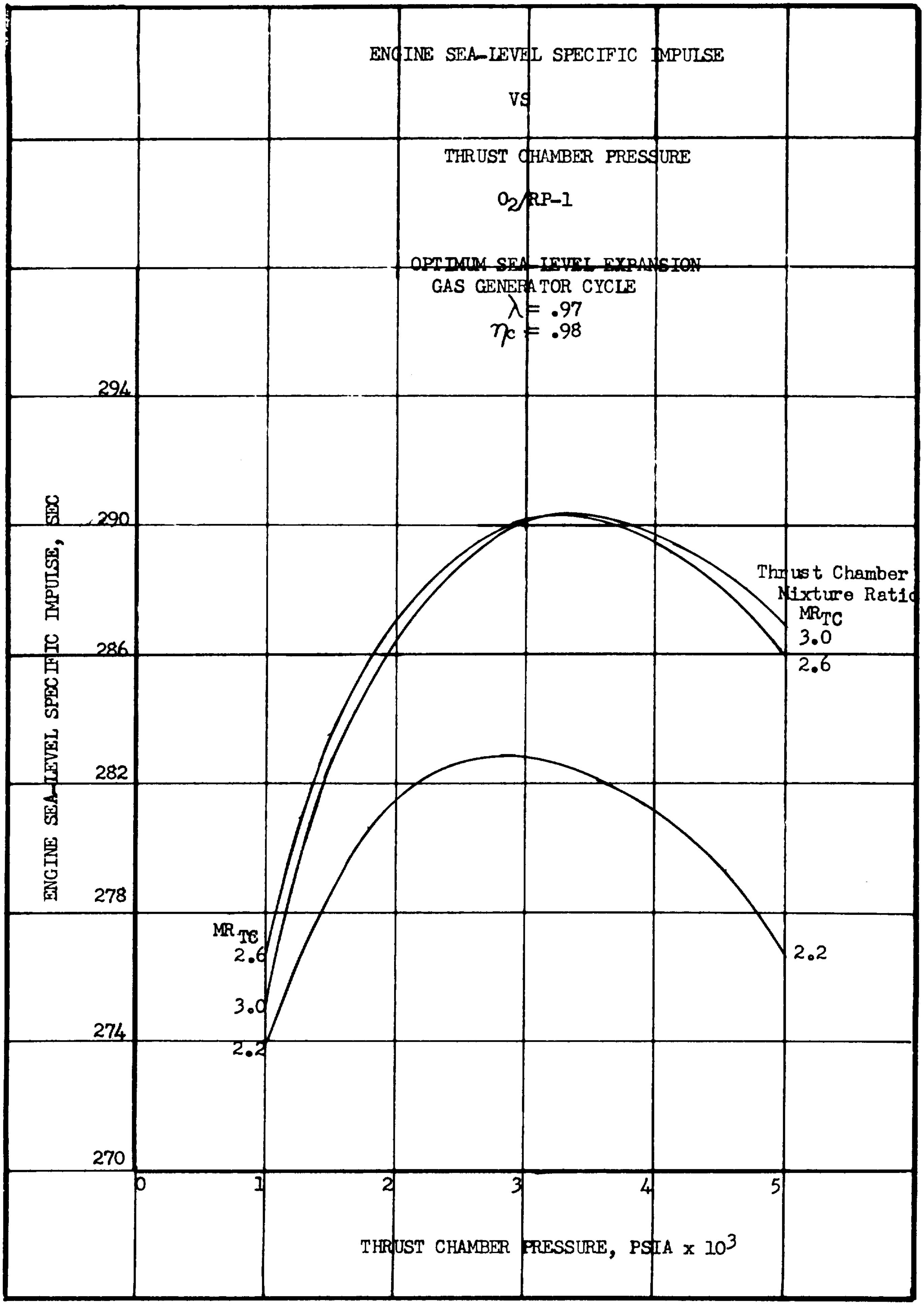

Figure III-13

STAGED COMBUSTION CYCLE

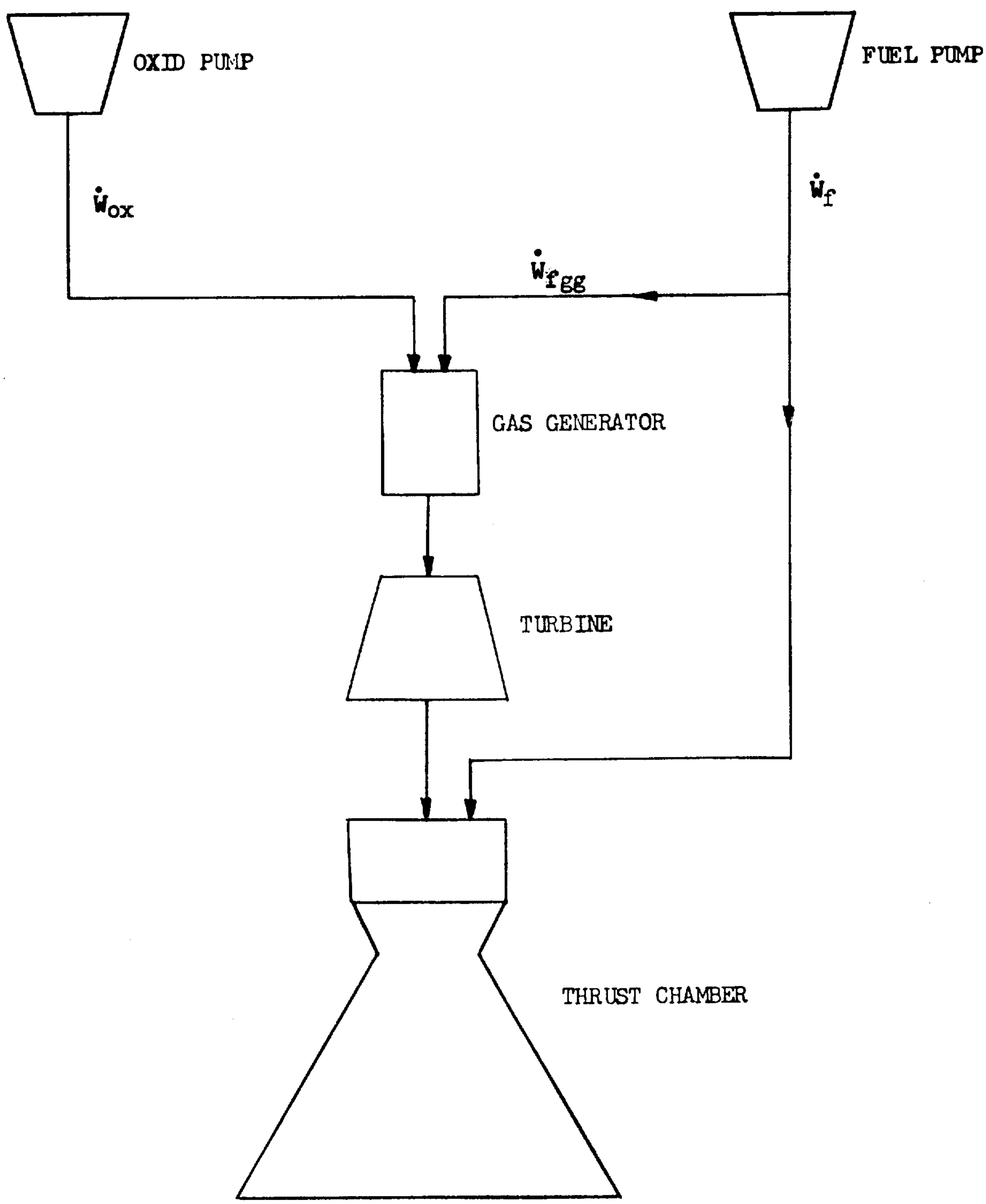

Figure III-14

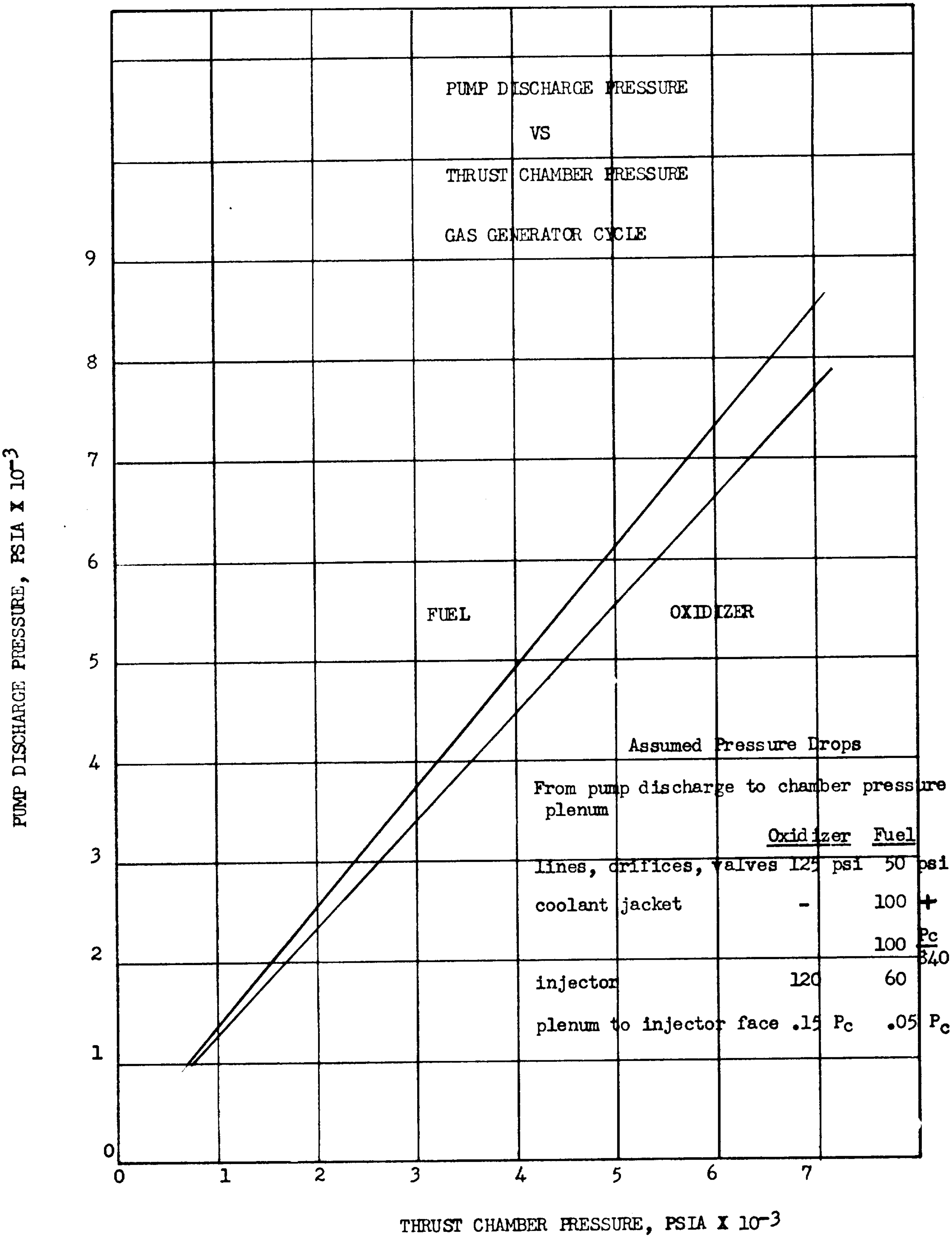

Figure III-15

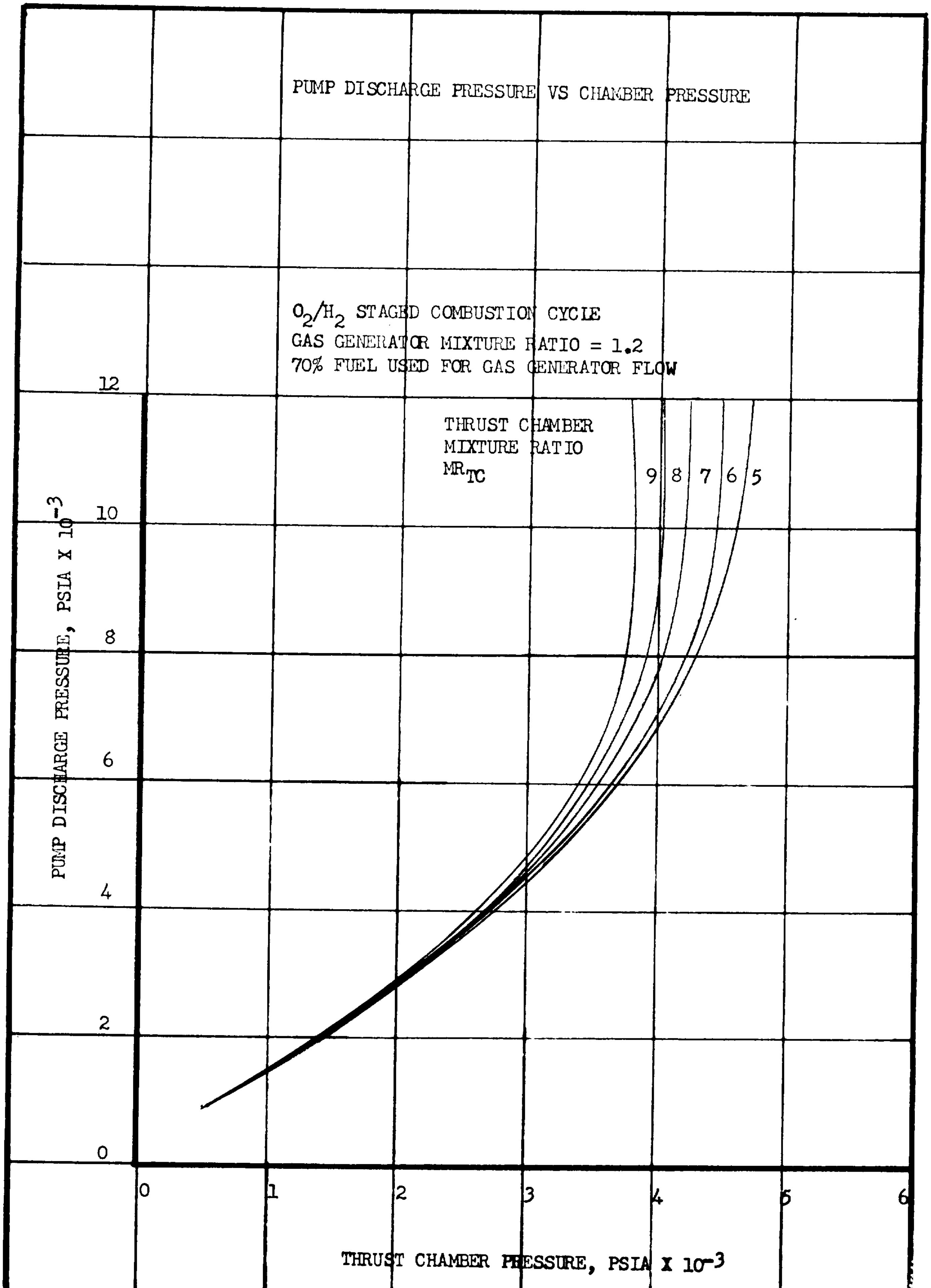

Figure III-16

PUMP DISCHARGE PRESSURE
VS
THRUST CHAMBER PRESSURE
O_2/RP-1
STAGE COMBUSTION CYCLE
GAS GENERATOR MIXTURE RATIO = 38.00

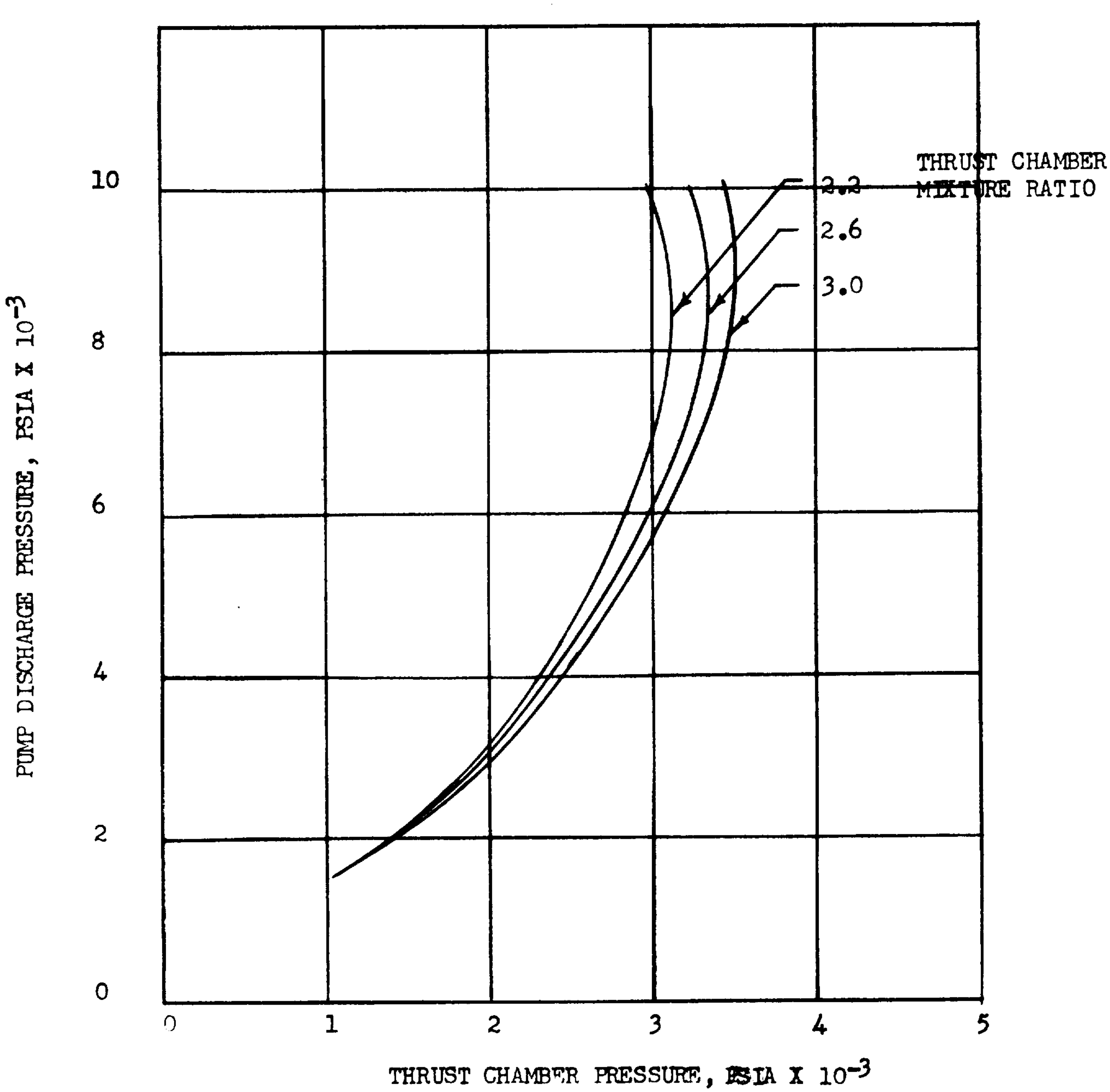

Figure III-17

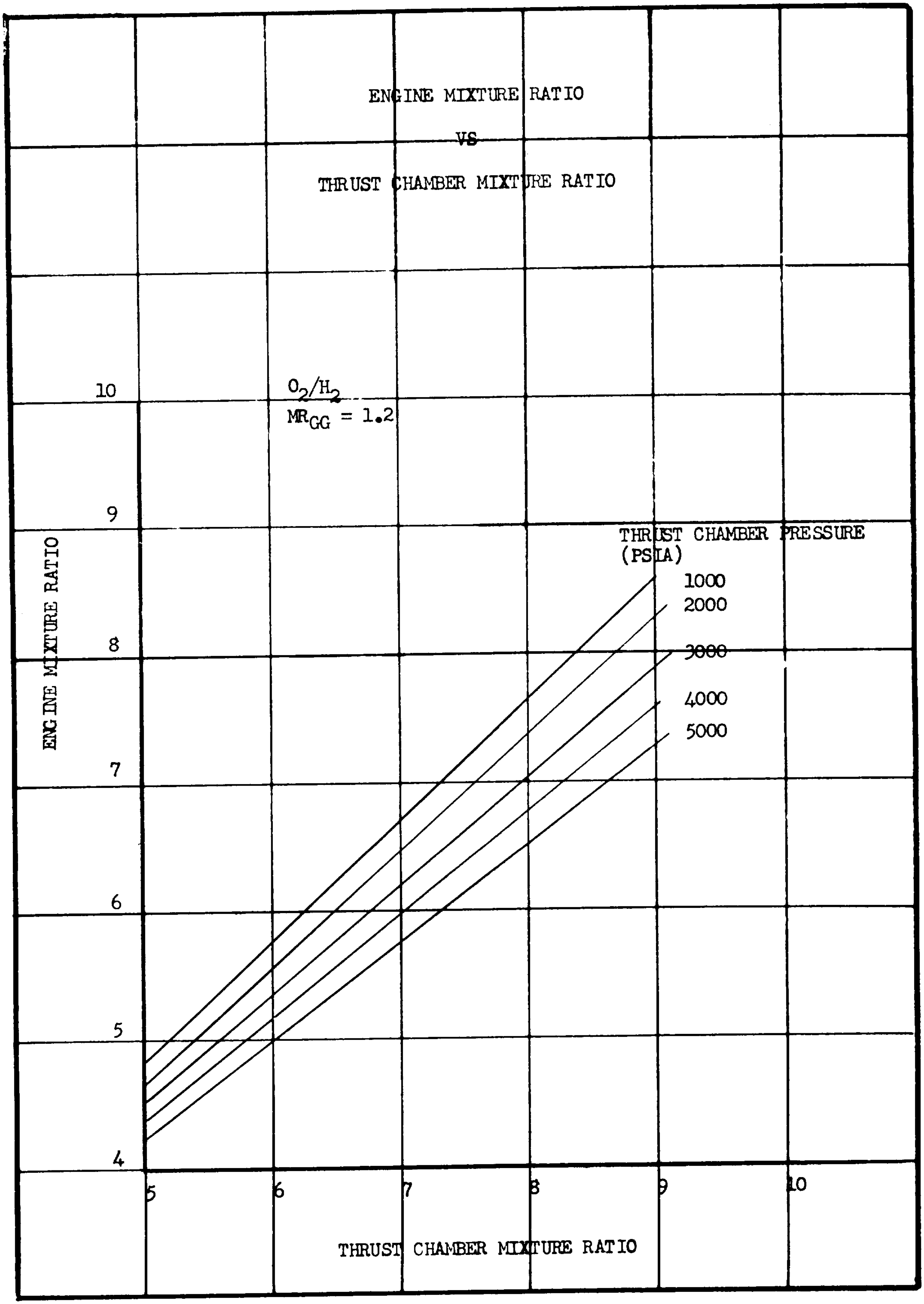

Figure III-18

ENGINE MIXTURE RATIO
VS
THRUST CHAMBER MIXTURE RATIO

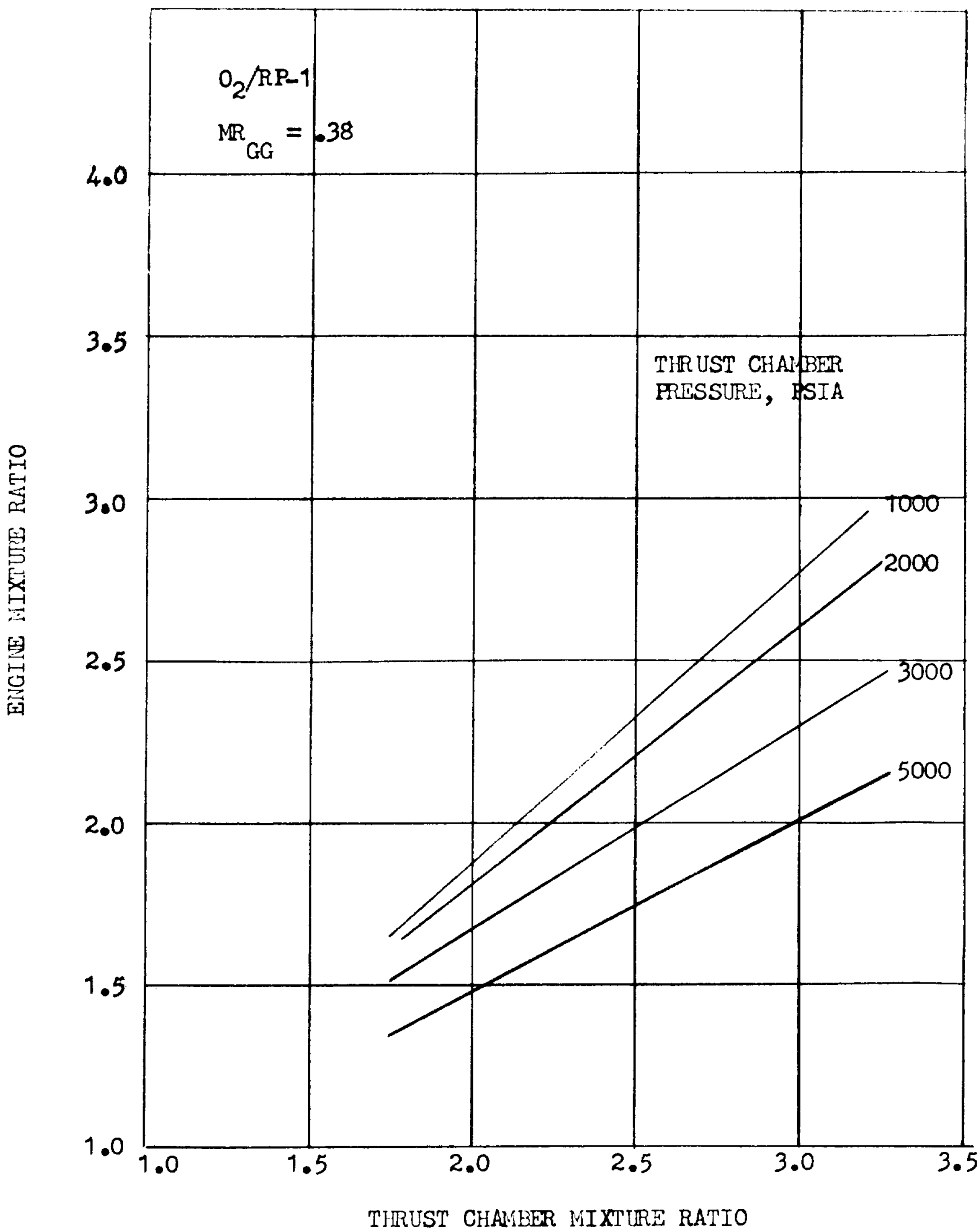

Figure III-19

THRUST CHAMBER MIXTURE RATIO SELECTION

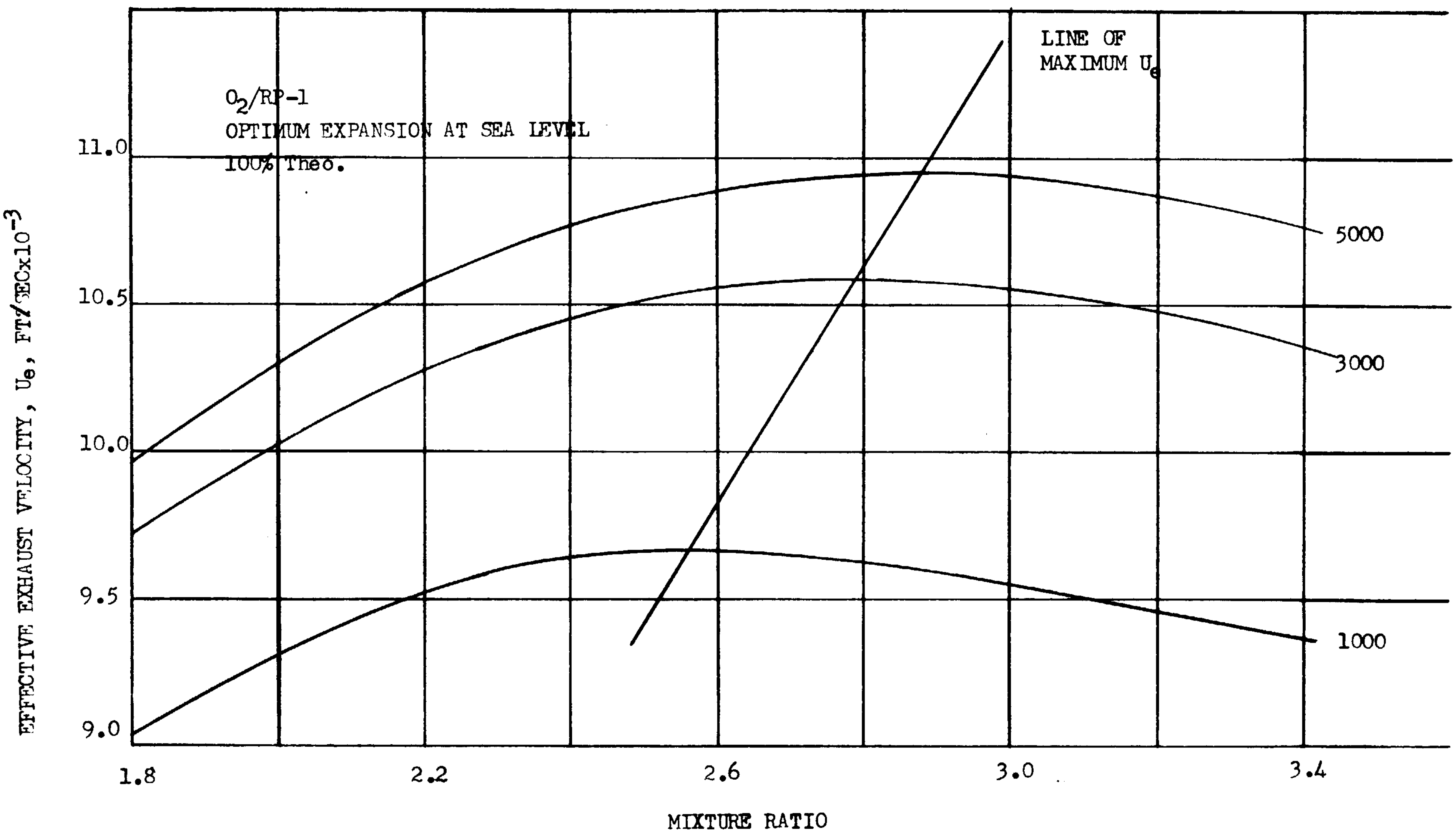

Figure III-20

SELECTED MIXTURE RATIOS

VS

THRUST CHAMBER PRESSURE

(O_2/RP-1

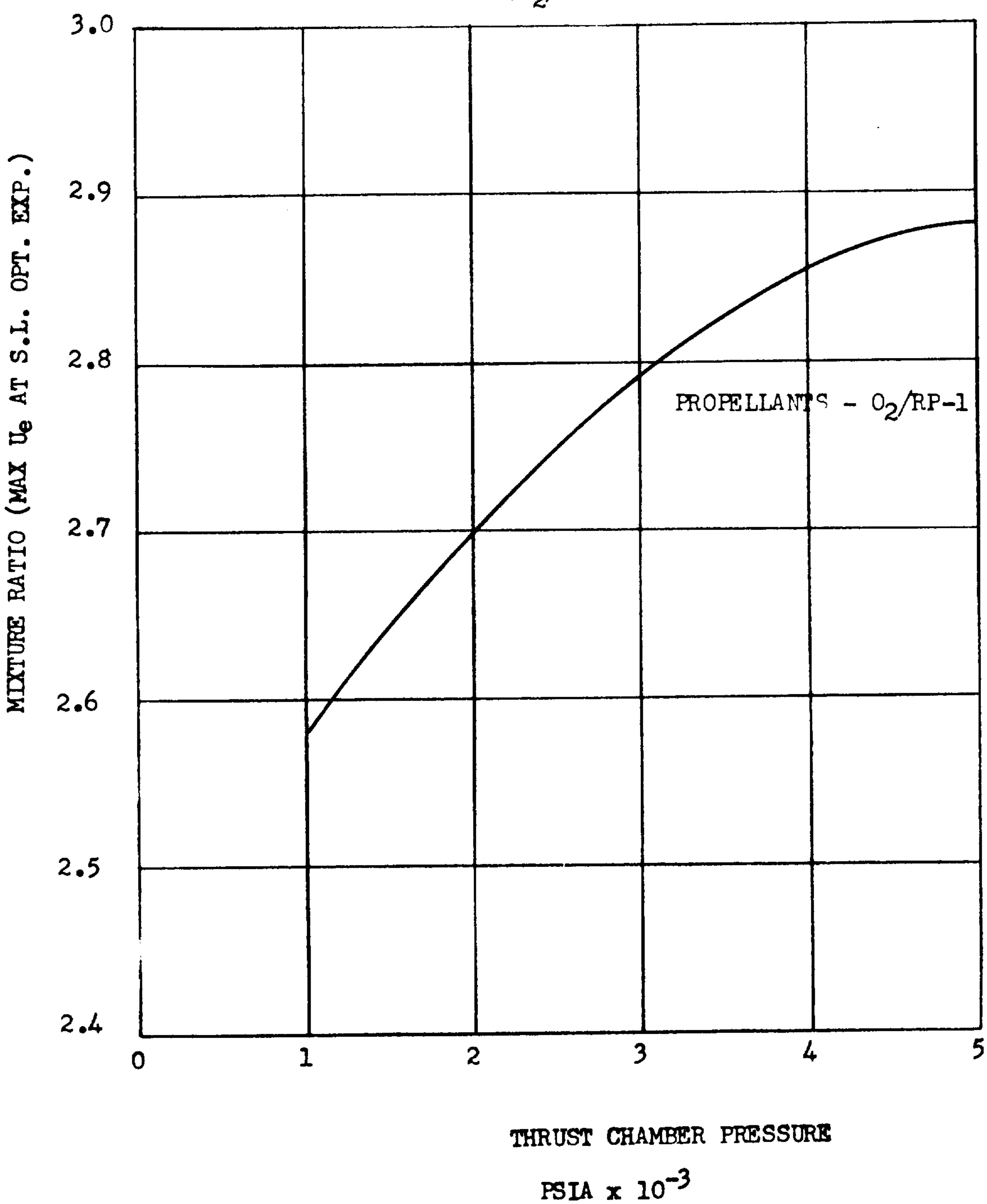

Figure III-21

SELECTED MIXTURE RATIOS

VS

THRUST CHAMBER PRESSURE

(O_2/H_2)

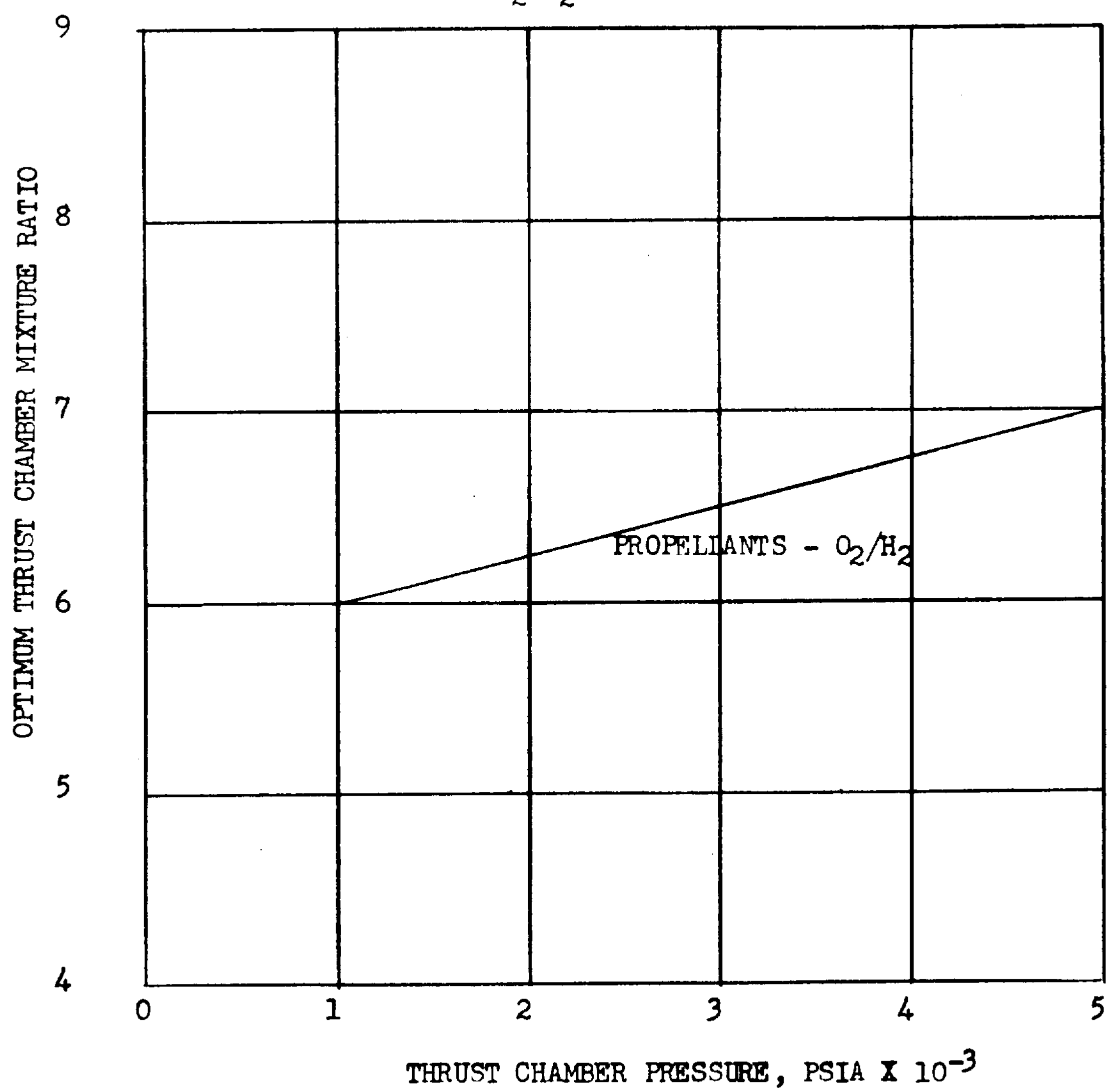

Figure III-22

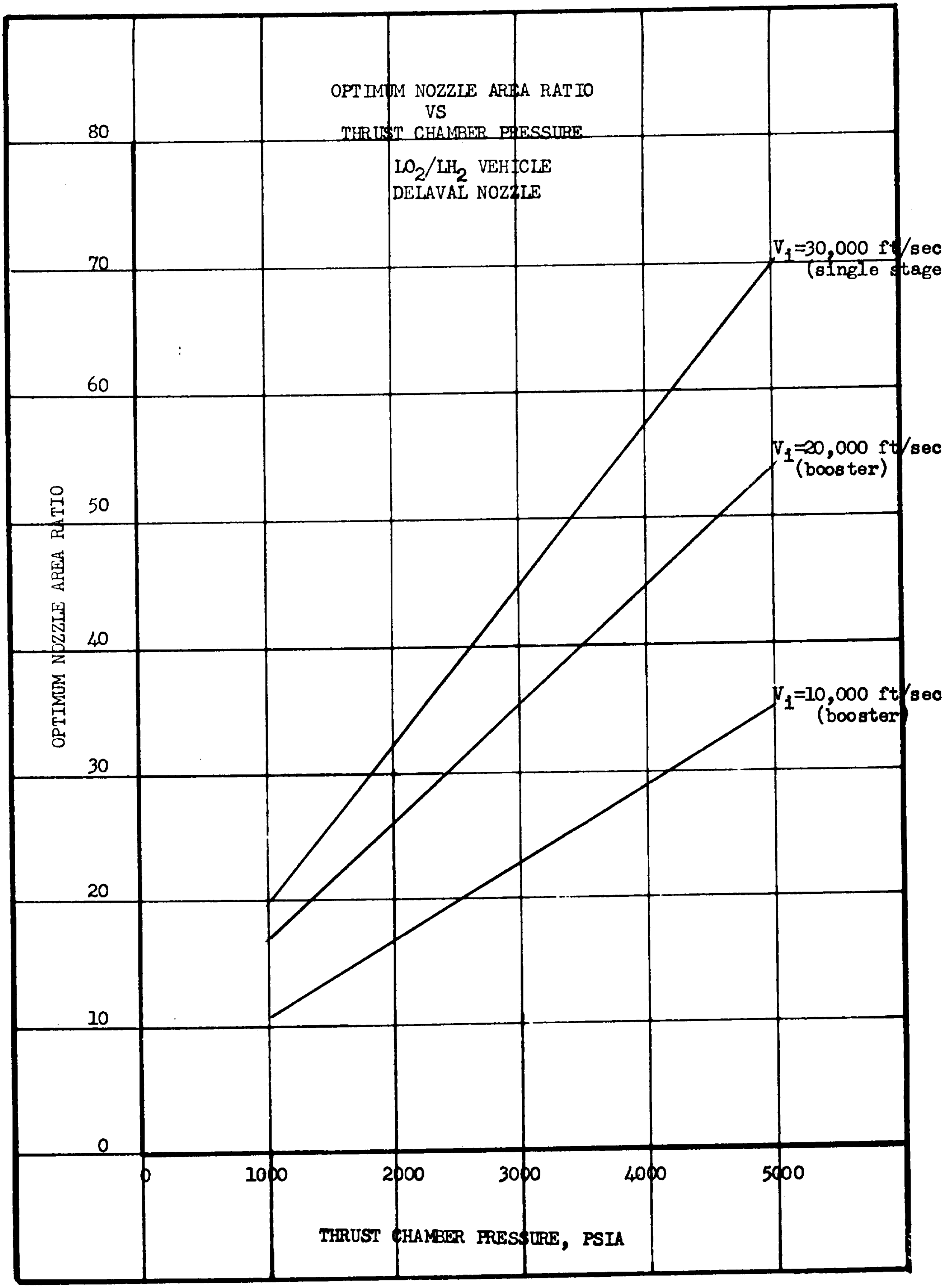

Figure III-23

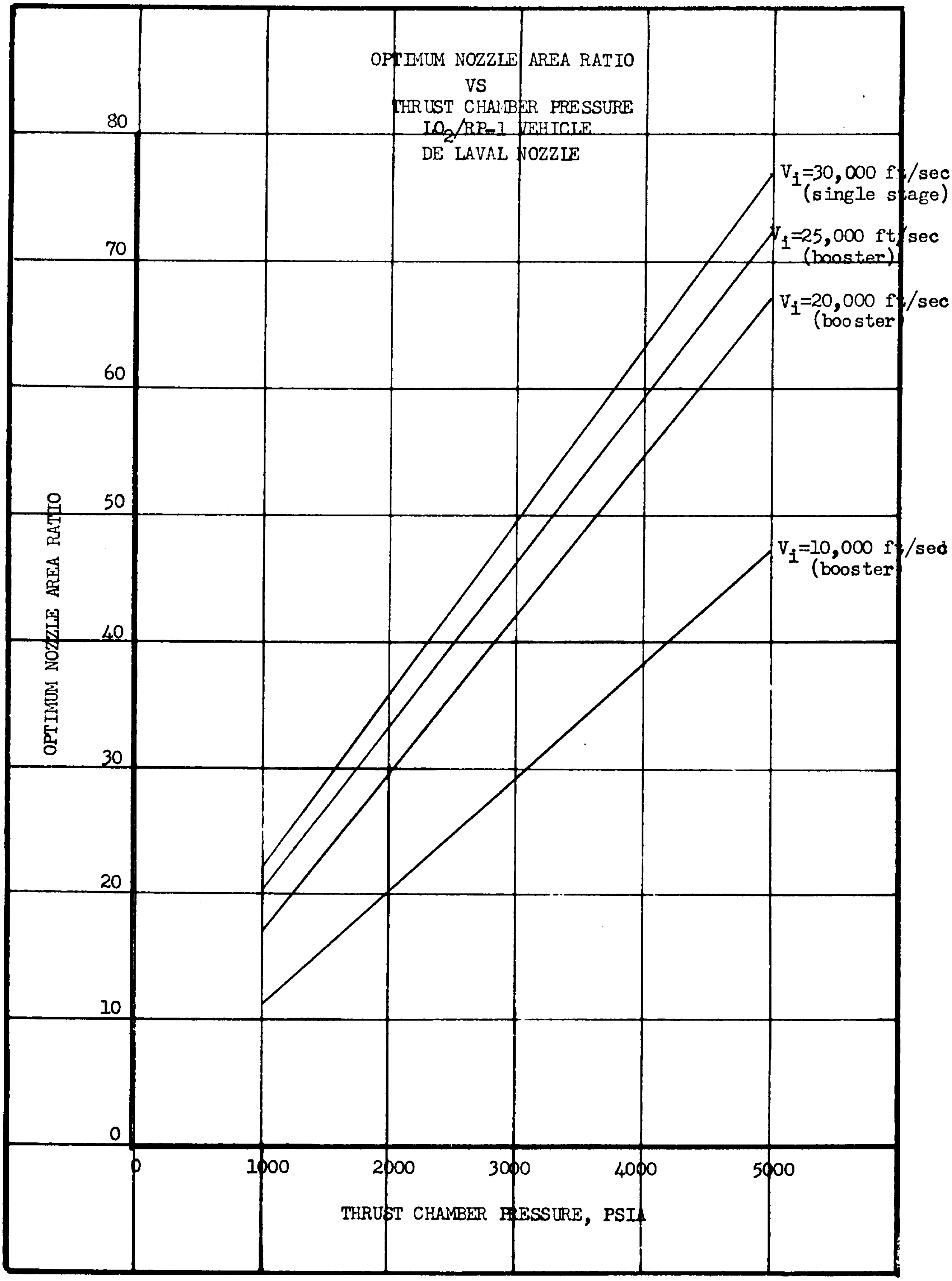

Figure III-24

OPTIMUM NOZZLE AREA RATIO
VS
THRUST CHAMBER PRESSURE
LO_2/LH_2 VEHICLE
FORCED-DEFLECTION NOZZLE

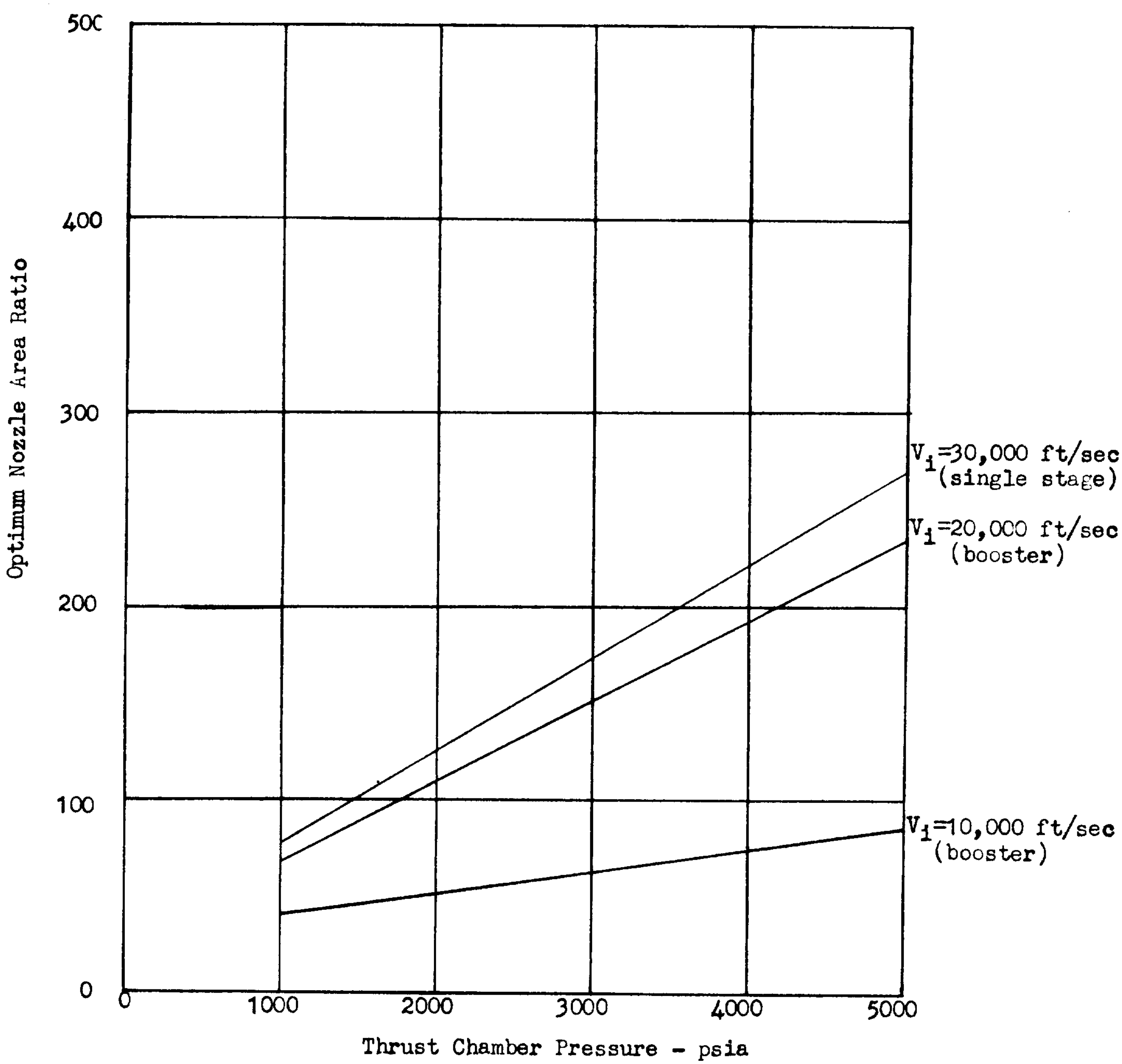

Figure III-25

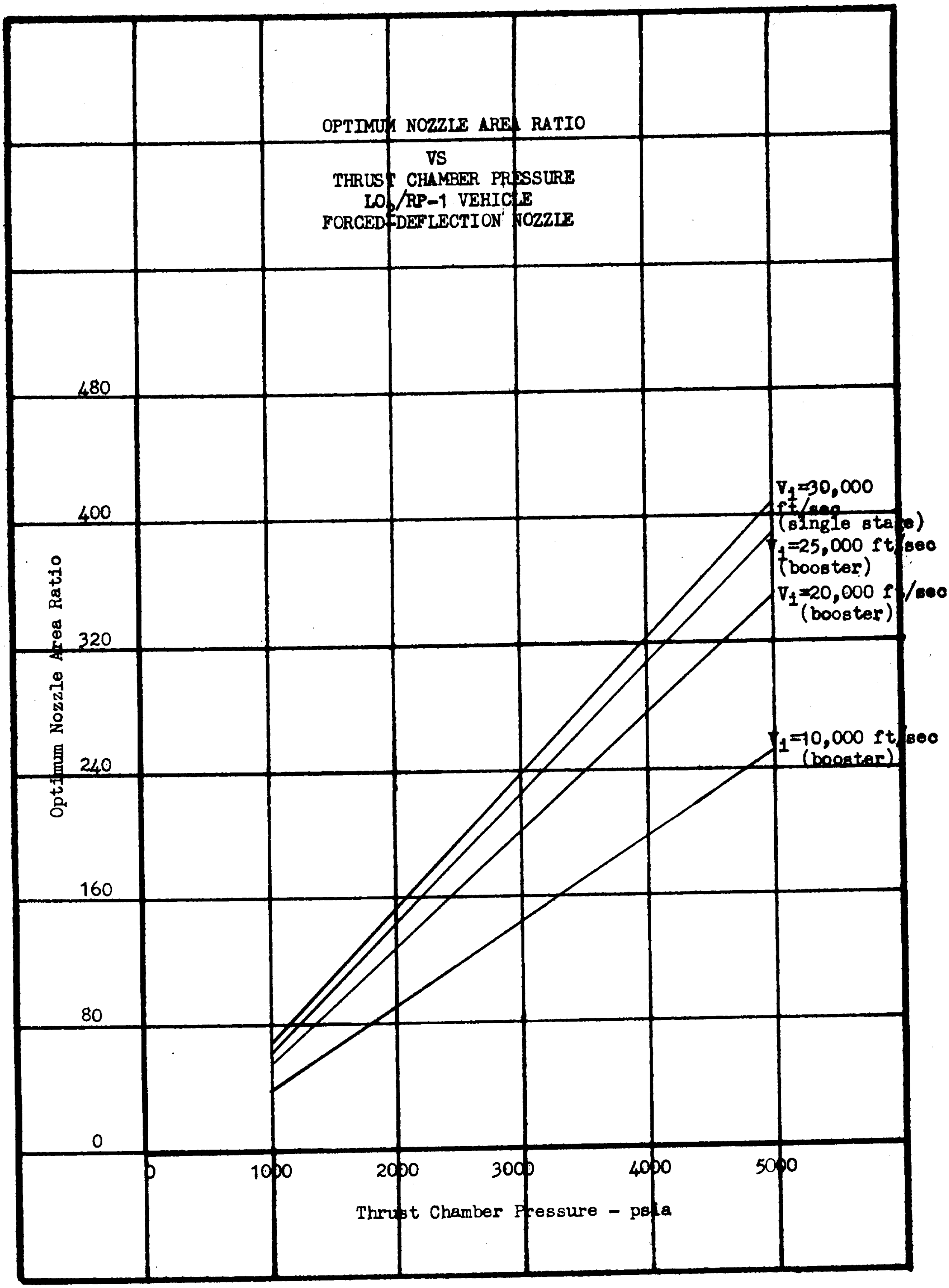

Figure III-26

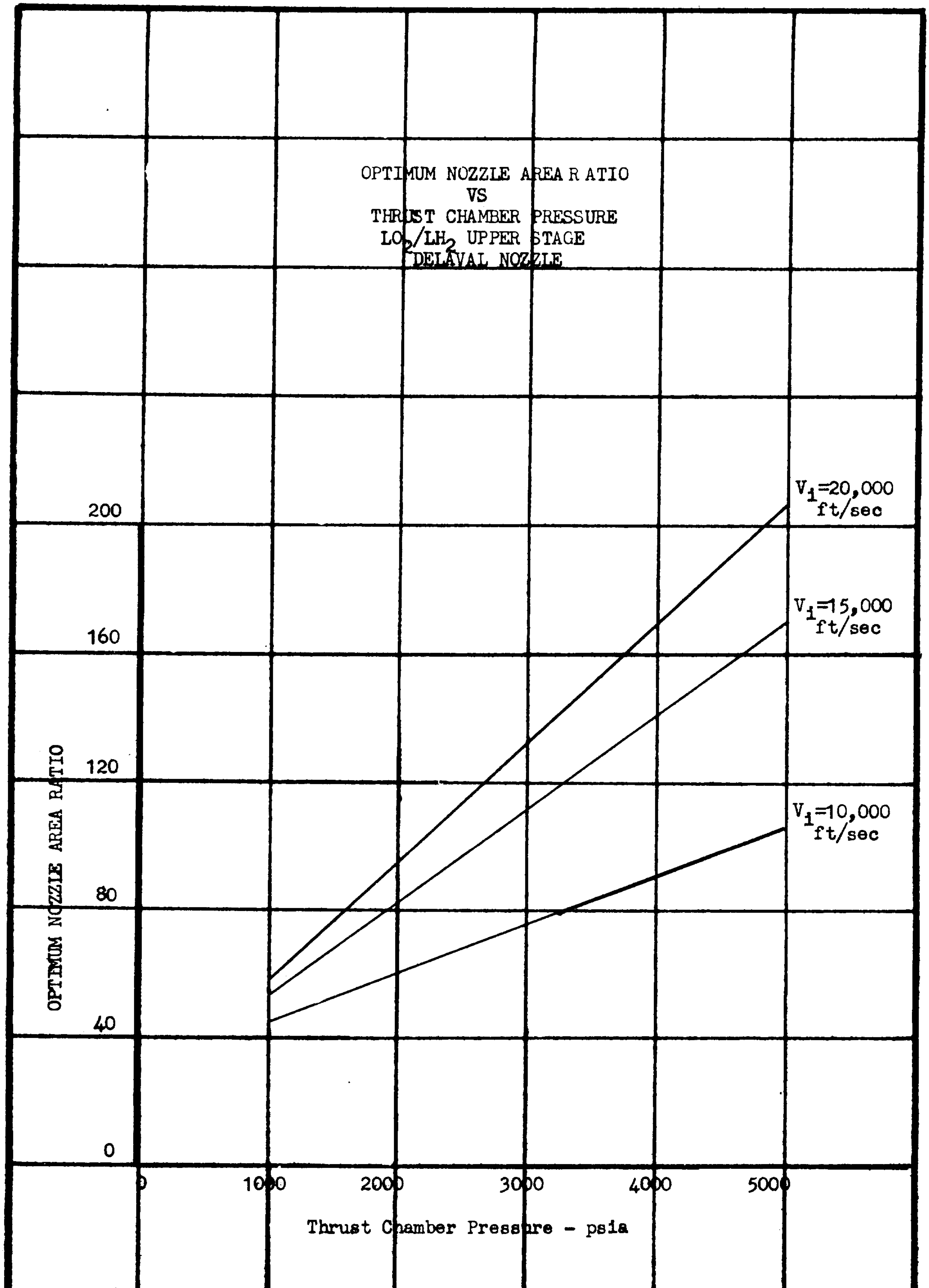

Figure III-27

RELATIVE PAYLOAD
vs
THRUST CHAMBER PRESSURE
LO_2/LH_2 VEHICLE

SINGLE STAGE TO 300 nm. ORBIT

— — FORCED DEFLECTION NOZZLE
——— DE LAVAL NOZZLE

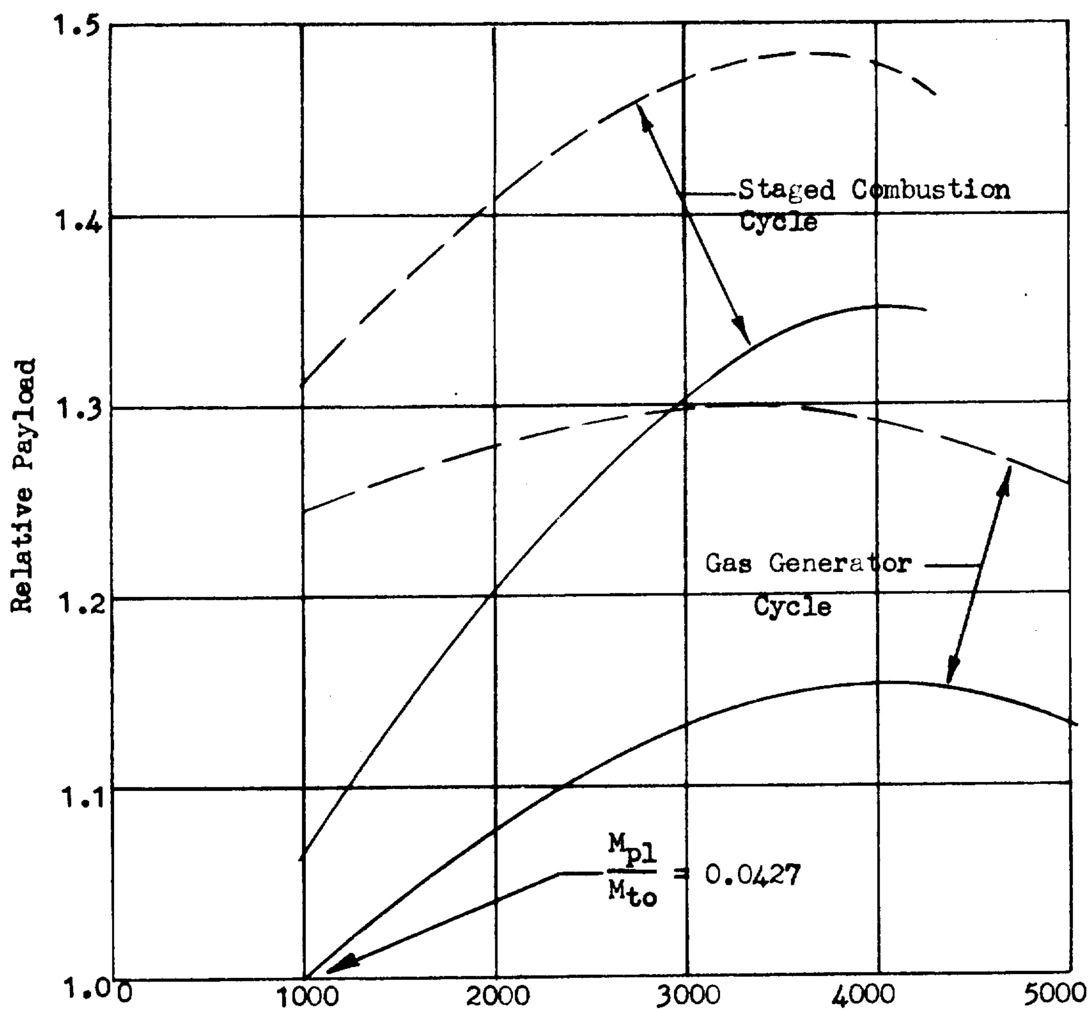

Figure III-28

RELATIVE PAYLOAD
vs
THRUST CHAMBER PRESSURE
LO_2/LH_2
V_i = 20,000 FT/SEC

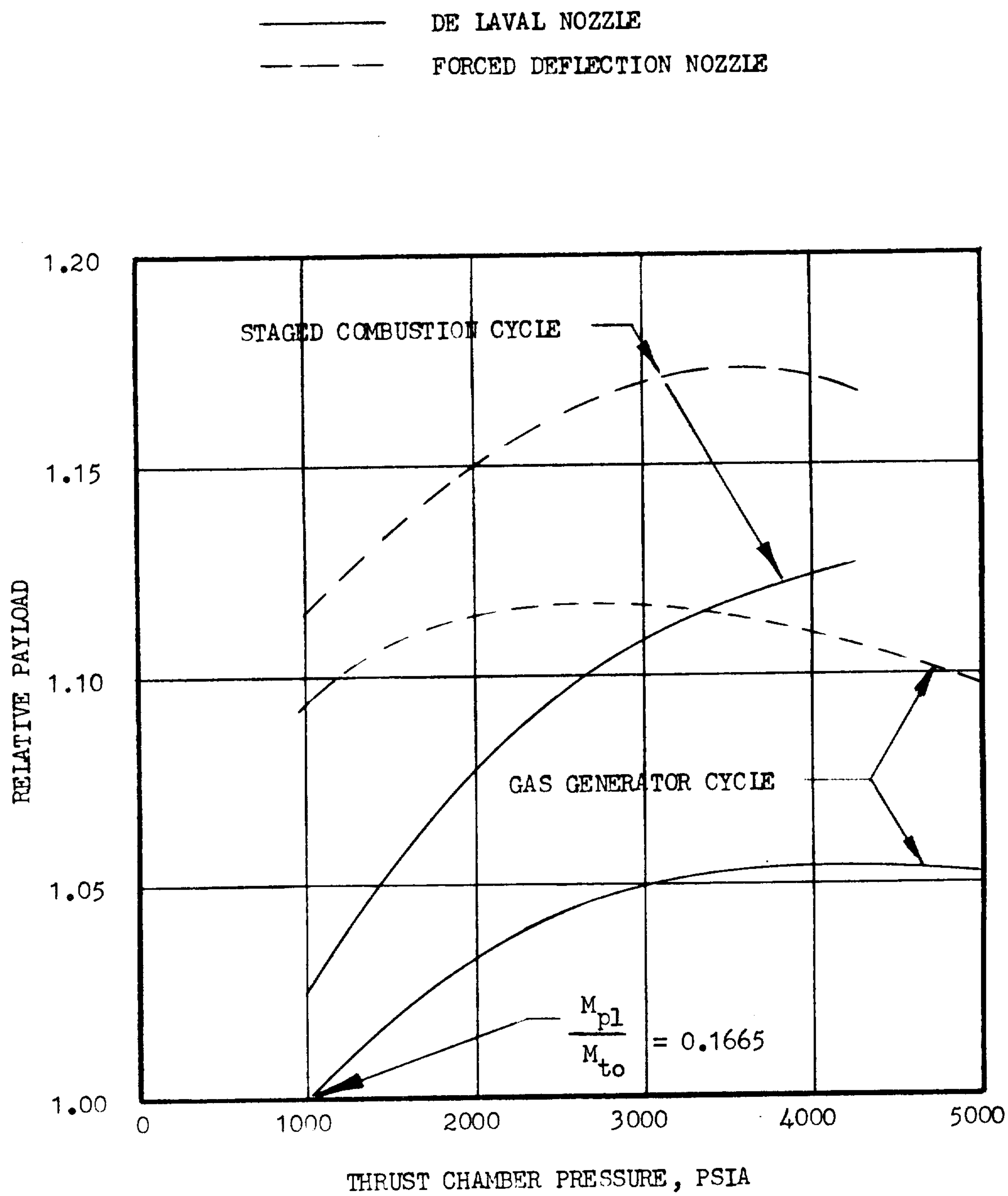

Figure III-29

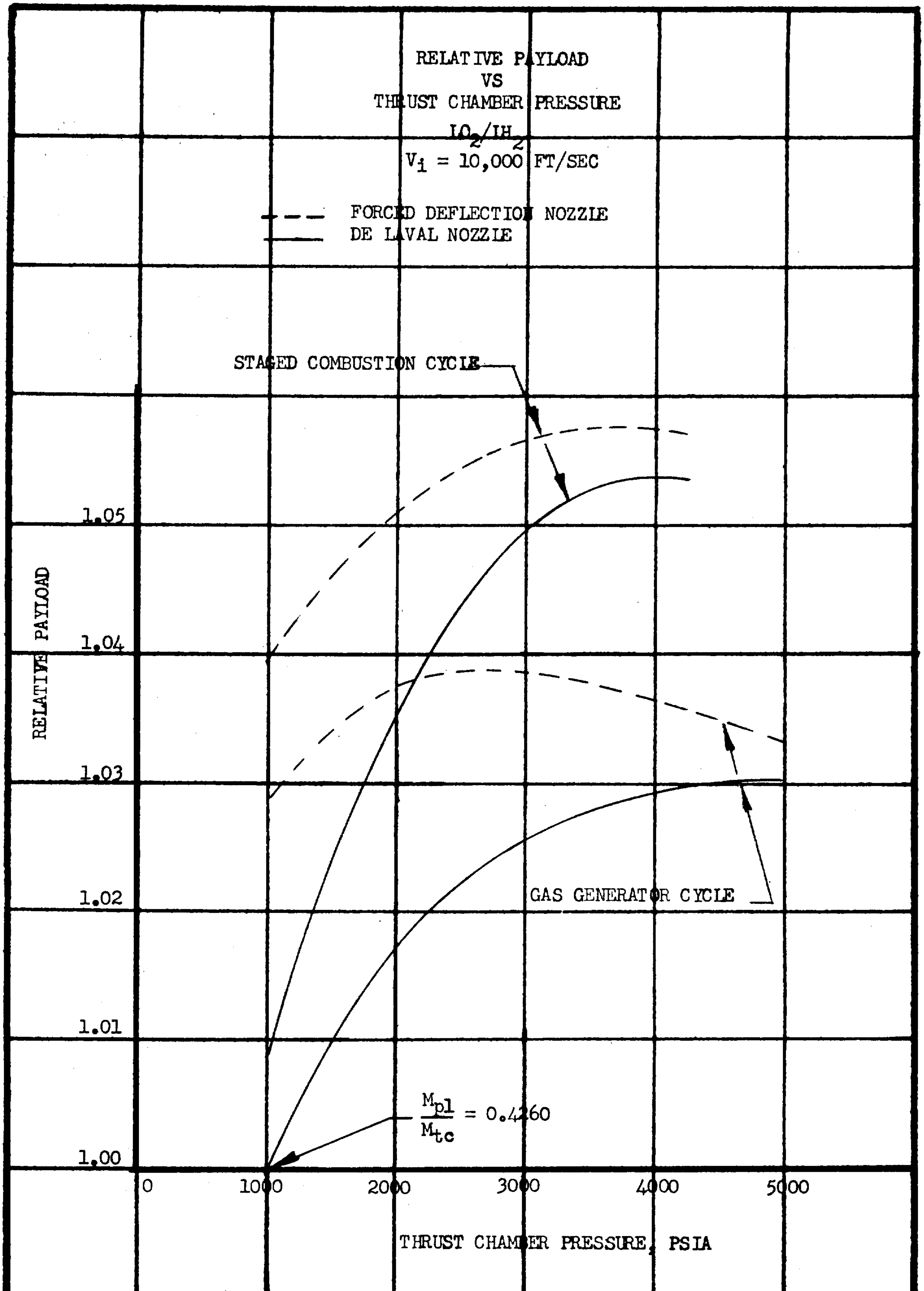

Figure III-30

RELATIVE PAYLOAD
vs
THRUST CHAMBER PRESSURE
LO_2/RP-1 VEHICLE
SINGLE STAGE TO 300 nm ORBIT

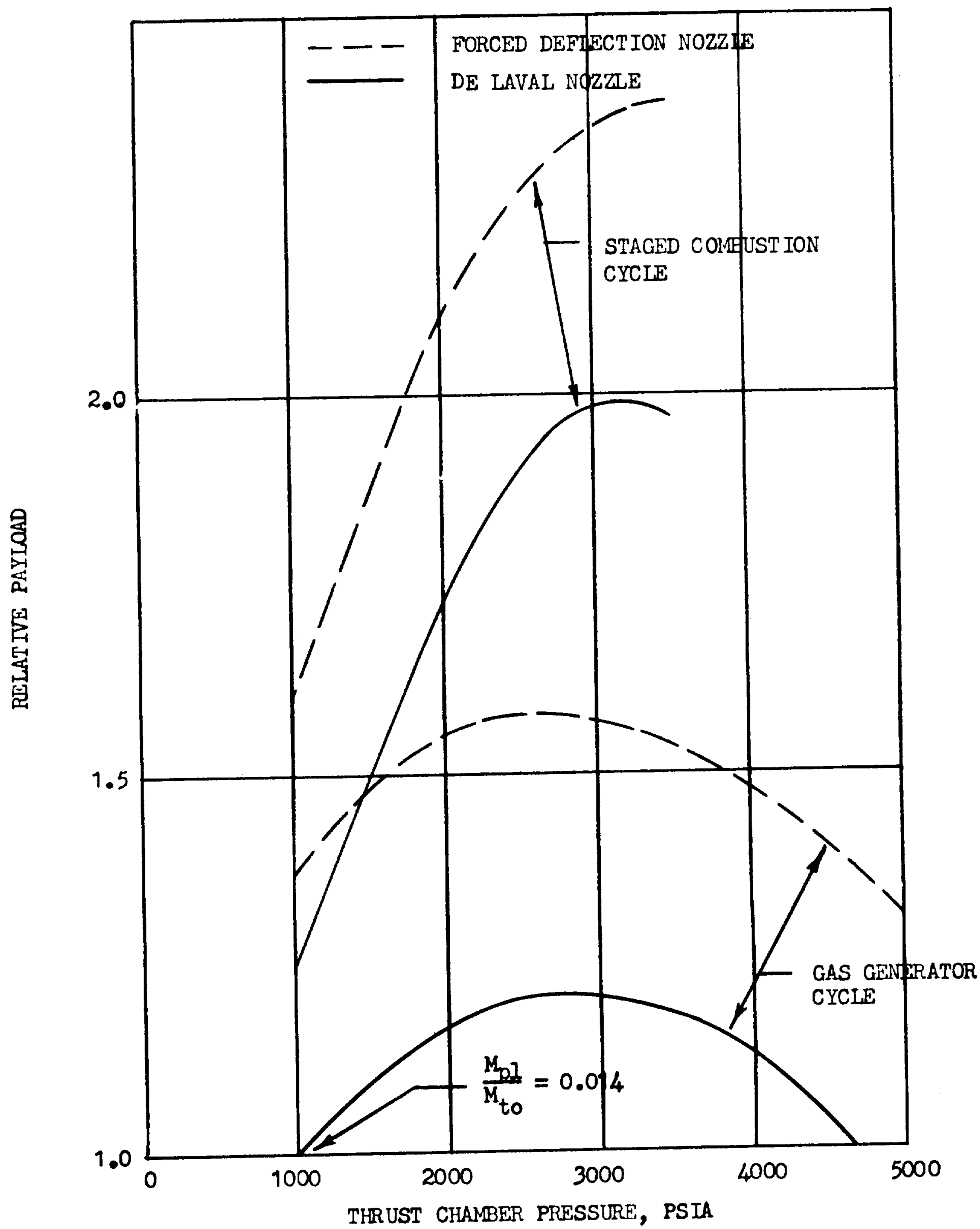

Figure III-31

RELATIVE PAYLOAD
VS
THRUST CHAMBER PRESSURE
LO_2/RP-1
FIRST STAGE VEHICLE
V_1 = 20,000 FT/SEC

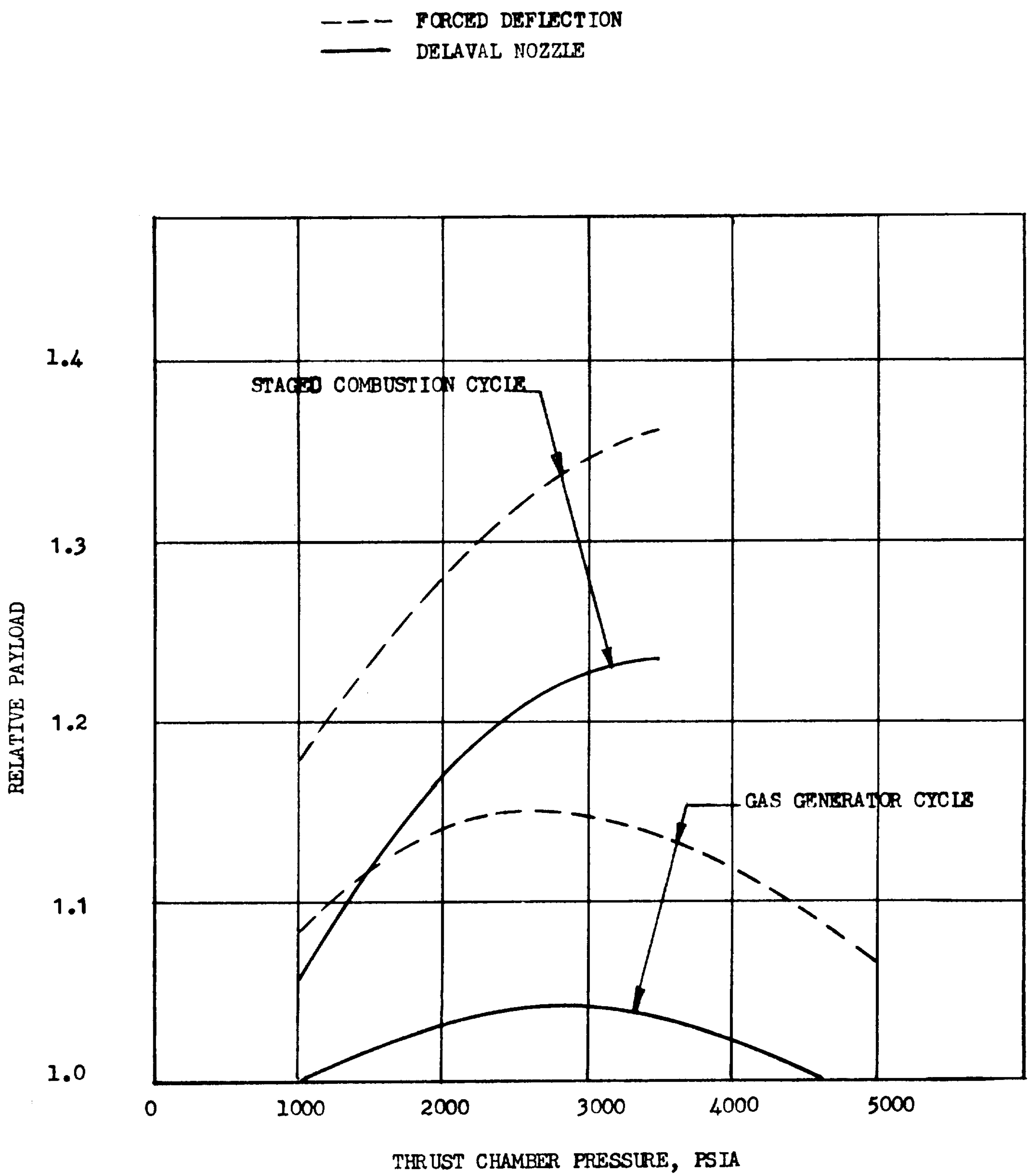

Figure III-32

RELATIVE PAYLOAD
vs
THRUST CHAMBER PRESSURE
LO_2/RP_1
FIRST STAGE VEHICLE
V_i = 10,000 ft/sec

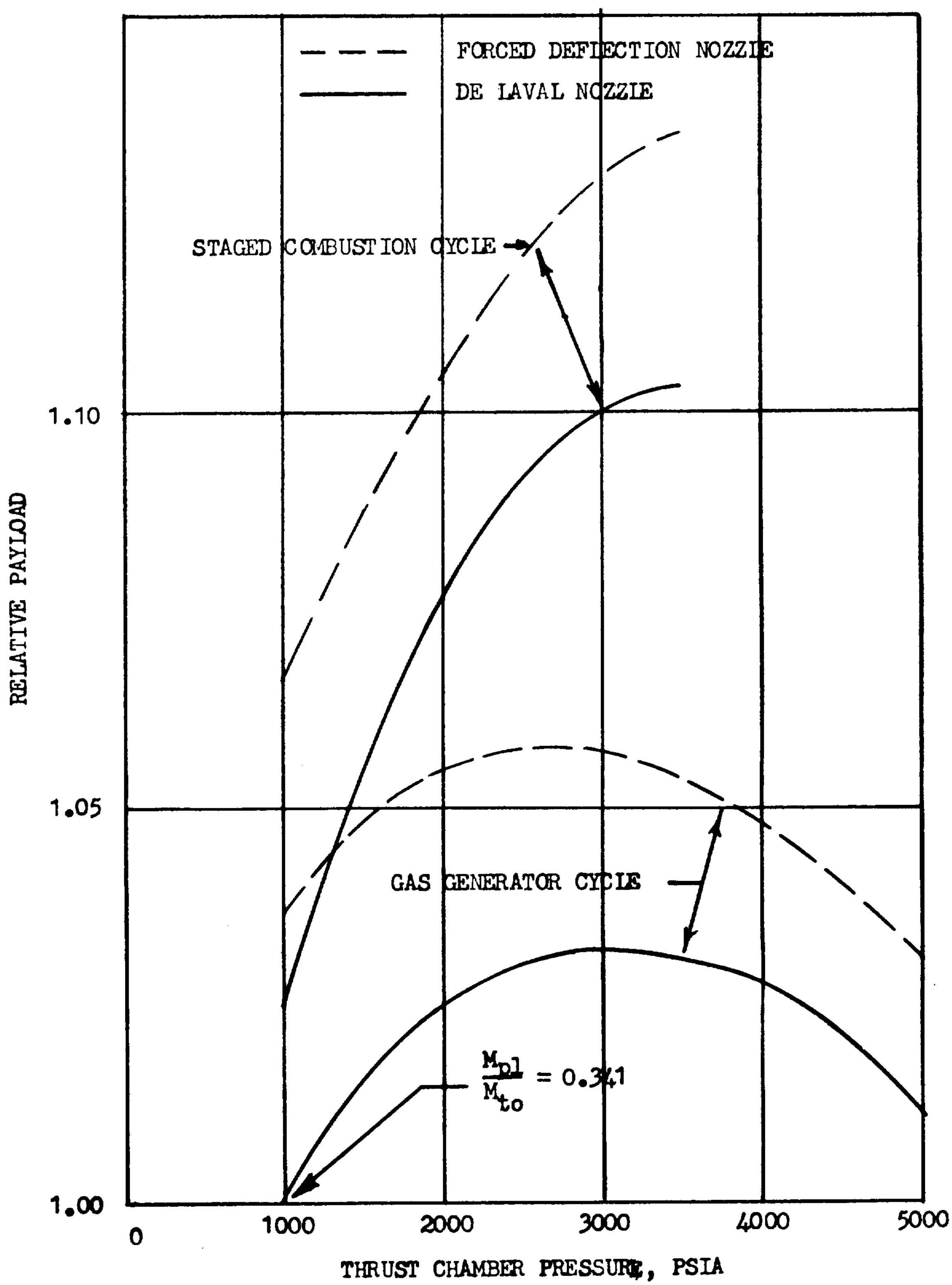

Figure III-33

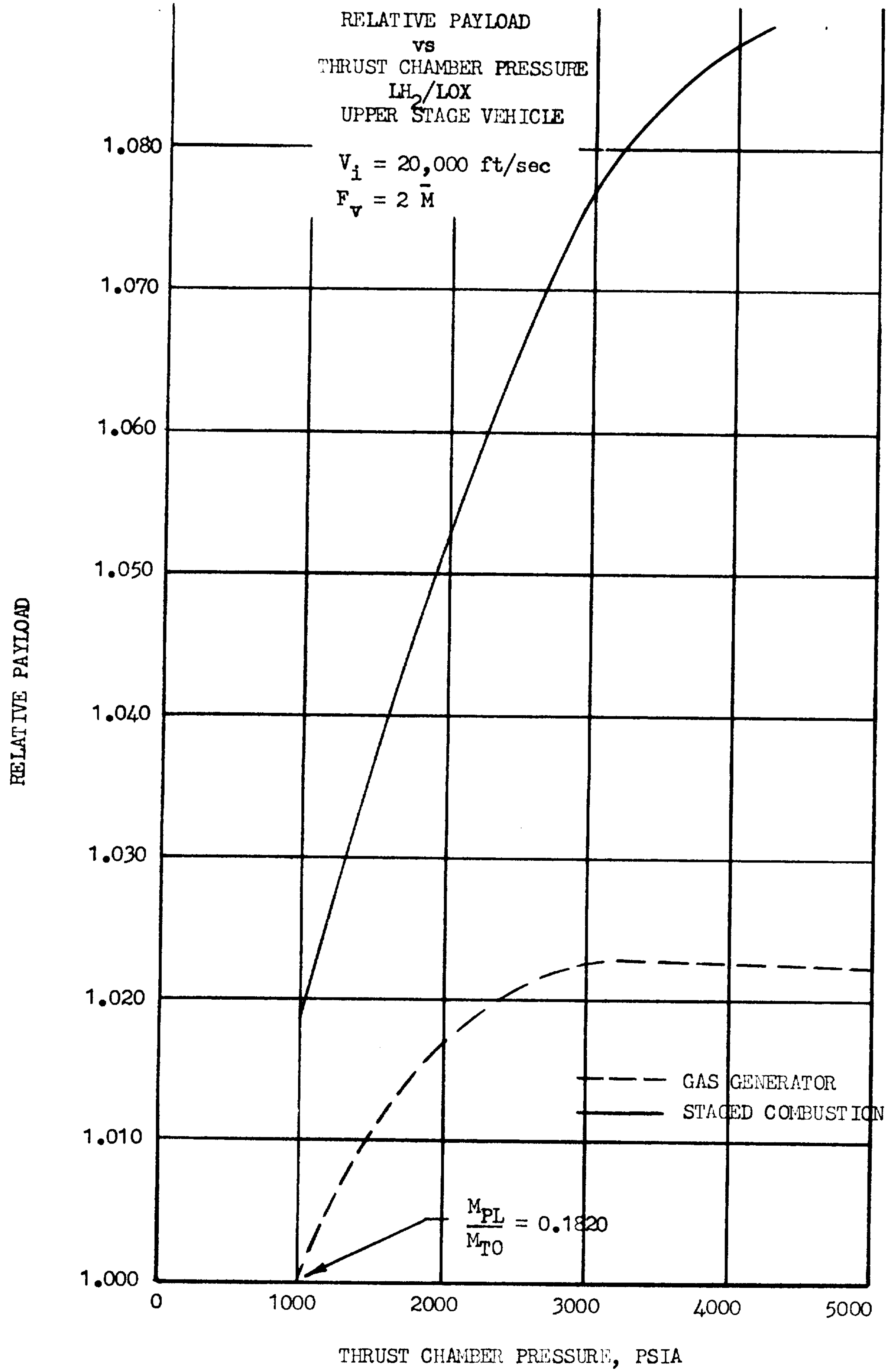

Figure III-34

RELATIVE PAYLOAD
vs
THRUST CHAMBER PRESSURE
LH_2/LOX
UPPER STAGE VEHICLE

$V_i = 15,000$ ft/sec
$F_v = 2\ \bar{M}$

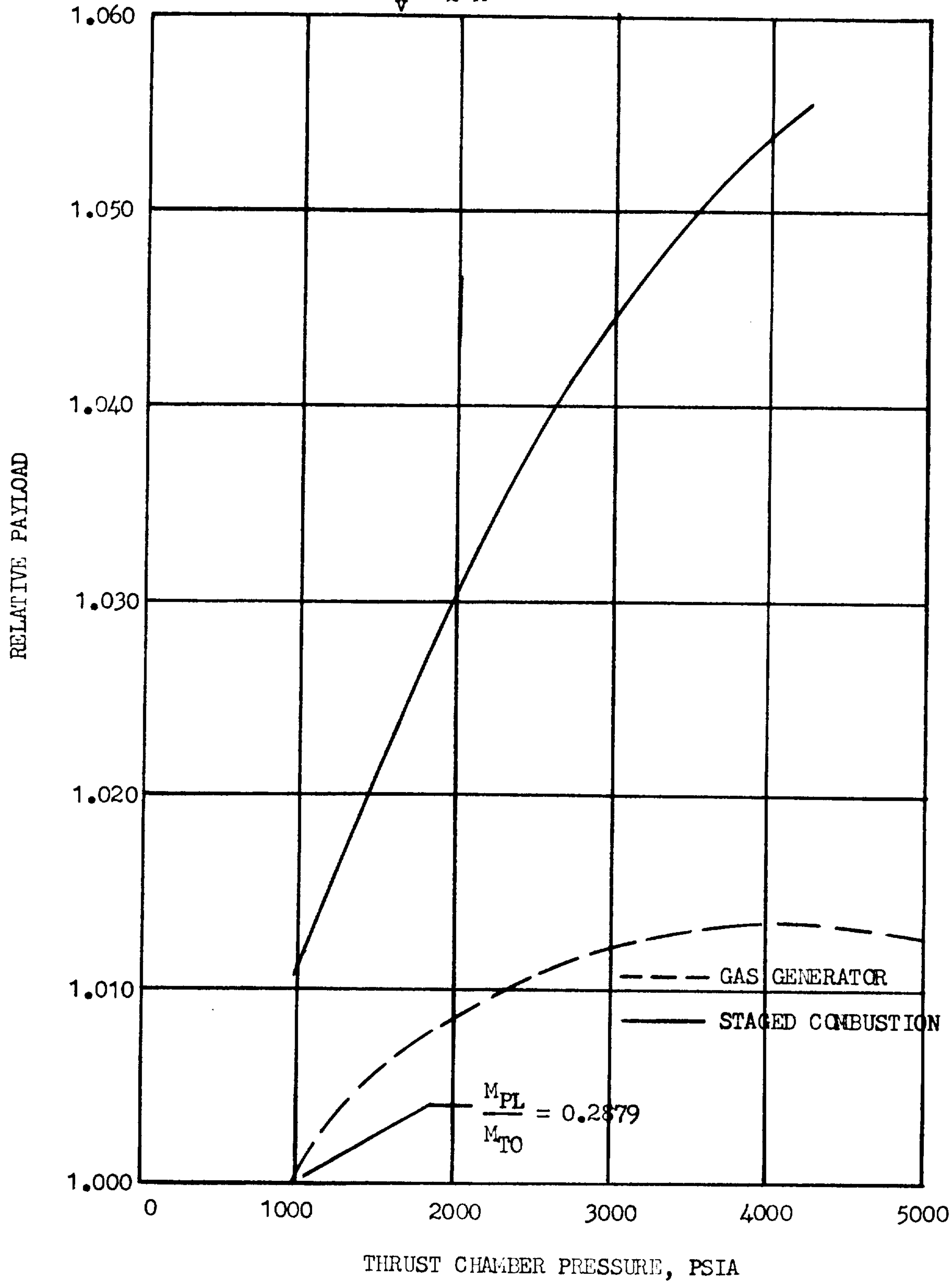

Figure III-35

RELATIVE PAYLOAD

vs

THRUST CHAMBER PRESSURE

LH_2/LOX

UPPER STAGE VEHICLE

$V_i = 10{,}000$ ft/sec

$F_v = 2\ \bar{M}$

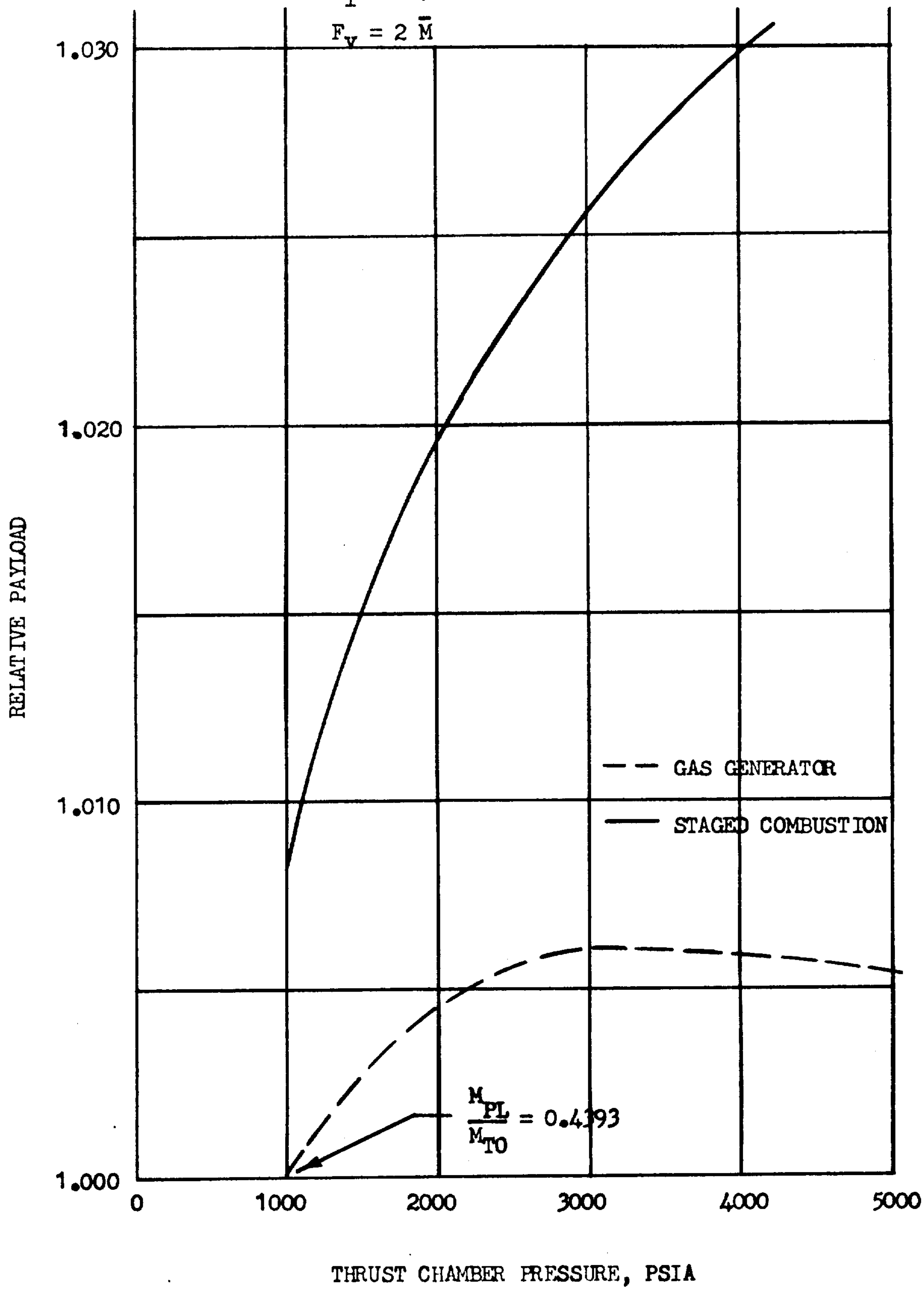

Figure III-36

THRUST CHAMBER PRESSURE VS INJECTION DENSITY

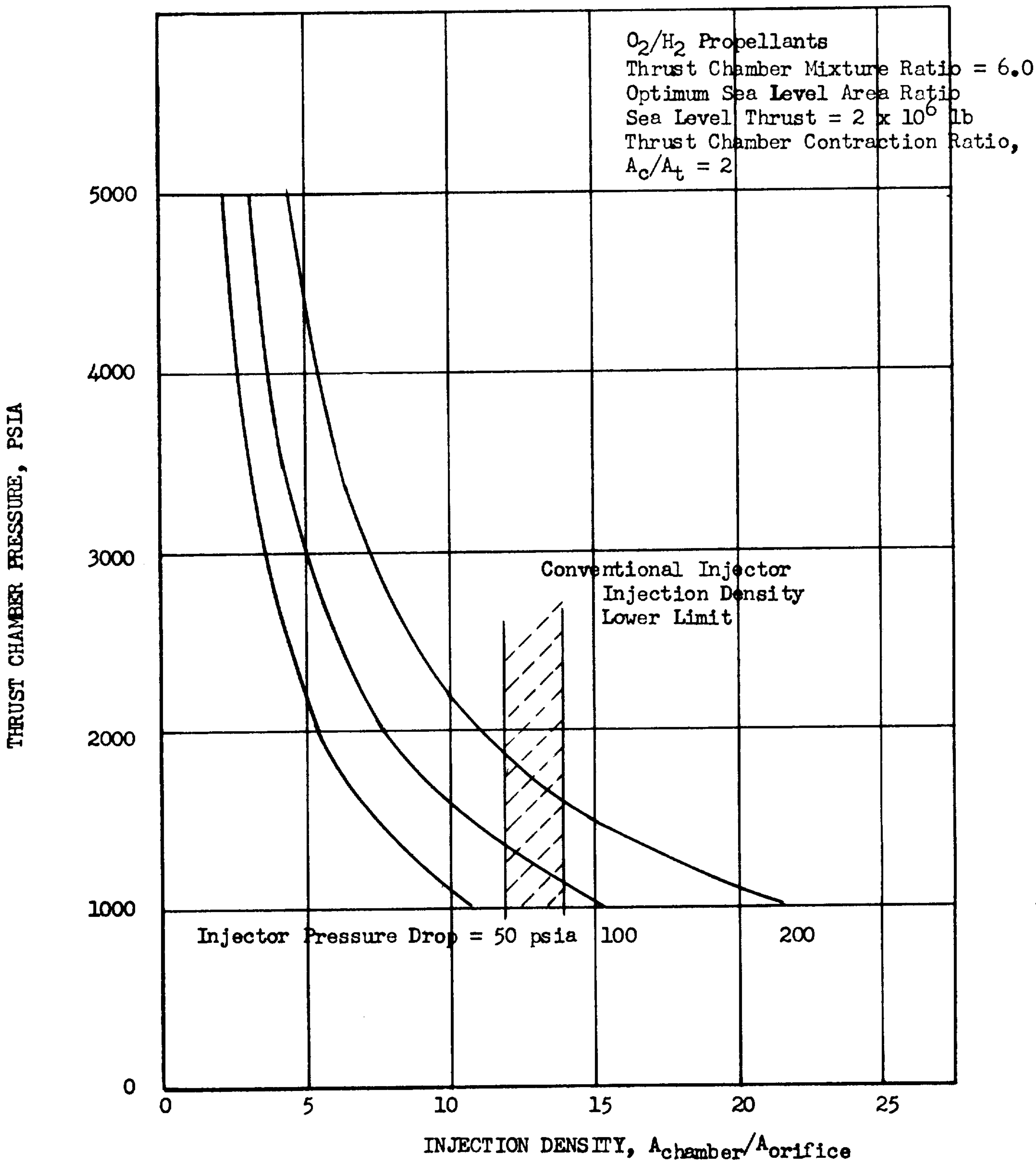

Figure III-37

THRUST CHAMBER PRESSURE VS INJECTION DENSITY

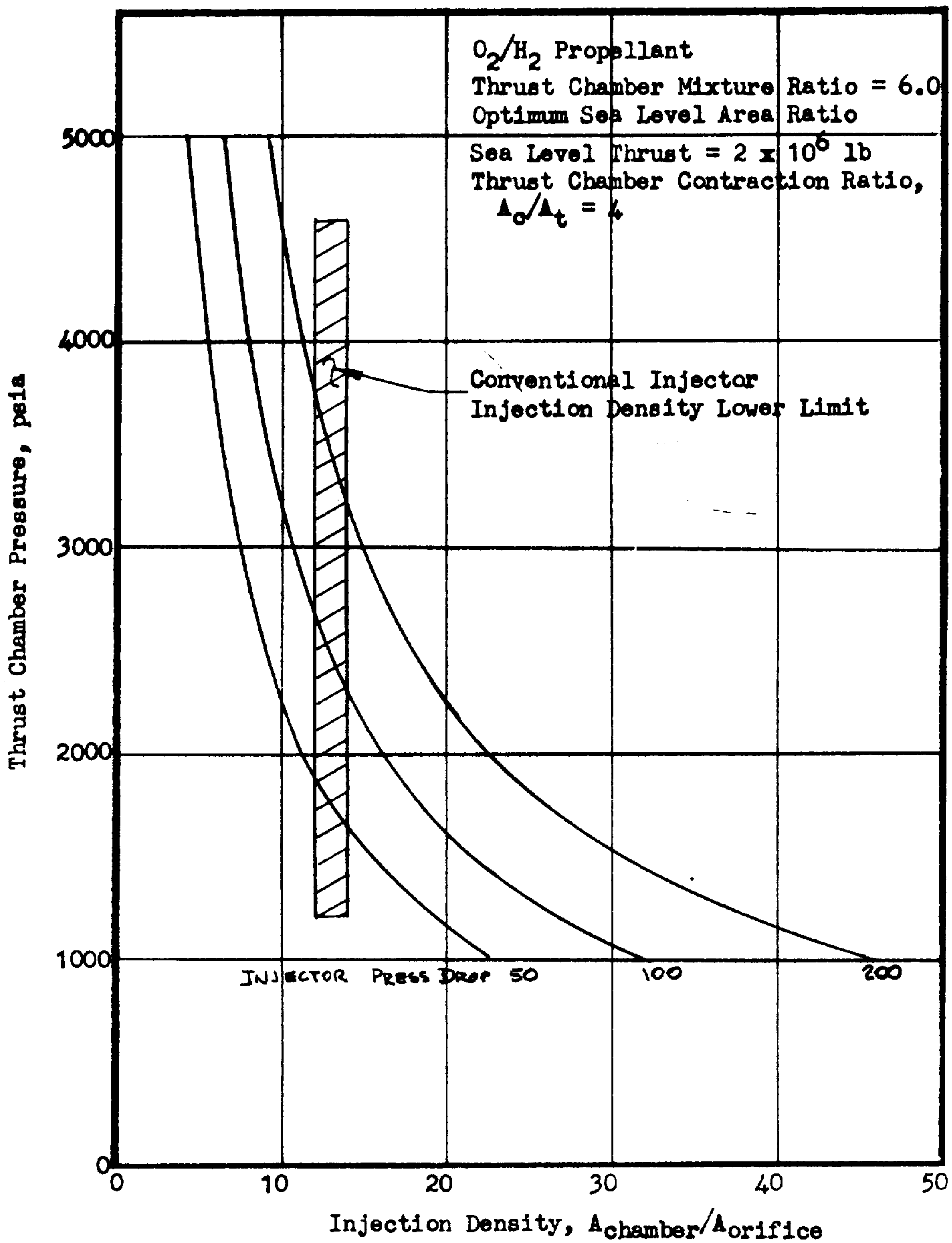

Figure III-38

THRUST CHAMBER PRESSURE VS INJECTION DENSITY

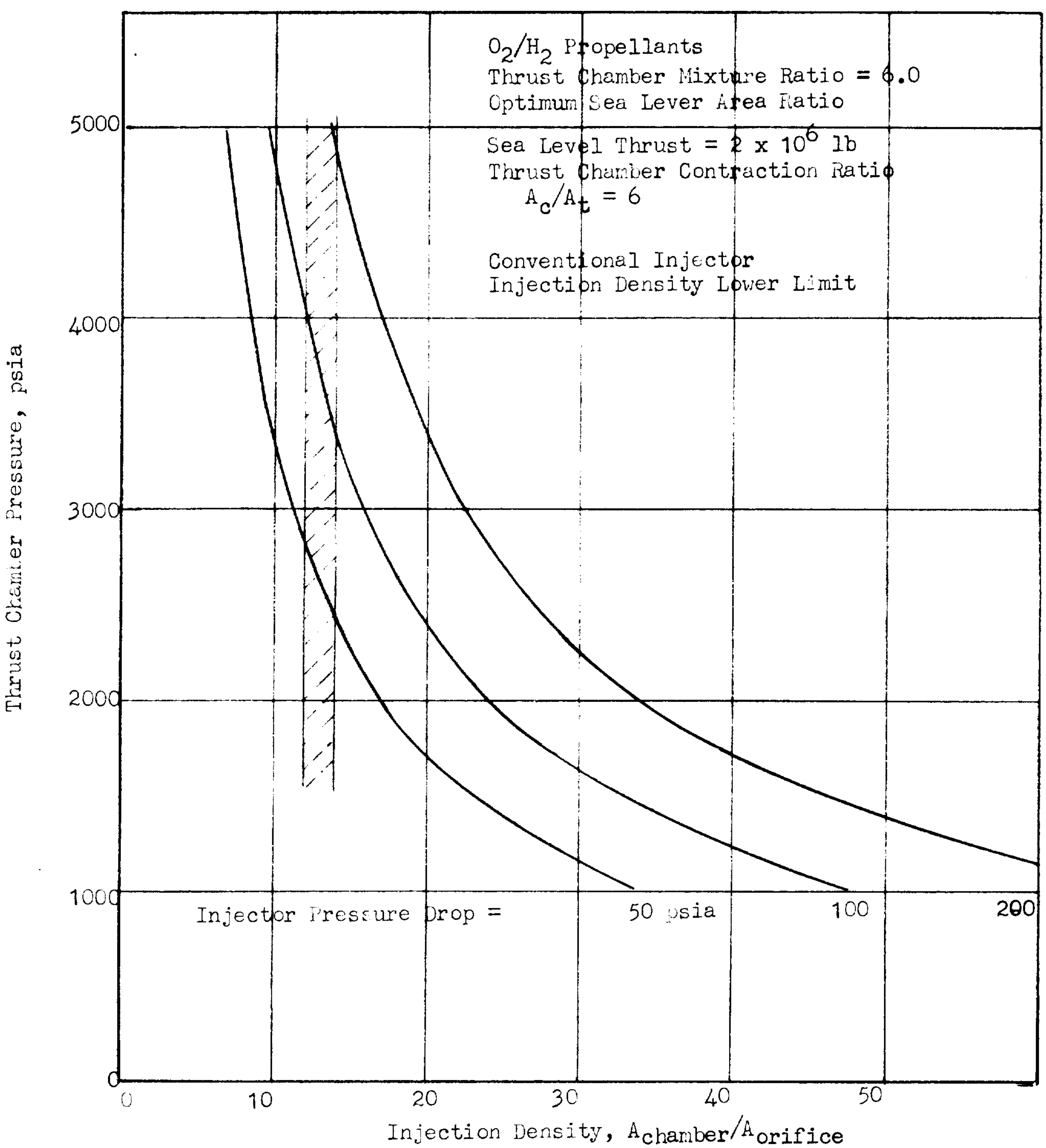

Figure III-39

THRUST CHAMBER PRESSURS VS INJECTION DENSITY

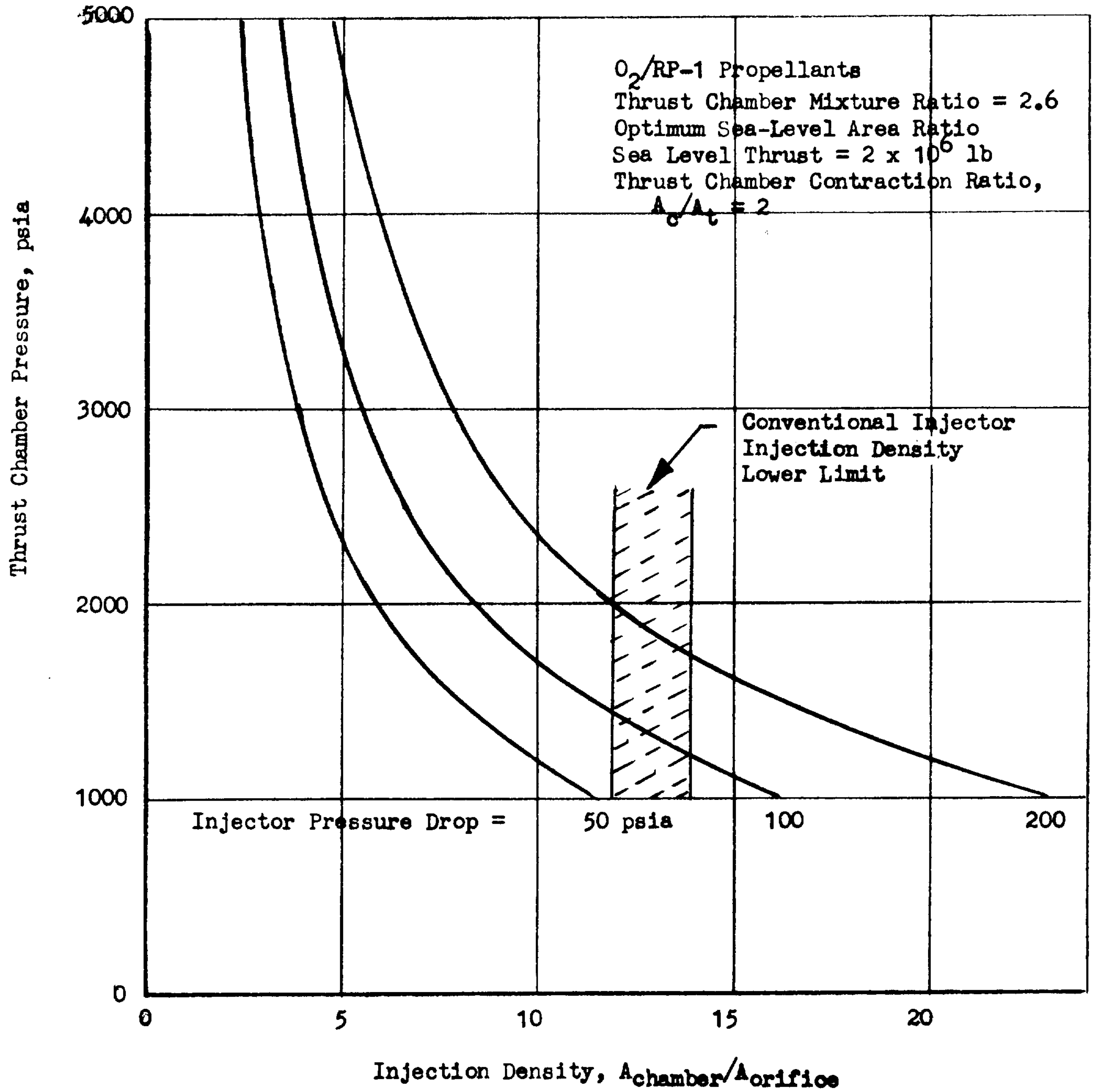

Figure III-40

THRUST CHAMBER PRESSURE VS INJECTION DENSITY

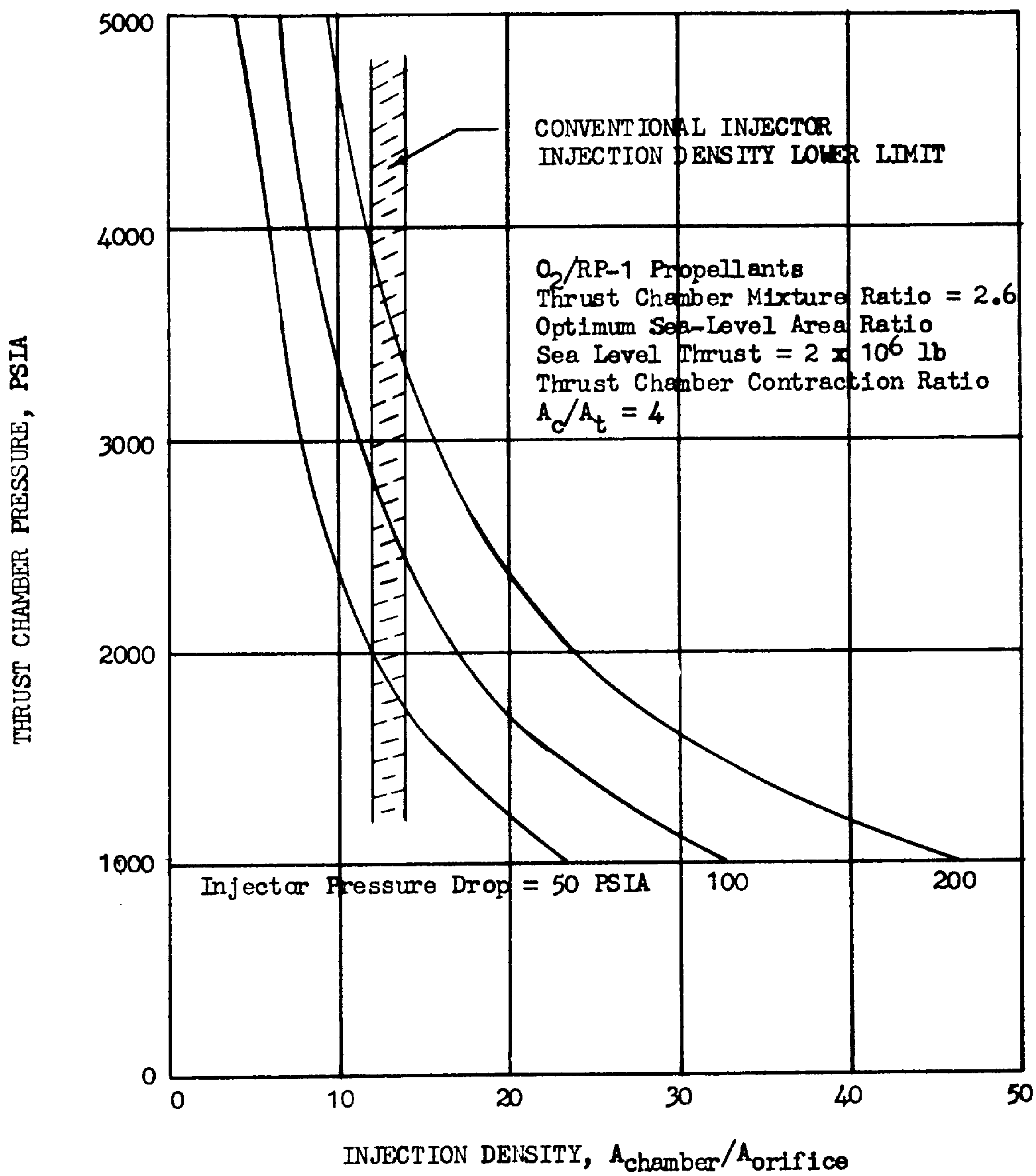

Figure III-41

THRUST CHAMBER PRESSURE VS INJECTION DENSITY

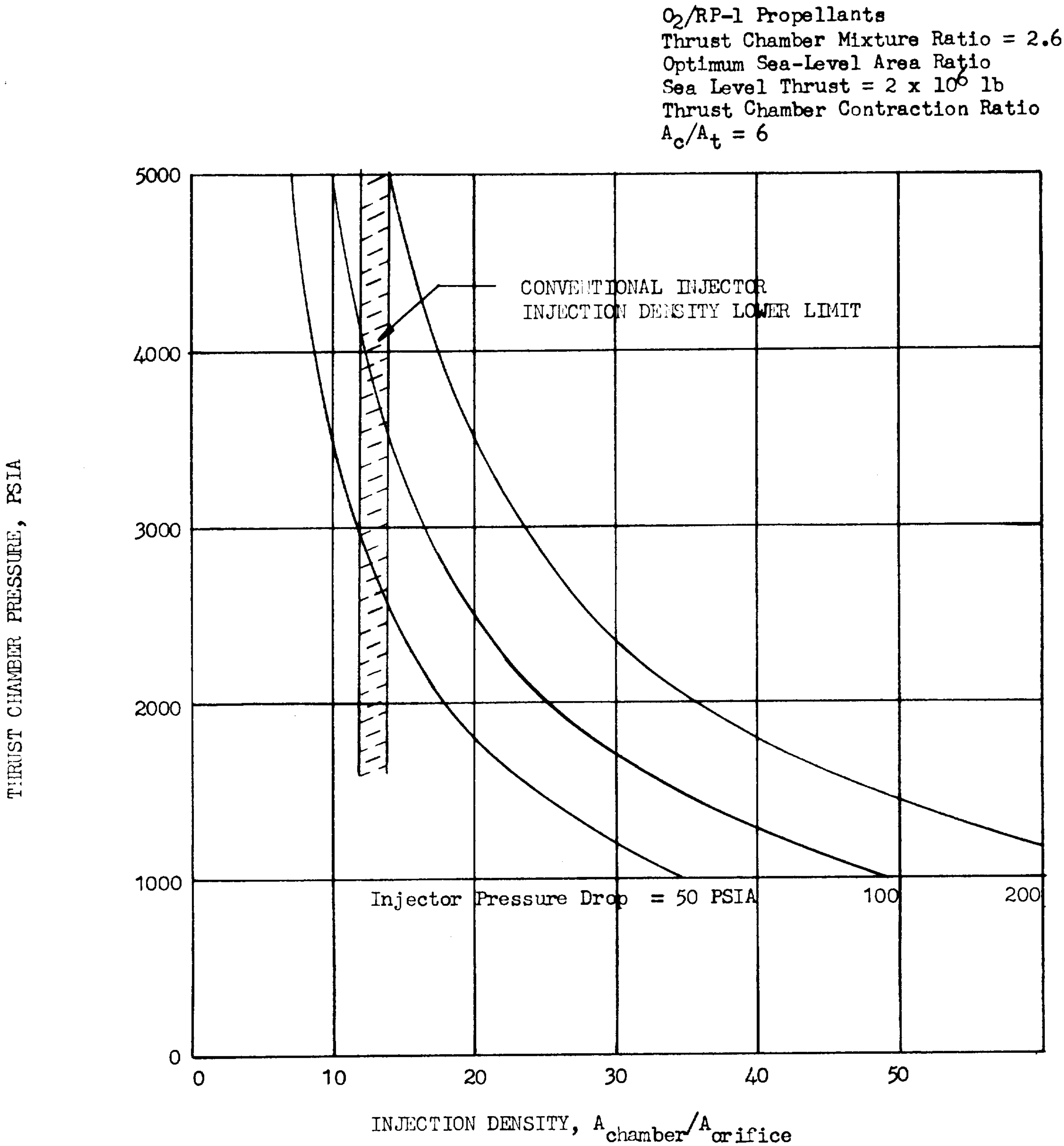

Figure III-42

IV. THERMODYNAMIC PERFORMANCE OF HIGH PRESSURE SYSTEMS

A. SUMMARY

The performance characteristics of LO_2/LH_2 and LO_2/RP-1 have been calculated for chamber pressures of 1000 psia, 3000 psia, 5000 psia, and 10,000 psia for both ideal and non-ideal gas theory. The non-ideal calculations consist essentially of a fugacity correction on the ideal (free energy) equilibrium coefficients. The results show that there is no significant difference between calculations performed using ideal gas laws and those performed using non-ideal gas laws.

B. INTRODUCTION

One criterion which may be used to compare the performance of propellant systems is specific impulse, since it is a measure of the thrust produced at unit propellant consumption rate. Thus high values of specific impulse are equivalent to a large total impulse produced by a given propellant weight. Especially at low pressure, it is well known that the methods of ideal gas thermodynamics may be used to obtain reliable estimates of specific impulse. It has not been equally clear that the method is applicable at very high pressures, where departures of real gas behavior would be most pronounced, due, for example, to the effects of compressibility.

In addition to a compressibility correction, the behavior of a mixture of real gases may be estimated by imposing on the free-energy equilibrium coefficients a correction factor based on the fugacity (a measure of chemical activity) of the individual gas species. Gas properties such as entropy and enthalpy are affected by the correction factor. An iterative program of computation is then used to obtain propellant system performance.

The computer program currently being used at Aerojet-General for propellant thermochemical calculations was modified to account for the effects of high chamber pressure conditions. The basic program (Reference 1) assumes the ideal gas equation of state. The modification of the program includes the effects of compressibility on the state properties. The P-V-T data were modified utilizing the compressibility factor. The thermodynamic functions and equilibrium relationships are modified according to the non-ideal equation of state. The general method of calculation and printout are the same as in Reference 1 .

C. TECHNICAL DISCUSSION

The methods for treating non-ideal gases are well known and the techniques vary, depending upon the equation of state used. The Aerojet-General thermochemical calculations program was modified by utilizing the correlations of References 2 and 3. This technique utilizes the compressibility factor:

$$Z = \frac{PV}{RT} \tag{1}$$

The equation of state

$$\rho = \frac{PM}{RT} \tag{2}$$

has been utilized in providing generalized correlations for the P-V-T data and the activity coefficients. The generalized correlations are based on the method of corresponding states.

The general thermochemical calculations program has been modified for non-ideal gas treatment only for propellants containing the

---

1. Crisman, P. A., Goldwasser, S.R., and Petrozzi, P. J., Proceedings of the Propellant Thermodynamics and Handling Conference, Special Report No. 12., Engineering Experiment Station, The Ohio State University, pp 293 - 313 (1959).
2. Hougen, O. A., Watson, K. M., and Ragatz, R. A., "Chemical Process Principles - Part II Thermodynamics", John Wiley & Sons, New York (1959).
3. Dodge, B. F., "Chemical Engineering Thermodynamics", McGraw-Hill, New York (1944).

chemical elements C, H, O, N, F, and Cl. Since the method of corresponding states requires the use of the critical constants for each gas species treated, these values were obtained. The generalized correlations each of thermodynamic relationships can be modified to account for the effects of non-ideality.

The equilibrium constant

$$K_f = \prod_i \chi_i^{\nu_i} f_i^{\nu_i} \tag{3}$$

and the activity coefficient for real gases

$$\gamma = f/p \tag{4}$$

can be defined as functions of the reduced conditions of the system (see below). The K_f defined at low pressures is the pressure equilibrium constant used in the ideal gas method of Reference 1. Thus, for some low-pressure (e.g. 1 atmosphere) thermodynamic standard-state defining a standard free-energy change:

$$F^o = - RT \ln K_f \tag{5}$$

In terms of the activity coefficient, a term which is not a function of composition can be defined

$$K_x = \prod_i \gamma^{\nu_i} \tag{6}$$

As K_f is a function of temperature only, a non-ideal gas constant, which is not a function of composition, can be defined

$$K_x = \frac{K_f}{K_\gamma} \cdot P^{\Sigma \nu_i} \tag{7}$$

The constant K_x can be calculated for each reaction having the standard free-energy change and the activity coefficients. With Equations (6) and (7), the real gas constant is evaluated as sub-routine and is "flagged" into the program when required. The use of K_x in the program is then the same as for the ideal gas case.

D. ACTIVITY COEFFICIENT

The activity coefficients, γ, are evaluated from the generalized plots in References 2 and 3. The reduced temperature $T_R = T/T_c$, and reduced pressure $P_R = P/P_c$, are evaluated at any temperature and pressure from the known values of the critical temperature and pressure for each of the gas species present.

E. THERMODYNAMIC FUNCTIONS

In the modified program, the ideal gas thermodynamic functions for each of the combustion product gases are obtained from the JANAF tables. These values are then modified for non-ideality by utilizing the generalized plots from References 2 and 3. The enthalpy correction is made on the ideal gas values from the JANAF tables

$$(H^o{}_T - H^o{}_{298.16})_i - \phi_i \, T_c \tag{8}$$

The heat of formation is not affected in the heat balance. The correction term ϕ is a function defined in References 2 and 3

$$\phi = \frac{H^* - H^o}{T_c} \tag{9}$$

The H^* is the real gas enthalpy.

By utilizing thermodynamic relationships, it is possible to avoid direct use of the entropy correction factors which are given in References 2 and 3. The entropy can be corrected by the correction factors already determined above. If entropy of the gas mixture at any temperature, T, is obtained by

$$S^o = \sum N_i \, S_{Ti} - N_g \, R \ln P - N_g \, R \sum X_i \ln X_i \tag{10}$$

then S^o is corrected by

$$S = S^o - \sum N_i \left[R \ln {}_i - \frac{\phi}{T_{Ri}} \right] \tag{11}$$

F. EQUATION OF STATE

The equation of state is Equation (2). The compressibility factor Z is obtained from the mixture from a generalized plot (Reference 2 and 3), and the density of the gas is determined from it. The pseudo-critical constants for a gas mixture can be obtained from the critical constants of the five components weighted by composition

$$T_c' = \sum_i X_i T_{ci} \tag{12}$$

and

$$P_c' = \sum_i X_i P_{ci} \tag{13}$$

The T_c and P_c are then used to determine the reduced conditions for the mixture.

G. CALCULATION PROCEDURE

1. Chamber

a. Assume a temperature.

b. Calculate T_R and P_R for each species i.

c. Obtain γ_i from tables at proper T_R and P_R.

d. Calculate K_f's in the same manner as the equilibrium constant was computed for ideal gas with no $\emptyset$ correction, since the thermodynamic standard-state is taken as one atmosphere; The k_f's are calculated for each reaction, which has been previously determined for the program.

e. Calculate K_γ from γ's, Equation (6) and (2).

f. Calculate K_x, Equation (7).

g. Have K_x's perform iteratim as outlined in Reference 1.

Obtain composition of combustion products (X_i's).

h. Obtain enthalph correction ϕ_i for each species.

i. Check enthalpy balance as per Reference 1, but correct enthalpy for non-ideality as Equation (9).

j. If enthalpy balance does not check, change temperature and repeat as in non-ideal cases.

k. When the enthalpy balance checks, calculate the entropy for that composition, Equation (10).

l. Correct entropy for non-ideality, Equation (11).

m. Obtain T_c, and P_c, and the pseudo-reduced conditions.

n. Obtain compressibility factor for mixture.

o. Calculate density, Equation (2).

2. <u>Any Expansion Point</u>

a. Select pressure.

b. Assume temperature.

c. Calculate T_R, P_R, K_f, γ_i, K_γ, and x_i's as before.

d. Calculate ϕ_i, S^o, and S, as before.

e. Compare S to entropy of chamber. Change temperature until the entropy is the same as that in chamber.

f. Calculate Z and density, Equation (2).

g. Obtain corrected local enthalpy from Reference 1 and Equation (9).

h. Calculate local gas velocity from difference of corrected enthalpies as in Reference 1.

i. Maximize the product (ρV) as in Reference 1 to obtain C*; the other performance parameters are treated in the same manner as in Reference 1.

H. NOMENCLATURE

C^*	Characterisic velocity
f	Fugacity of a component
F^o	Standard free-energy change for a reaction
H^o	Ideal enthalpy
H^*	Real gas enthalpy
$H^o{}_T - H^o{}_{298.16}$	Ideal gas enthalpy function from tables
K_f	Equilibrium constant for real gases forming an ideal solution
K_x	Non-ideal gas equilibrium constant, not a function of composition
K_γ	Activity equilibrium constant
M	Molecular weight of combustion product mixture
N_g	Moles of combustion product species, gaseous only
N_i	Moles of any combustion product species
P	Pressure of system
P_c	Critical pressure of any species
P_R	Reduced pressure of a species
P_c'	Psudocritical pressure for a mixture
R	Universal gas constant
S	Non-ideal entropy of combustion product mixture
S^o	Ideal standard-state entropy for mixture
$S^o{}_T$	Ideal standard-state entropy at same temperature T
T	Temperature
T_c	Critical temperature of a component
T_R	Reduced temperature of a component
T_c'	Pseudocritical temperature of a mixture

V	Molar volume
v	Cas stream velocity in a nozzle
X	Mole fraction of a component in mixture
Z	Compressibility factor

GREEK LETTERS

π	Product sign
ν	Stoichiometric coefficients in a given reaction, positive for products and negative for reactants
ρ	Density
γ	Activity (or fugacity) coefficient
ϕ	Enthalpy correction function

SUBSCRIPTS

i	Any combustion product species
g	Gaseous combustion product species

I. COMPUTED PERFORMANCE RESULTS

For the LO_2/LH_2 and LO_2/RP-1 propellant combinations, calculations made using ideal gas laws showed no significant difference from those made using non-ideal gas laws in the pressure range up to 5000 psia. Results are shown in Table I.

TABLE I

SEA LEVEL SPECIFIC IMPULSE, lb_f - sec/lb_m

LO_2 - LH_2

	M/R	2	4	6	8	10
P_c, psia	I_{sp}, ideal	373.8	391.0	383.3	361.9	336.7
1000	I_{sp}, non-ideal	374.4	391.3	383.4	462.0	336.7
3000		396.8	419.3	415.8	398.2	268.6
		397.2	419.5	415.9	398.3	368.7
5000		405.0	429.7	428.0	412.5	380.9
		405.0	429.9	428.1	412.6	381.0

LO_2 - RP-1

		1.8	2.2	2.6	3.0	3.4
1000		281.2	296.1	300.5	297.1	291.3
		281.4	396.2	300.6	297.1	291.3
3000		301.5	319.7	328.0	327.8	322.1
		302.0	320.0	328.3	328.1	322.5
5000		309.3	328.6	338.4	340.1	334.7
		309.8	329.0	338.9	340.6	335.3

Apparent differences between the ideal gas results and the non-ideal gas results are somewhat larger for the LO_2/RP-1 system than for the LO_2/LH_2 system. The effect may be due to the additional gas species produced by the former. For both systems, the differences tend to be slightly larger at high pressures. Further comparative calculations were therefore made to investigate more thoroughly the effects of additional gas species and high pressures.

To study the effect of gas species, calculations were performed for the propellant system N_2O_4/Aerozine -50 (50% N_2H_4 + 50% UDMH, by weight). The assumed chamber pressure was 5,000 psia. Plots of C* vs mixture ratio, and I_{sp} vs mixture ratio are shown in Figure IV-1 and IV-2 respectively. Depending on the mixture ratio region, and thus the exhaust gas composition (and the corresponding reduced conditions), the difference in characteristic velocity amounts to about 1%. The effect on specific impulse, for a given pressure ratio, is also about 1%. However, this is primarily due to the density discrepancy and its effect on the continuity equation. For a given area ratio, the variation in specific impulse will be quite small, since the thermodynamic effects seem to cancel each other.

To study the effect of increased chamber pressure, calculations were made for LO_2/LH_2 and LO_2/RP-1 at 10,000 psia. The results are shown in Table II, where such small trends as do appear are generally consistent with the trends indicated at low chamber pressures.

TABLE II

THERMODYNAMIC PERFORMANCE, P_c = 10,000 psia

		LO_2/LH_2			LO_2/RP-1		
M/R		2	6	10	1.8	2.6	3.4
C*	Ideal	7814	7720	6720	5862	6041	5831
	Non-Ideal	7823	7753	6793	5889	6153	5923
I_{sp},sl	Ideal	414.28	442.13	395.18	318.89	350.66	350.52
	Non-Ideal	414.40	442.22	395.18	319.51	351.17	351.23
I_{sp},A/A* = 1000	Ideal	-	495.13	447.89	362.37	397.04	408.20
	Non-Ideal	-	495.18	447.96	362.97	397.44	408.71

It is observed that in rounding-off to the nearest unit value in specific impulse, for example, almost all values reported are identical. Thus, it is not likely that smaller differences could be experimentally verified, except possibly by statistical means. Average random errors in thrust measurement and total propellant flow rate measurement of 1% each would result in an error of about 1.4% in the determination of specific impulse.

J. CONCLUSIONS

In general, small differences in thermodynamic performance have been shown to exist, depending on whether ideal gas criteria or non-ideal gas criteria are the basis of calculation. Relatively larger differences occur when,

1. Additional gas species occur;
2. higher chamber pressures prevail.

Since the chemical combustion products may vary widely in type and composition, depending on the propellants used and the mixture ratio range, there is no definite criterion available which will indicate at which pressure the non-ideal gas effects become important. For any given propellant system, the non-ideal gas effects should be checked at chamber pressures above 2,000 psia.

For LO_2/LH_2 and LO_2/RP-1, ideal gas laws are adequate to at least 5000 psia. Specific impulse for these two propellant system combinations is shown in Figures IV-3 and IV-4.

CHARACTERISTIC VELOCITY

VS

MIXTURE RATIO

N_2O_4 /AEROZINE − 50

P_C = 5000

IDEAL GAS & NON-IDEAL GAS

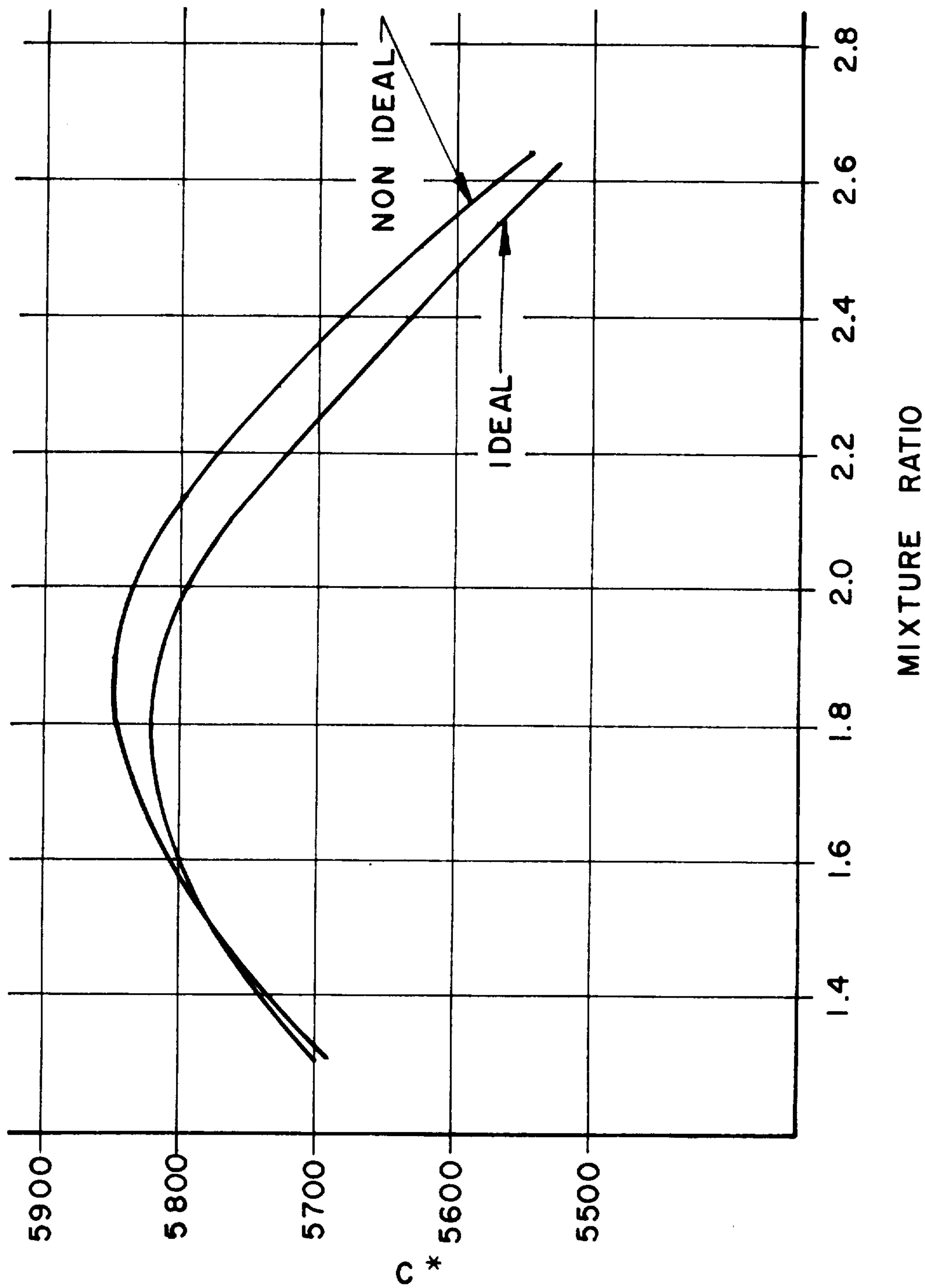

Figure IV-1

SPECIFIC IMPULSE
VS
MIXTURE RATIO
N_2O_4/AEROZINE-50
IDEAL GAS & NON-IDEAL GAS

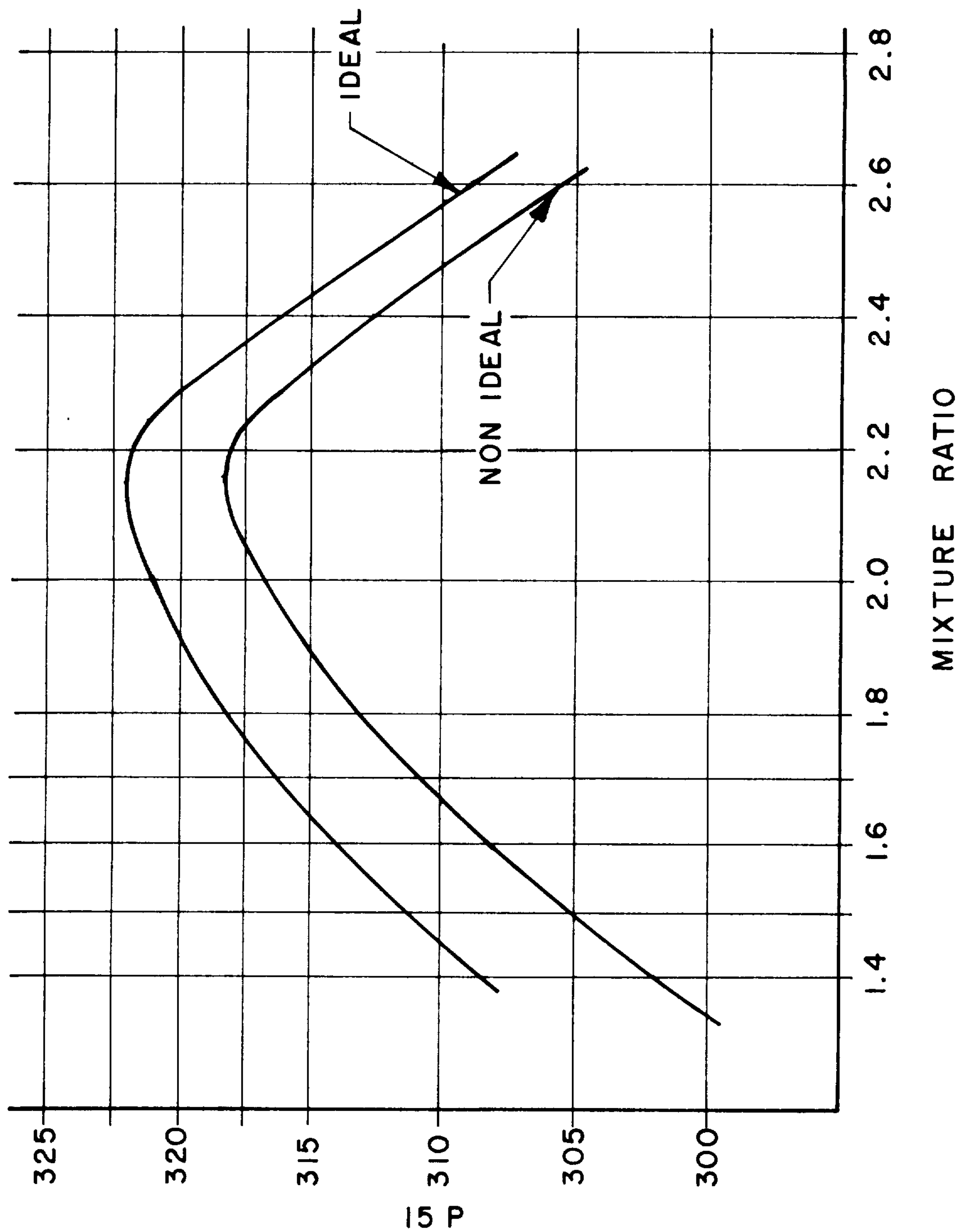

Figure IV-2

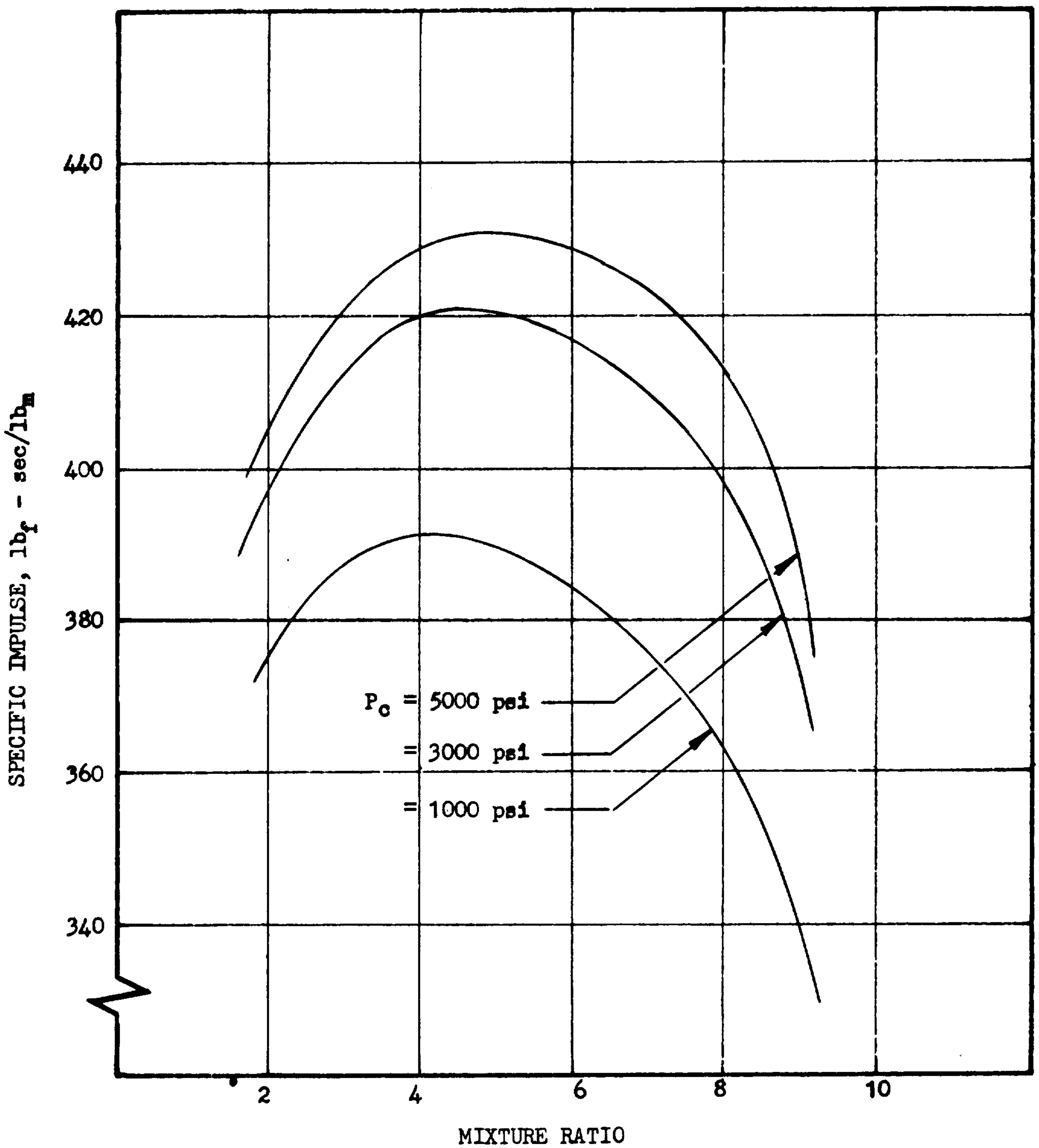

SEA LEVEL PERFORMANCE OF LO_2/LH_2

Figure IV-3

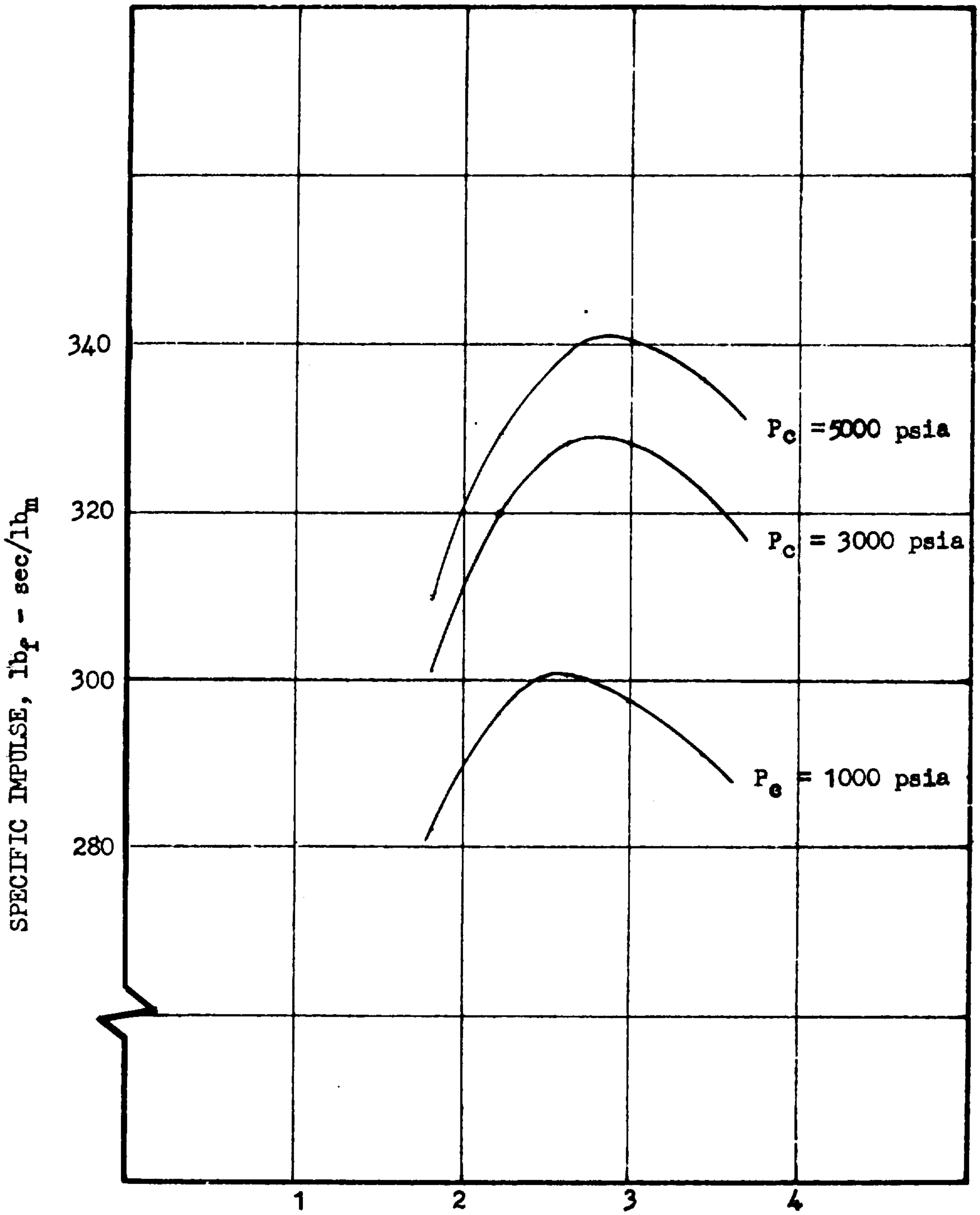

MIXTURE RATIO

SEA LEVEL PERFORMANCE OF LO_2/RP-1

Figure IV-4

V. COMBUSTION STABILITY BEHAVIOR

A. PRELIMINARY INVESTIGATIONS

1. Comparison of Approaches

In order to determine the best method of correlating the results of the experimental program, the current approaches to the problem of combustion instability in liquid propellant rocket engines were compared and evaluated. The activities of the various agencies and institutions conducting investigations of this problem were surveyed and classified into the following three groups:

a. Primarily Theoretical

Lewis Research Center, NASA

Advanced Research Division, Aerojet-General Corporation

Massachusetts Institute of Technology

Armour Research Foundation

b. Primarily Experimental

Purdue University (gas rocket)

Space Propulsion Division, Aerojet-General Corporation

Edwards Air Force Base

Marshall Space Flight Center, NASA

c. Combined Theoretical and Experimental

Rocketdyne Division, North American Aviation, Inc.

Princeton University

Polytechnic Institute of Brooklyn

The first group includes those agencies which are not known to be carrying out any experimental work at all (MIT, ARF) and also those whose experimental efforts are designed to obtain information concerning the basic combustion processes, and are not intended as direct verification of theoretical predictions. In the second group are the investigators who have not as yet attempted to formulate a quantitative theoretical description. Finally, the third category includes the group whose experimental efforts are intended to serve as verification of theoretical predictions as well as for exploration of the unstable combustion processes.

An examination of the published theoretical studies of high frequency combustion instability shows three main lines of approach:

a. The Sensitive Time Lag Theory of Crocco and his coworkers at Princeton University;

b. The Mechanistic Theories developed by Morrell, Priem, and Guentert at NASA - Lewis Research Center and by Torda, et al, at Brooklyn, and

c. The Available Energy Concept of Ellis, Pickford, and Peoples at the Aerojet-General Corporation.

The theoretical work of Culick (MIT) makes some use of the available energy concept, although there are significant differences in approach. A bibliography of the most important publications pertaining to each approach is included in Section D.

The theoretical approach taken by the Princeton workers is that of the classical, linear, small perturbation stability theory. That is, each of the quantities describing the flow in the combustion chamber is assumed to oscillate about its steady state value. For certain unstable operating conditions, the oscillation amplitudes will increase with time, even for arbitarily small initial amplitudes. Theoretical conditions can be established for the existence of neutral oscillations, the amplitudes of which neither increase or decrease with time. The assemblage of operating points of the thrust chamber which satisfy the conditions for neutral stability forms the "stability limits" which divide the unstable from the stable regions of operation. The complete stability behavior of the rocket engine is thus described by specifying the stability limits and indicating the unstable regions.

The unique feature of the Princeton theory is the use of the sensitive time lag concept. The idea of a combustion time lag as a coordinating influence to excite organized oscillations in a liquid propellant rocket combustion chamber originated in von Karman's group at the Jet Propulsion Laboratory in 1941. Several analyses were made of low frequency instability (which depends upon the interaction between the feed system and combustion process) based on a constant time lag. In order to explain high frequency modes of instability, Crocco introduced the time varying, or sensitive, combustion time lag.

In the time lag concept, the gradual evolution of combustion products from each portion of propellant mixture traveling through the combustion chamber after injection is approximated by a discontinuous conversion from reactants to products after a certain time, the total time lag, has elasped. If the combustion chamber conditions fluctuate, the time lag also must vary. In order to simplify the description of the effect of the chamber conditions on the time lag, the total time lag is taken as the sum of a "sensitive" part (τ) and an "insensitive" part. The various physical conditions are assumed to affect the combustion process rates only during the sensitive portion of the total time lag. The magnitude of the response of the combustion process rate to changes in thermodynamic state is expressed by a "pressure interaction index" (η). Similarly, the effects of transport phenomena are measured by a velocity index (ℓ, which is vectorial).

The synthetic representation of the combustion process by means of the time lag concept eliminates the need for information on any of the specific processes occurring in the chamber, such as atomization, vaporization, mixing, chemical kinetics, etc. This fact constitutes the primary advantage of the time lag type of analysis, since very little quantitative information is available concerning the details of the various unsteady combustion processes.

For analytical simplicity, the Princeton theory assumes that the steady state flow is one dimensional, with particle velocities small compared to the sonic velocity, and that the flow is inviscid within a rigid, adiabatic thrust chamber. Solutions of the conservation equations have been obtained in closed form as first order corrections to the acoustic wave patterns.

The application of the sensitive time lag theory to the longitudinal modes was first made by Crocco in 1951. The expanded and generalized theory of longitudinal mode combustion instability was published, but without experimental verification, in 1956 by Crocco and Cheng. Subsequently, the validity of the theory was shown in a series of experiments reported by Crocco, Gray, and Harrje. In the latter paper a simple means for measuring the combustion parameters η and τ through stability limit tests was presented. The first application of the sensitive time lag concept to transverse modes was made by Scala, who considered only thermodynamic effects. The importance of velocity (or hydrodynamic) effects in transverse modes was shown by Reardon, who was able also to present some experimental verification. Recently, the crucial connection between longitudinal and transverse modes was established experimentally at Princeton.

The workers at the Lewis Research Laboratory of the National Aeronautics and Space Administration have approached the problem of combustion instability from a more mechanistic viewpoint. That is, their theoretical formulations include rate expressions for assumed rate controlling processes. They have also included nonlinear effects associated with both the combustion processes and with the fluid mechanical flow processes. Associated theoretical and experimental studies of vaporization and mixing under steady and unsteady conditions are also carried out by this group.

A similitude study of the general conservation equations by Priem and Morrell disclosed two major similarity parameters. One parameter, a measure of viscous dissipation, is a Reynolds number based on the average acoustic velocity in the combustor. The second parameter is a measure of the heat release rate. Values of these parameters were calculated for a series of hydrocarbon-liquid oxygen rocket engines, using two assumptions as to the rate controlling process: one was steady state spray vaporization, the other was drop or jet shattering by a shock wave. With both rate expressions they obtained group separation of stable and unstable combustors for the cases considered, indicating the suitability of the parameters for first order prediction of combustion stability.

A much more ambitious effort has been begun with one dimensional analysis by Priem and Guentert of unstable combustion. The model used is that of an annular section of a combustor having very small thickness and length. The viscous dissipation and heat release rate similarity parameters discussed above are utilized in the analysis. The nonlinear equations of conservation of mass, momentum, and energy, are solved numerically for an assumed initial disturbance. Two different rate controlling processes, vaporization and chemical reaction, are considered.

At present, calculations have been performed only for the case of an initial disturbance having a first tangential mode amplitude distribution. For this case, the results are obtained that the vaporization model produces a rapid wave steepening effect (such as observed experimentally) which is not shown by the chemical reaction model. Even with the latter model, tthe effects on stability of the reaction order and activation energy are small. For the annular combustor considered in this analysis, the viscous dissipation parameter has been found to have a negligible influence, because the model does not include a boundary layer or other wall effects. One of the most interesting results of this study is that the controlling mechanism for small laboratory combustors may be chemical in nature, while the corresponding mechanisms for large production engines may be related to vaporization. Thus, research studies with small combustion chambers may not simulate properly the stability behavior of large engine systems.

The available energy concept of the workers of the Aerojet-General Corporation in Azusa has developed, mostly inductively, from the initial wave motion descriptions of Ellis and Pickford. The application of this approach of the tangential modes of high frequency instability has been discussed by Pickford and Peoples. Briefly, the conceptual basis of the Azusa approach is as follows: In steady state, the injection of a given mass of propellants is followed by the processes of atomization, vaporization, and mixing, which require a certain time to be accomplished. Thus prepared, the reactants are then "available" for the final process of chemical reaction which results in the release of energy. The reaction proceeds over a time interval $\widehat{\tau}$, during which the reactants are sensitive to a disturbance in pressure. The amount of pressure sensitive available energy per unit volume is found to be proportional to the time $\widehat{\tau}$ and to the local intensity of combustion, measured by the gas velocity gradient, $\frac{dU}{d\tau}$.

The effect of a perturbation, which in the Azusa approach is assumed to be of very short duration, is to increase the rate of reaction, thereby releasing excess energy and depleting the local available energy. The consequent expansion of the combustion products causes enhancement of the rates of the preparation processes so that the concentration of available energy may overshoot the steady state value after a time τ_a has elapsed. If no further disturbance occurs, the available energy will return to its steady state value at a time $\widehat{\tau}_b$ after the disturbance has passed.

In the case of a periodic disturbance, amplication may result if the cycle period τ_w is in the range $\tau_a < \tau_w < \tau_b$. Because of energy dissipation effects, there is probably a threshold perturbation value below which the energy release by the perturbation is not sufficient to cause the available energy concentration to overshoot its steady state value. This statement is based on experimental observations of stability testing using the Aerojet pulse motor. In this device, a series of calibrated powder charges is fired tangentially into the combustion chamber in order to disturb the combustion and flow patterns. Each charge is stronger than the preceding one. Shutdown of the rocket motor is effected automatically following the onset of instability. The number of charges fired is thus a measure of the relative stability of the thrust chamber at the particular operating conditions of the test.

Of the three theoretical approaches considered in this survey, only the Princeton one has been extensively developed. The sensitive time lag concept has been applied to both longitudinal and transverse modes, and velocity, or transport, effects as well as thermodynamic effects have been included analytically. Experimentally, the validity of the theory has been shown for several combinations of injector type and propellants, and for both longitudinal and tangential modes.

However, the very nature of the sensitive time lag approach makes it impossible to calculate the values of the stability parameters from basic principles. In addition, as presently developed, the solutions are not valid for engines with nozzle contraction ratios less than two. The required extension, while complex, is straightforward. A more serious restriction is that of linearity. The effect of large amplitude, shock-type pulses can be handled only qualitatively. In spite of these limitations, the sensitive time lag approach has in its favor the facts that the theory is well developed, has been verified experimentally, and can be used to correlate test data in a general and systematic fashion, permitting prediction of stability behavior of related but geometrically dissimilar thrust chambers.

The other two approaches have as their ultimate goal the analytical prediction of stability behavior. Of these, the mechanistic approach is more rigorous and quantitative. However, to date it has been possible to obtain solutions only for a single transverse mode for an annular section of a combustor. The extension to the full three dimensional case is being made, but presents extreme difficulties. No help is thus available at the present time for the evaluation of the stability of the entire combustion chamber.

The available energy approach has not yet been developed into a quantitative theory. The concepts involved have been formulated on the basis of a large number of experimental observations. Therefore, when properly expanded, it should be quite useful to researchers and designers in the liquid rocket industry. Although the available energy concentration can be derived experimentally, this process involves two successive differentiations. Thus, extremely accurate and precise measurements are required, which may not be possible in all cases of interest. In addition, it is not clear at present how the concept is to be extended beyond local considerations to include the combustion and flow in the thrust chamber as a whole.

On the basis of the comparison above, it was decided to utilize the Sensitive Time Lag Theory in the correlation of the data from the experimental program.

2. Theoretical Instability Zones

According to the Sensitive Time Lag Theory, the stability of an injector-propellant combination can be described by two parameters: the interaction index, n, which measures the sensitivity of the combustion process to fluctuating chamber conditions; and the sensitive combustion time lag, τ, which is a characteristic time of the combustion process. A given mode of high frequency instability can occur only if the sensitive time lag is in proper relation to the period of the corresponding acoustic oscillation and if the interaction index is sufficiently large, so that the exciting forces can overcome the damping forces. The stability parameters n and τ are functions of the combustion process and, hence, of the injection pattern, propellant combustion, and operating conditions. Although it is not yet possible to calculate n and τ directly from physical and chemical property data, values can be inferred from appropriate experiments.

The investigation of the high-frequency combustion stability of a given thrust chamber assembly depends upon the following considerations. From information regarding the size and shape of the combustion chamber and the general character of the combustion process and products, zones of instability can be drawn for each mode on the n, τ plane (Figure 1).

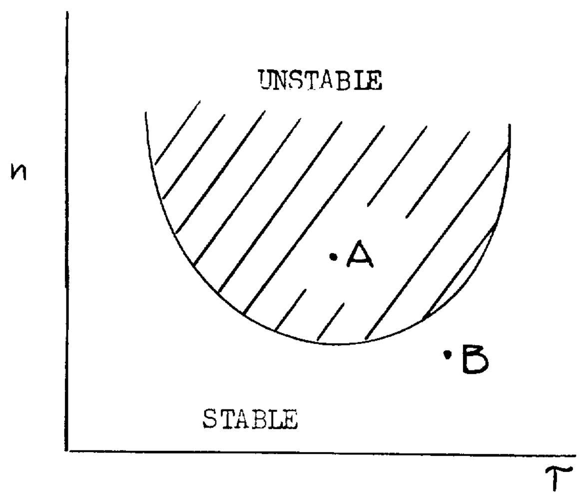

Typical Instability Zone for One Mode of High-Frequency Instability

Figure 1

Then if the n, τ point corresponding to the particular combustion process under consideration lies within the instability zone (point "A" in Figure 1) spontaneously unstable comb stion is to be expected. That is, small disturbances, always present in the combustion "noise", will amplify to levels that are likely to result in hardware damage. For operating n, τ points outside, but sufficiently near, a zone of instability (point "B"), a larger disturbance, such as that produced by the Aerojet-General Corporation pulse generator, will result in instability. Although there is not at present any quantitative nonlineal theory, it can be reasoned intuitively that the nearer the n, τ point lies to an unstable zone, the smaller is the distance required to excite oscillatory combustion.

Theoretical instability zones for the 8-inch diameter combustion chamber are shown in Figures V-1 through V-4 . The unstable zones for the 6-inch chamber length at 2500 psi chamber pressure are given in Figure V-1 . It can be seen that the first tangential mode zone occurs at lower interaction index values than either the second tangential or first longitudinal zones. Therefore, the first tangential is the most unstable of the three modes considered. Typically, the stability parameters have been observed to lie in the ranges

$$0.4 < n < 1.0 \quad ; \quad 0.1 < \tau < 0.3 \text{ millisec}$$

Therefore, the first tangential mode is the only one expected for the 8 x 6-inch chamber.

Figure V-2 shows the theoretical instability zones for the 12.75-inch long chamber at 2500 psi. Because of the added length and the decreased damping effect of the nozzle, the first longitudinal mode has become the most unstable mode. The instability zones for the transverse modes have shifted to slightly higher interaction index values, reflecting the theoretical prediction that the additional volume of combustion products has a slight stabilizing effect.

The zones of instability calculated for the 12.75-inch long combustion chamber at a chamber pressure of 1500 psi are shown in Figure V-3. It can be seen that the decreased nozzle contraction ratio has had a stabilizing effect, since the instability zones have moved to higher n values. The unstable zones for the 6-inch long chamber are shown in Figure V-4 . As with the higher chamber pressure, the effect of decreasing the length is to stabilize the longitudinal modes and to shift the transverse modes to slightly lower interaction index values.

3. Calibration of Pulse

A series of pulse calibrations was made in the 8 by 6.5 in. combustion chamber in order to determine the characteristics of the disturbance produced by the Aerojet-General pulse generator. From work done at Princeton University(*), the following picture of the disturbance has been obtained. Following the bursting of the diaphragm, a shock wave moves down the tube of the generator and into the combustion chamber. From there, it propagates across the chamber as a spherical shock wave, and reflects from the wall, tending to set up a standing first tangential mode. The driver gas from the shock generator expands into the chamber shortly after the shock wave. Because the pulse generator is aimed tangentially, the entering driver gas causes the wave pattern to rotate, forming a spinning tangential mode. In the absence of combustion interaction effects, this wave motion damps according to the law,

$$|p'| = P e^{-\delta t}$$

when P is the amplitude at $t = 0$, and δ is the damping factor.

The results of a typical calibration test are shown in Figure V-5 , for a 20 grain pulse at a chamber pressure of 1500 psia. It can be seen that the disturbance has decayed to one-tenth its initial value by 60 millisec after the passage of the initial shock wave. Figures V-6 and V-7 show the effect of charge size and chamber pressure on the initial pulse amplitude P and damping factor, δ . Both P and δ increase with increasing charge size. However, within the experimental accuracy, there appears to be little effect from pressure.

(*) Non-Linear Aspects of Combustion Instability in Liquid Propellant Rocket Motors - Second Yearly Progress Report. Princeton University, Aero Eng. Rept. No. 553b 1 June 1962.

B. EXPERIMENTAL RESULTS

1. Summary of Test Conditions and Results

Table III presents a summary of the tests conducted in the experimental phase of the program. Considerable difficulty was experienced in preventing burnout of the flush-mounted pressure transducers. Further discussion of this aspect of the program is contained in the following section. It can be seen that only three tests were completely successful. However, these tests produced extremely interesting results, which are discussed in detail below.

2. Test Installation

a. Summary

The test installation schematic shown in Figure V - 8 defines the pressurizing system, propellant tankage, valves and related instrumentation. The liquid hydrogen tanks and propellant line are vacuum jacketed to minimize boil-off. The hydrogen line vacuum jacket extends from the tank up to the thrust chamber valve. The oxidizer supply line is insulated from the oxidizer tank up to the thrust chamber valve. All tests were conducted with the test hardware installed in the horizontal position. A typical test set-up is shown in Figures V-9 and V-10.

Ignition was accomplished by two ALCLO igniters which were sequenced to fire at the time the oxidizer valve opens, or 100-150 milliseconds before fuel is introduced into the chamber. These units provide a high temperature gas stream for approximately one second. One unit was mounted in an igniter boss located in the side of the thrust chamber; the other was mounted on an expendable aluminum tube which is inserted through the nozzle throat.

TABLE III TEST SUMMARY

Test No.	Date	Design Level P_c (psia)	Chamber Diameter (inches)	Chamber Length (inches)	Injector Configuration	Pulse Gun Charges (grain)	Remarks
D-495LM -2	7/20/62	1500	8.0	6.0	4.5K Pentad	10,15,30,40	No high frequency instability. One Photocon burned out.
-3	8/20/62	2500	8.0	6.0	4-K Pentad	10,20,40,80	No high-frequency instability. Four Photocons burned out.
-4	10/12/62	2500	22.0	20.0	3-5K Pentad	20,40,80	Bolt spacers failed, 80 grain charge initiated 470 psi, 3100 cps instability.
-5	11/20/62	1500	8.0	12.75	4-5K Pentad	10,20,40,80	Oxidizer valve die not fully open. Low P_c shutdown.
-6	11/21/62	1500	8.0	12.75	4-5K Pentad	10,20,40	40 grain charge initiated 500 psi 4000 cps instability.
-7	1/11/63	1500	8.0	12.75	Conventional		High-frequency instability initiated before sequence of pulse charges.
-8	1/22/63	1500	8.0	9.5	4-5K Pentad	10,20,40,80	High-frequency oscillations, 450 psi, 5200 cps, initiated by 80-grain pulse, damped after 59 millisec

NOTES:

a. Design pressure achieved.

b. Test mixture ratios not given because of inadequacy of flow rate measurements.

c. Characteristic Velocity, C^*, not given because of inadequacy of flow rate requirements.

Pulse generators were sequenced to fire at 50 millisecond intervals after steady-state conditions were reached. These units provide pressure pulses at a leveldefined by a calibrated charge. Figure V-11 shows a typical pulse generator assembly.

A high-frequency sensing device was used to stop the run in the event of an instability. This unit was pre-set to initiate a shutdown if any chamber pressure oscillations with a frequency greater than 1000 cps and a peak to peak amplitude greater than 120 psi occurred for a duration longer than 20 milliseconds.

b. Instrumentation

(1) Instrumentation was located as shown in Figure V-12. A discussion of individual components follows.

(a) Propellant Flow Rates

Fuel flow measurements were made using two differential pressure transducers connected in parallel across an orifice which was installed near the fuel tank outlet; oxidizer flow measurements were made using a differential pressure transducer connected across a venturi section in the oxidizer line.

(b) Propellant Pressures

Propellant pressures were measured using Type P-1871 Wiancko transducers of the 5000 psi range.

(c) Propellant Temperatures

The fuel temperature was measured with Rosemount platinum resistance probes; standard copper-constantan thermocouples were used to measure the oxidizer temperature.

(d) Chamber Pressure

Mod. 352A, 3000 psi Photocon pressure transducers were used to measure any high frequency chamber pressure oscillations; due to the inability of these units to withstand directly the heat flux in the combustion chamber, a recessed Photocon installation was developed; this system incorporated an adapter which spaced the Photocon approximately .750 from the inside diameter of the chamber, and acted as a heat sink for the hot combustion gases; Figure V-13 shows a typical recessed Photocon installation.

(e) Heat Flux

Heat flux was measured by using HY-CAL molybdenum slug calorimeters; these units were mounted with the sensing unit flush with the inside diameter of the chamber.

3. Design and Fabrication of Hardware

a. 8-in. Diameter Pulse Motor

(1) Chamber

(a) An 8-in.-dia variable length thrust chamber was designed to match existing nozzles and injectors; chamber length can be varied between 6.00-in. and 12.75-in. by inserting spacers between the chamber and nozzle, as shown in Figures V-14 and V-15.

Four equally spaced bosses were provided on the thrust chamber periphey for mounting pulse generators in a radial plane near the injector face; the bosses are orientated such that the pulse generators fire tangential to a 4-in. diameter circle.

Mounting holes for four high frequency response pressure transducers are also provided; three transducers are in the same radial plane as the four pulse generators, and the fourth is placed axially downstream from one of the other three; this arrangement of transducers allows the detection and identification of both tangential and longitudinal modes of instability.

Two calorimeter mounting bosses are provided and are located in the same axial plane 0.750-in. and 5.45-in. from the injector face.

The thrust chamber is constructed of 1.5-in.-thick 1020 steel; a 0.030-in. "Rokide Z" coating was applied to the inside diameter of the chamber, spacers, and nozzles, to provide protection from the combustion gases.

(2) Four Element Pentad Injector

This large-thrust-per-element injector shown in Figure V-16 consists of four 5K pentad elements; each element consists of four oxidizer streams impinging at an included angle of 60° on a central fuel stream; the fuel injection velocity was 500 ft/sec and the oxidizer injection velocity was 80 ft/sec; the injector plate and propellant tubes were made from Type 347 stainless steel; no special machining techniques were required during the construction of this unit; a water flow test is shown in Figure V-17.

(3) Conventional Pattern Injector

The pattern of the conventional injector shown in Figure V-18 is made up of 90 elements, each consisting of two showerhead oxidizer holes impinging on a fuel fan formed by two impinging fuel holes; the propellant orifices are fed through concentric ring channels which are manifolded from the back side; the fuel injection velocity was designed for 240 ft/sec, and the oxidizer injection velocity was designed for 190 ft/sec; a water flow test is shown in Figure V-19.

b. 22-in. Diameter Pulse Motor

A 1020 steel nozzle adapter was designed to allow installation of 20K pulse motor nozzles on the existing 120K pulse motor chamber. A pentad injector pod, with the same physical configurations and dimensions as the pentad elements used for the 8-in.-dia chamber, was designed for the 22-in.-dia pulse motor. Three of these injector pods were used to provide a total thrust of 14,000 lb.

c. Hydrogen Pump

Previously, the pressurization of the liquid hydrogen run tank was accomplished by using a nitrogen compressor to provide high pressure nitrogen to pressurize gaseous hydrogen in an ullage tank, which in turn, pressurized the liquid hydrogen. This system allowed a considerable amount of nitrogen to accumulate in the hydrogen tank, thus adversely affecting engine performance.

In order to provide uncontaminated pressurization of the hydrogen run tank, a Corblin high pressure gaseous hydrogen compressor was installed. This diaphragm-type compressor provides a convenient and rapid means of pressurization. Approximately thirty minutes is required to bring the 20 ft^3 hydrogen ullage bottle up to the 4500 psi operational level with a compressor inlet of 1500 psi. The hydrogen compressor was installed for test D495 LM-7 and has demonstrated satisfactory performance since that time.

4. Instrumentation

A serious problem encountered during the testing program was the inability of the water cooled Photocon pressure transducers to sustain the heat flux generated in the combustion chamber. Designs incorporating water cooled flame shields and Rokide coatings proved to be inadequate. It was, decided, therefore, to determine the applicability of an adapter which would permit a recessed installation, as shown in Figure V-13. The purpose of the adapter was to limit the heat flux experienced by the transducer.

The response characteristics of three adapter configurations were measured using the shock tube apparatus shown in Figure V-20 . Adapter "A" had seven 1/8-in. diameter holes; "B" had seven 3/16-in. diameter holes, and "C" had a single, 11/16-in. diameter hole. In all cases the holes were 3/4-in. long and there was a gap of 0.010-in. between the adapter and the Photocon flame shield.

The frequency response curves for the three adapter configurations are compared in Figure V-21 . Configuration "B", with seven 2/16-in. diameter holes had the best overall response characteristics, being flat within 25% to nearly 1500 cps. Under combustion chamber conditions, the sonic velocity of the gas in the transducer and adapter cavities is estimated to be approximately three times the sonic velocity of the working fluid in the shock tube calibrations. Therefore, the frequency response of adapter "B" will be flat within 25% for frequencies up to 4500 cps, which is approximately the frequency of the first tangential mode of the 8-in. diameter combustion chamber.

5. Discussion of Test D495LM-6, -7, and -8

Test No. D-495-LM-6 was conducted using an 8 in. dia chamber with a cylindrical length of 12.75 in. The injector pattern consisted of four 5K pentad elements. The test was made at a chamber pressure of 1490 psia and a mixture ratio of 6.22. Pulse charges of 10, 20, and 40 grains were fired, with instability in the first tangental mode resulting from the

40 grain pulse. The 10 grain charge did not produce a sufficiently large disturbance to emerge from the combustion noise. Both the 20 and 40 grain pulses produced longitudinal as well as tangental wave motion. Ths signals were separated by filtering so that the amplitude - time characteristics of the two modes could be studied independently.

Figure V-22 shows the variation of amplitude with time for each of the components of the oscillation produced by the 20 grain charge. Both modes exhibited an exponential decay. The initial amplitudes were nearly equal, but the decay rate of the longitudinal oscillation was approximately three times that of the tangential. A probable explanation of the pulse characteristics is the following: The pulses were introduced at the injector end of the chamber, which had a length-to-diameter ratio of 1.6. The initial propagation of the pulse was as a spherical shock wave, with the initial amplitude dependent primarily on the pulse charge characteristics (i.e., size of powder charge and burst disk). Since the pulse was initiated at the injector end, oscillations were set up by reflection in both the longitudinal and transverse directions. The subsequent damping of the pulse reflects the acoustic properties of the combustion chamber. It has been shown both experimentally and theoretically that the exhaust nozzle exerts a stronger damping effect on the longitudinal modes than on the transverse ones.

The 40 grain pulse behaved initially in a similar fashion (Figure V-23). The longitudinal mode damped out approximately twice as fast as the tangential, starting from the same initial amplitude (180 psi). However after 2 milliseconds (eight cycles), the oscillation amplitude increased rapidly to greater than 350 psi (peak-to-peak). Phase and amplitude data indicate the following series of events (see Figure V-24): The initial pulse oscillation traveled in a counter-clockwise direction (looking from the nozzle toward the injector), corresponding to the orientation of the pulse gun. The initial amplifying (unstable) oscillation also traveled in the counter-clockwise direction. However, at ten milliseconds after the pulse initiation, the oscillations recorded by transducer No. 2 decreased rapidly to about 25 psi with a frequency of 8000 cps, while that of transducer No. 1 remained unchaged. This pattern is that of a standing first tangential with a pressure node at transducer No. 2 and a pressure antinode at No. 1. The standing pattern was maintained for four milliseconds after which rotation began again, but in the clockwise direction. The remainder of the oscillation was a clockwise-spinning first tangential mode.

An interesting comparison may be made with the pulse charge calibrations discussed above (Section V-A-3):

	O_2/H_2 Test (tangental mode)	N_2 Calibration
20 grain pulse		
Initial amplitude	106 psi	150 to 230 psi
Damping rate	183 sec^{-1}	22 to 40 sec^{-1}
Frequency	4000 cps	1200 cps
40 grain pulse		
Initial amplitude	190 psi	190 to 290 psi
Damping rate	260 sec^{-1}	37 to 43 sec^{-1}
Frequency	4000 cps	1200 cps

The initial amplitudes obtained by the two methods are in reasonable agreement. However, the damping rate with combustion was approximately six times that observed with the nitrogen-pressurized chamber. The frequencies, as expected, are in the same ratio as the sound velocities.

Test No. D-495LM-8 was conducted with the same large thrust (4-5K pentad) injector as Test No. -6. However, the chamber length was reduced to 9.5-inches. Ten, 20, 40, and 80 grain pulse charges were fired at 50 millisecond intervals. The 10 grain charge produced no pressure oscillations, but the 20 and 40 grain charges produced low amplitude 4200 cps oscillations which damped out prior to the succeeding pulse. The 80 grain charge resulted in oscillations at 4200 cps with a peak-to-peak amplitude of 450 psi. This oscillation damped out after 59 millisec. Performance calculations indicate that the 10, 20, and 40 grain charges were fired at a mixture ratio of approximately 5. The mixture ratio decreased following the 80 grain charge; the oscillation damped out at a mixture ratio of about 7.5.

Because of the varying mixture ratio in Test No. -8, no clear effect of chamber length could be detected. The results of the two large thrust injector tests indicate that the tendency to instability is greatest at the design mixture ratio of 6. Below that value, oscillations appear to be more difficult to initiate, whereas above 6, fully developed oscillations damped out.

The relative stability of the conventional, multiple orifice type of injector (showerhead) compared with the large-thrust-per-element type (4-5K) was investigated on Test No. D-495LM-7. The chamber length was 12.75 inches, the same as that used on Test No. -6. A high frequency instability occurred at 0.130 sec after 90% of chamber pressure was reached. The instability sensing device signaled for a shutdown 0.160 sec after 90% of P_c. The total test duration was 0.300 sec. The shutdown was initiated before any of the pulse charges were sequenced. Post-test examination showed that the burst-diaphragm on the 10 grain charge was ruptured and the powder charge burned. This charge was either burned due to a failure of the burst-diaphragm upon the initiation of combustion in the chamber, or due to erosion of the burst-diaphargm which occurred during the high frequency instability. There was no indication from the oscillograph records of the time that this charge burned.

The chamber pressure oscillations developed smoothly, without any trace of a disturbance, and achieved a maximum amplitude of about 500 psi (peak-to-peak). Following the usual procedure, the test was initiated with an oxidizer lead. The oscillations began at the time the fuel valve reached the fully open position. In the shutdown procedure, the oxidizer valve was closed first. As a result, there was a continuous decrease in mixture ratio throughout the test. This mixture ratio variation was evident in the frequency of oscillation, which began at 4200 cycles per second, increased to 4820 cps and then decreased to 4530 cps. Assuming 95% combustion efficiency, these frequencies correspond to mixture ratios of about 8, 4, and 2, respectively.

C. CONCLUSIONS

Because of the linear nature of the Sensitive Time Lag Theory and the limited number of valid tests, precise values of the stability parameters n and τ could not be determined. However, approximate values were estimated for the two types of injection used, as follows:

a. Conventional injector: $1.0 < n < 1.4$; $0.09 < \tau < 0.15$ millisec;

b. large-element injector: $0.7 < n < 1.0$; $0.09 < \tau < 0.15$ millisec.

These results are compared with other data available* in Figures V-25 and V-26.

In general, the interaction index decreases with increasing element size (see Figure V-25). This is a gross dependence; its physical basis has not yet been determined. The dependence of n on chamber pressure as inferred from these data is $n \sim p_c^{\frac{1}{2}}$. Recent tests conducted at Princeton University, using the propellant combination LO_2/ethanol and a very low thrust-per-element injection pattern, have indicated a similar pressure dependence of the interaction index.

The results from the present, high chamber pressure, program do not show a clear trend with element size of the sensitive time lag. Low pressure testing, however, indicates that the time lag increases with increasing thrust-per-element, as shown in Figure V-26 . For the low thrust, multiple-element injectors, the dependence of τ on chamber pressure is approximately, $\tau \sim p_c^{-\frac{1}{2}}$, in agreement with results obtained at Princeton.

The implications of the available data are twofold:

a. The large-thrust-per-element type of injector is more stable than the conventional, multiple orifice type (since the interaction index is smaller). In addition, the sensitive time lag is greater for the large element injector. Since the occurrence of a given mode of instability

---

* Stability parameter data was obtained from the following sources:
Addoms, J. F., et al; Unique Injector Concepts Development (UNICODE), Aerojet-General Report 0518-00-5 (Quarterly), September 1962.

Reardon, F. H., Combustion Stability Behavior of the Nitrogen Tetroxide/AeroZINE 50 Propellant Combination with the 2SIN Injector Pattern, Aerojet-General Report TMC 9616/003, 13 March 1962.

High Pressure Chamber Operation Launch Vehicle Engine. Aerojet-General Report 4008-Q3 (Quarterly), 2 January 1963.

depends on the matching of the oscillation period, T, with the sensitive time lag, τ, (actually $\tau \approx \frac{1}{2}T$), and the period is proportional to the chamber diameter: a larger diameter is required to obtain the same mode for a large-thrust-per-element injector as compared to a conventional one. For any value of time lag, there is a maximum chamber size that can be operated stably without baffles. With a large-element injector, the maximum stable diameter will be larger than that for a conventional type. If baffles are necessary to stabilize combustion with a large-element injector, the required baffle spacing should be larger than for the corresponding small-element injector.

b. Increasing the chamber pressure is likely to result in a greater tendency to combustion instability. The sensibility of the combustion process to disturbances is greater at higher pressure and the characteristic time is smaller. Although, for a given thrust level, the combustion chamber decreases with increasing pressure, the combustion time may decrease faster (size); thus higher modes, with more complex wave patterns than those observed at present, may be experienced.

It should be noted that these conclusions are based on a very small amount of data. Further work is necessary to explore their limitations, and to determine the processes that govern the variations in the stability parameters.

D. BIBLIOGRAPHY

1. Crocco, L., and Cheng, S. I., Theory of Combustion Instability in Liquid Propellant Rocket Motors, AGARDograph No. 8, Butterworths Scientific Publications, London, 1956.

2. Scala, S. M., Transverse Wave and Entropy Wave Combustion Instability in Liquid Propellant Rockets, Princeton University Aeronautical Engineering Report No. 380, 1 April 1957.

3. Crocco, L., Gray, J., and Harrje, D. T., "Theory of Liquid Propellant Combustion Instability and Its Experimental Verification," ARS Journal, Vol 30, No. 2., February, 1960.

4. Reardon, F. H., An Investigation of Transverse Mode Combustion Instability in Liquid Propellant Rocket Motors, Princeton University Aeronautical Engineering Report No. 550, 1 June 1961.

5. Crocco, L., Harrje, D. T., and Reardon, F. H., "Transverse Mode Combustion Instability in Liquid Propellant Rocket Motors", ARS Journal, Vol. 32, No. 3, March, 1962.

6. Reardon, F. H., Combustion Stability Behavior of the Nitrogen Tetroxide/Aerozine-50 Propellant Combination with the 2 SIN Injector Pattern, Aerojet-General Corporation, Thrust Chamber Department, LRP, TM9616/003, 13 March 1962.

7. Reardon, F. H., Combustion Stability Behavior of the Liquid Oxygen/Liquid Hydrogen Propellant Combination, Aerojet-General Corporation, Liquid Rocket Plant, TM 9616/002, March 1962.

8. Priem, R. J., and Morrell, G., "Application of Similarity Parameters for Correlating High-Frequency Instability Behavior of Liquid Propellant Combustors", American Rocket Society Paper No. 1721-61, presented at the Propellants, Combustion, and Liquid Rockets Conference, Palm Beach, Florida, April 26-28, 1961.

9. Priem, R. J., and Guentert, D. C., Combustion Instability Limits Determined by a Nonlinear Theory and a One-Dimensional Model, NASA Technical Note, 1962.

10. Ellis, H. B., and Pickford, R. S., High-Frequency Instability, Aerojet-General TN-17 (AFOSR TN-56-547), September, 1956.

11. Pickford, R. S., and Peoples, R. G., Inherent Stability of the Combustion Process, Aerojet-General TN-36 (AFOSR 676), November 1960.

12. Peoples, R. G., and Pickford, R. S., Analytical and Experimental Scaling of Thrust Chambers, Aerojet-General TN-40 (AFOSR 677), November, 1960.

13. Peoples, R. G., Baker, P. D., and Knowles, L. S., High-Frequency Combustion Instability, Aerojet-General Report No. 2126 (AFOSR 1802), November, 1961.

14. Mirsky, I., Transverse Gas Motions in Cylindrical and Annular Thrust Chambers, Rocketdyne Report R-2903 (AFOSR-124), 28 February 1961.

15. Moore, F. K., and Maalen, S. H., Transverse Oscillations in a Cylindrical Combustion Chamber, NACA TN 3152, October, 1954.

16. Kogarko, S. M., "Amplification of Compression Waves in Interaction with a Flame Front," Soviet Physics-Technical Physics, Vol. 5, No. 1, pp. 100-108, July, 1960.

17. Hurrell, H. G., Analysis of Injection-Velocity Effects on Rocket Motor Dynamics and Stability, NASA TR R-43, 1959.

18. Pickford, R. S., Krieg, H. C., and Ellis, H. B., Basic Research in Liquid Rocket Thrust Chambers, Aerojet-General Report 1193 (AFOSR-TR-56-61), January, 1957.

19. Krieg, H. C., Schults, L. O., and Gray, P. D., Liquid-Thrust-Chamber Development Tools, (Confidential), Aerojet-General Report 1858, August 1960.

20. Gray, P. D., and Krieg, H. C., Pulse-Motor Evaluation of Injector-Pattern Combustion Stability with Storable Propellants, Aerojet-General Report 1664, (Confidential), 29 July 1960.

21. Baker, P. D., Peoples, R. G., and Mills, T. R., Two-Dimensional Motor Program, Aerojet-General Report 2185, January, 1962.

22. Cramer, T. B., Webber, W. T., and Lawhead, R. B., Research on the Basic Fluid Dynamic Phenomena Related to Rocket Combustion Instability, Rocketdyne, WADC-TN-57-426, June, 1958.

23. Rabin, E., and Cramer, F. B., Shattering of Burning and Non-Burning Propellant Droplets by Shock Waves, Rocketdyne Report R-695 (AFOSR TN 58-62), 20 February 1958.

24. Rabin, E., Schallenmuller, A. R., and Lawhead, R. B., Displacement and Shattering of Propellant Droplets, Rocketdyne Report R-2431 (AFOSR-TR-60-75), March, 1960.

25. Tau-Yi Toong, "A Theoretical Study of Interactions Between Two Parallel Burning Fuel Plates," Combustion and Flame, Vol. 6, No. 3, September, 1961.

26. Webber, W. T., Effects of Gas Motion on Heterogeneous Combustion, etc., Rocketdyne Report R-1421 (WADC-TC-59-50), April, 1959.

27. Wharton, W. W., Connaughton, J. W., Allan, B. D., and Williams, W. D., The Effect of Sound Oscillations on Combustion and Heat Transfer, ARGMA TR 1C36R, 15 December 1959.

28. Wieber, P. R., and Mickelson, W. R., Effect of Transverse Acoustic Oscillations on the Vaporization of a Liquid-Fuel Droplet, NASA TN D-287, May, 1960.

29. Dityakin, I. F., and Yagodkin, V. I., Effect of Periodic Oscillations of Velocity and Density of a Medium on Disintegration of Liquid Jets, NASA TT F-63, April, 1961.

30. Drain, D. J., Sebum, H. J., and Wasserbauer, C. A., Relations of Combustion Dead Time to Engine Variables for a 20,000-Pound-Thrust Gaseous-Hydrogen-Liquid-Oxygen Rocket Engine, NASA TN D-851, June, 1961.

31. Blackshear, P. L., "The Growth of Disturbances in a Flame-Generated Shear Region," Sixth Symposium on Combustion, Reinhold Publishing Corporation, New York, N. Y., 1957.

32. Putman, A. A., Clough, G. M., and Kenworthy, M. J., Final Report on Studies of Turbulent Premixed Flames and Methods of Suppressing Combustion Oscillations, WADC TR 56-583, December 1956.

33. Lambiris, S., and Combs, L. P., Steady-State Combustion Measurements in a LOX/RP-1 Rocket Chamber and Related Spray Burning Analysis, Rocketdyne Research Report RR 61-13, 10 May 1961.

34. Markstein, G. H., "A Shock-Tube Study of Flame Front-Pressure Wave Interaction," Sixty Symposium on Combustion, Reinhold Publishing Corporation, New York, N. Y., 1956.

35. Mickelsen, W. R., Effect of Standing Transverse Acoustic Oscillations on Fuel-Oxidant Mixing in Cylindrical Combustion Chambers, NACA TN 3983, May, 1957.

36. Morrell, G., Critical Conditions for Drop and Jet Shattering, NASA TN D-677, February, 1961.

37. Male, T., Kerslake, W. R., and Tishler, A. O., Photographic Study of Rotary Screaming and Other Oscillations in a Rocket Engine, NACA RM E54A29, 25 May 1954.

38. Zucrow, M. J., and Osborn, J. R., "An Experimental Study of High-Frequency Combustion Pressure Oscillations," Jet Propulsion, Vol. 28, No. 10, October, 1958.

39. Osborn, J. R., and Bonnell, J. M., "Importance of Combustion Chamber Geometry in High Frequency Oscillations in Rocket Motors," ARS Journal Vol. 31, No. 4, April, 1961.

40. Pelmas, R., Glassman, I., and Webb, M., An Experimental Investigation of Longitudinal Combustion Instability in a Rocket Motor Using Premixed Gaseous Propellants; Princeton University Aeronautical Engineering Report No. 589, December, 1961.

41. Bortzmeyer, H. G., and Crocco, L., Analysis of Longitudinal High Frequency Combustion Instability In a Gas Fueled Rocket Motor, Princeton University Aeronautical Engineering Report No. 587 (AFOSR TN-1957), 5 December 1961.

42. Feiler, C. E., Effect of Fuel Drop Size and Injector Configuration on Screaming in a 200-Pound-Thrust Rocket Engine Using Liquid Oxygen and Heptane, NACA RM E58A20a, 11 July 1958.

43. Morse, P. M., Vibration and Sound, McGraw-Hill, New York, Second Edition, 1948.

44. Fuhs, A. E., Spray Formation and Breakup, and Spray Combustion, Sundstrand Turbo TN No. 4 (AFOSR TN 58-414), 5 February 1958.

45. Griffith, J. D., and Sabersky, R. H., "Convection in a Fluid at Supercritical Pressures," ARS Journal, Vol. 30, No. 3, March, 1960.

46. Hendricks, R. C., Graham, R. W., Hsu, Y. Y., and Medeoros, A. A., "Correlation of Hydrogen Heat Transfer in Boiling and Supercritical Pressures States," ARS Journal, Vo. 32, No. 2, February, 1962.

47. Il'yaehemko, S. M., "Evaporation and Combustion of a Single-Component Fuel in a Chamber of a Liquid Rocket Engine ZHRD," ASTIA, 28 August 1961.

48. Ingebo, R. D., Drop-Size Distributions for Impinging-Jet Breakup in Airstreams Simulating the Velocity Conditions in Rocket Combustors, NACA TN 4222, March, 1958.

49. Ingebo, R. D., "Size Distribution and Velocity of Ethanol Drops in a Rocket Combustor Burning Ethanol and Liquid Oxygen," ARS Journal, Vol. 31, No. 4, April, 1961.

50. Priem, R. J., and Heidman, M. F., Propellant Vaporization as a Design Criterion for Rocket-Engine Combustion Chambers, NASA TR R-67, 1960.

51. Belles, F. E., and Ehlers, J. G., "Shock Wave Ignition of Hydrogen-Oxygen-Diluent Mixtures Near Detonation Limits," ARS JOURNAL, Vol. 32, No. 2, February, 1962.

52. Eisen, C. L., Gross, R. A., and Rivlin, T. J., Theoretical Calculations in Gaseous Detonations, Fairchild Engine Division Report AFCSR-TN-58-326, March, 1958.

53. Fowell, L. R., and Korbacher, G. K., A Review of Aerodynamic Noise, University of Toronto UTIA Review No. 8, July, 1955.

54. Heidman, H. D., Injection Principles for Liquid Oxygen and Heptane Using Two-Element Injectors, NACA RM E56D04, 26 June 1956.

55. Hersch, M., Combined Effect of Contraction Ratio and Chamber Pressure on the Performance of a Gaseous-Hydrogen-Liquid-Oxygen Combustor for a Given Propellant Weight Flow and Oxidant-Fuel Ratio, NASA TN D-129, February, 1961.

56. King, C. R., Compilation of Thermodynamic Properties, Transport Properties, and Theoretical Rocket Performance of Gaseous Hydrogen, NASA TN D-275, April, 1960.

57. Barney, J. D., and Magee, P. M., "Vol. VI - Compilation of Hydrogen Properties," Aerojet-General Report 1999 (Final), June, 1961.

58. Lewis, B., and Von Elbe, G., Combustion, Flames, and Explosions of Gases, Academic Press Inc., New York, 1961.

59. Penner, S. S., Chemistry Problems in Jet Propulsion, Pergamon Press, New York, 1957.

60. Putnam, A. A., et al., Injection and Combustion of Liquid Fuel, WADC Tech. Rept. 56-344, Battele Memorial Institute, March, 1957.

61. Sievers, G. K., Tomasio, W. A., and Kinney, G. R., Theoretical Performance of Hydrogen-Oxygen Rocket Thrust Chambers, NASA TR R-111, 1961.

62. Unknown, Performance and Properties of Liquid Propellants, Aerojet-General, Liquid Rocket Plant, Report 8160-65, March, 1961.

E. EXPERIMENTAL PROPULSION PERFORMANCE

Among several methods of measuring rocket engine performance, the most generally suitable is that of determining the characteristic velocity, C*. From the definition,

$$C^* = P_c A_t \left(\frac{g}{\dot{W}} \right)$$

It is evident that this criterion is independent of thrust level, and therefore back pressure and area ratio. The characteristic velocity is essentially a measure of the success of conversion of chemical energy. From an experimental standpoint, measurement of the characteristic velocity has the advantage that it should be possible to measure accurately all the variables appearing in the definition.

In the present program, determination of the characteristic velocity yielded unsatisfactory results. Test operations were limited to approximately 0.5-sec durations because of the adverse heating effect on uncooled hardware developed at the high experimental pressures, i.e., about 2500 psia. It will be seen in the defining equation that accurate measurement of propellant flow rates is basic to the determination of the characteristic velocity.

As shown in Figure V-27 , which is typical of experimental results, flow response did not occur until 0.30 sec after fire switch, and it is clear that steady state conditions were not developed before (nor after) shut-down at 0.5 seconds. Theoretical characteristic velocity is shown only as a point of reference. It is not considered that performance was adequately demonstrated.

For future operations, the installation of a direct-calibrated hydrogen flow meter of the turbine-type will be of advantage in establishing improved flow measurements. The degree of improvement will not be apparent until flow meter response under the test conditions has been determined. For uncooled hardware operating at high pressures it is not likely that test durations can be extended much beyond the present limit.

As a consequence of the severity of thermal damage to the pressure transducers encountered early in the test program, an attempt was made to determine the heat flux imposed on the instrumentation and chamber. High pressure , high temperature slug-type calorimeters were mounted in the chamber walls. It will be evident from Figure V-28 that the calorimeter response was totally inadequate. No evidence of heating rate was indicated until after shutdown fire switch.

Independent studies of Photocon pressure transducers conducted at Princeton University have indicated a probable suitability at heat flux levels as high as 15-16 Btu/in^2 sec. In view of the recurrence of thermal damage problems early in the test program, and the ultimate necessity of providing the installation adapters described above, it is clear that improved instrumentation will be required in order to establish high pressure heat fluxes with confidence.

THEORETICAL INSTABILITY ZONES

FOR 8" DIA X 6" LONG CHAMBER

AT 2500 PSIA

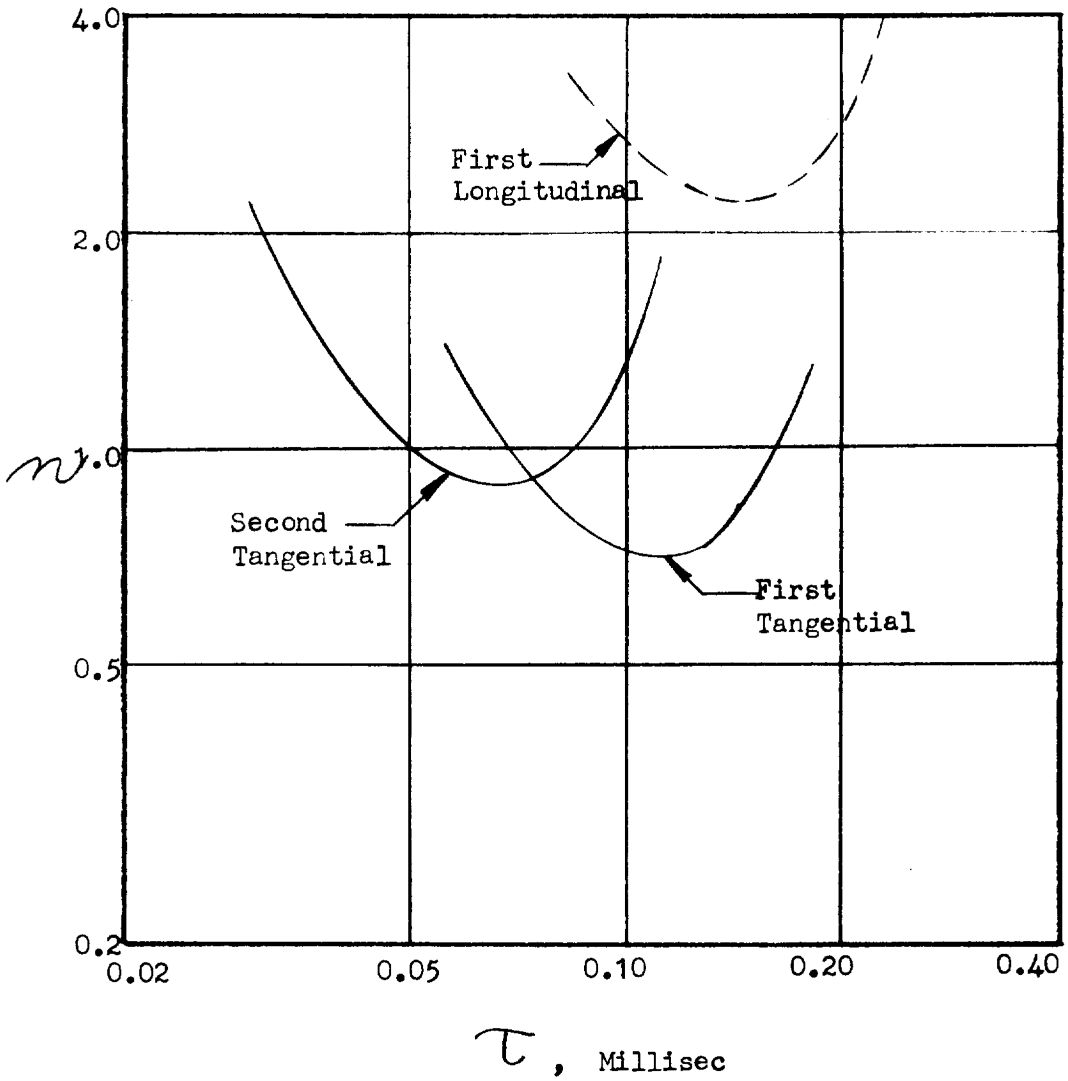

Figure V-1

THEORETICAL INSTABILITY ZONES

FOR 8" DIA X 12.75" LONG CHAMBER

AT 2500 PSIA

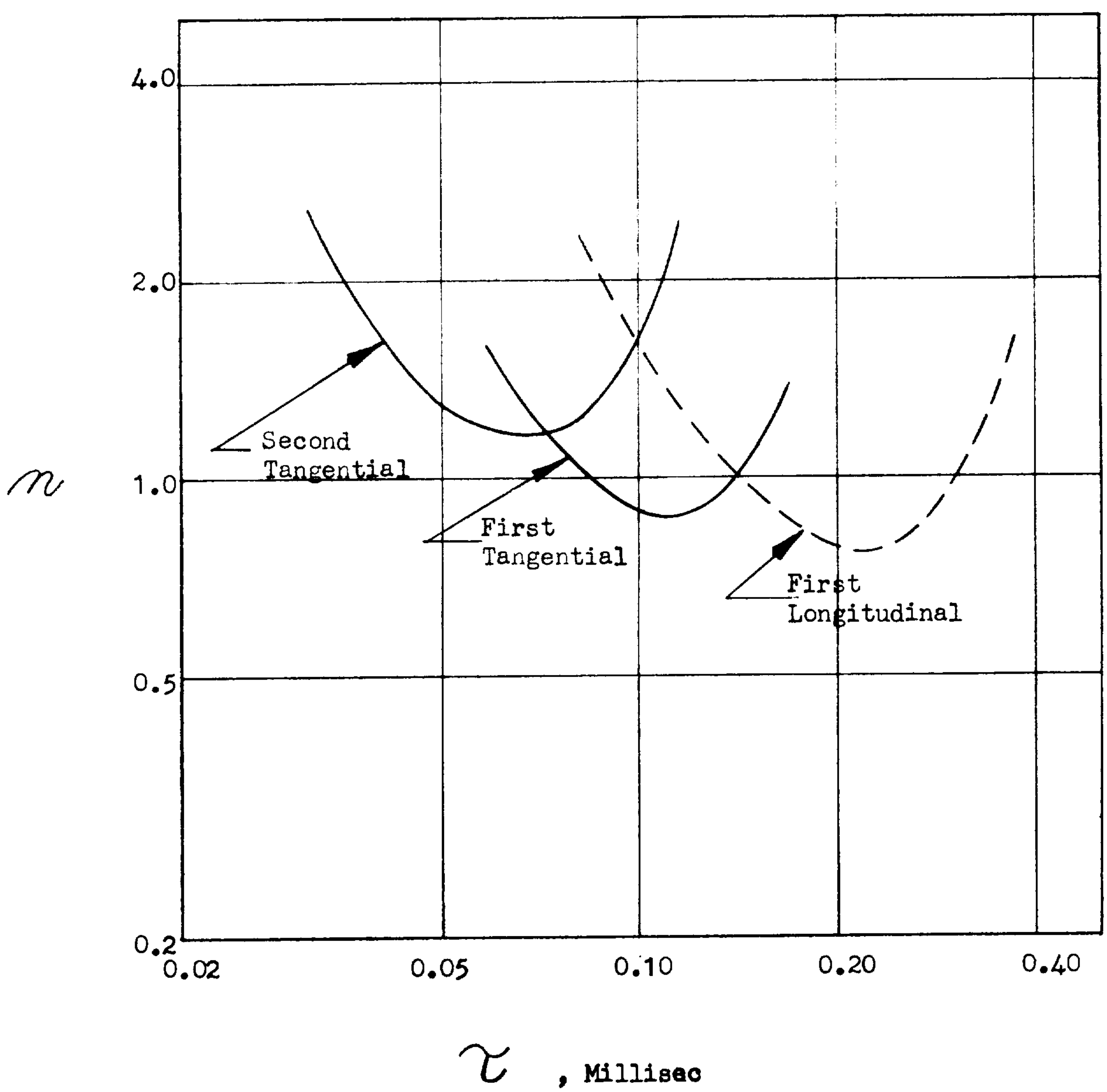

Figure V-2

THEORETICAL INSTABILITY ZONES

FOR 8" DIA X 12.75 " LONG CHAMBER

AT 1500 PSIA

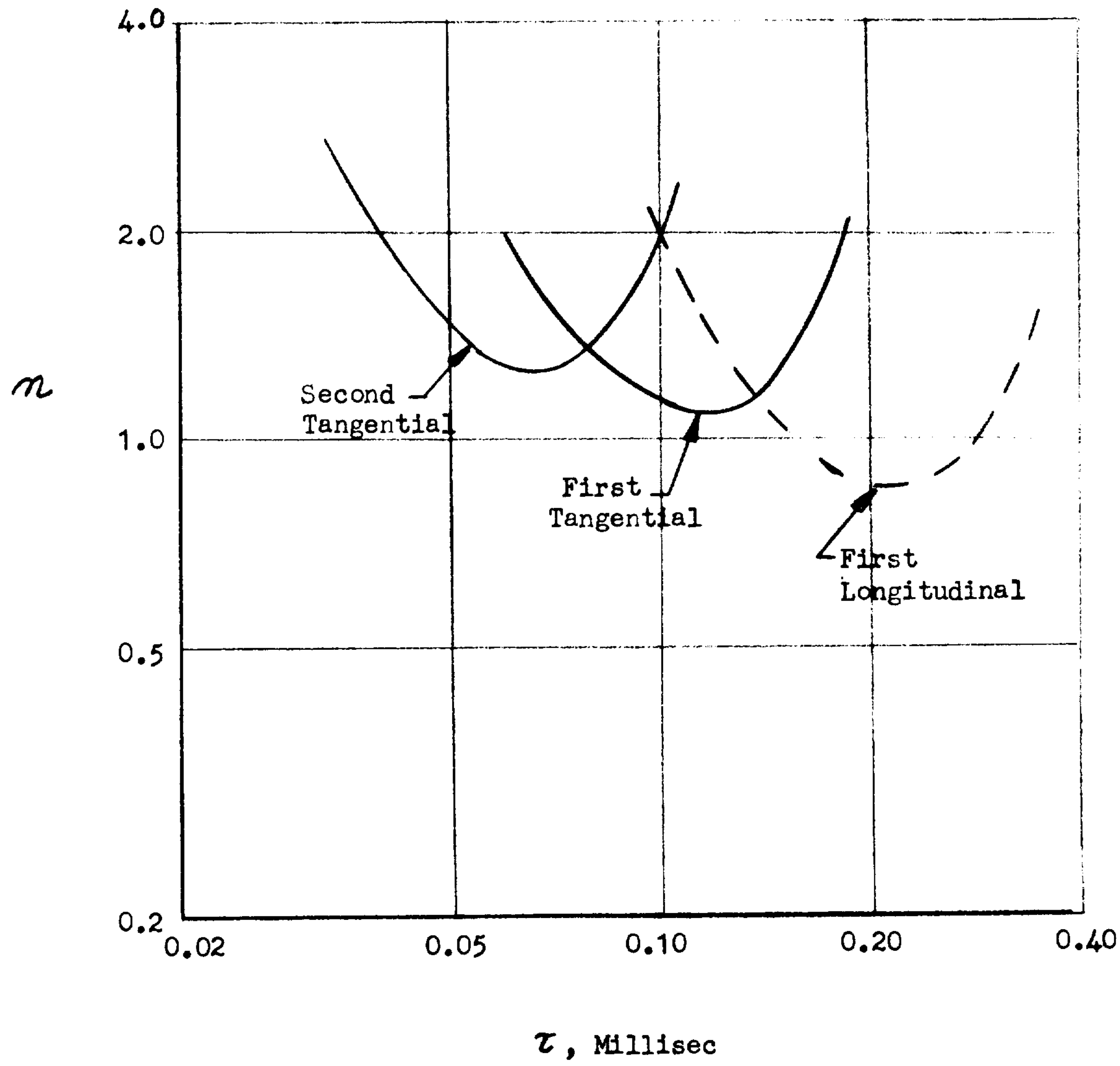

Figure V-3

THEORETICAL INSTABILITY ZONES

FOR 8" DIA X 6" LONG CHAMBER

AT 1500 PSIA

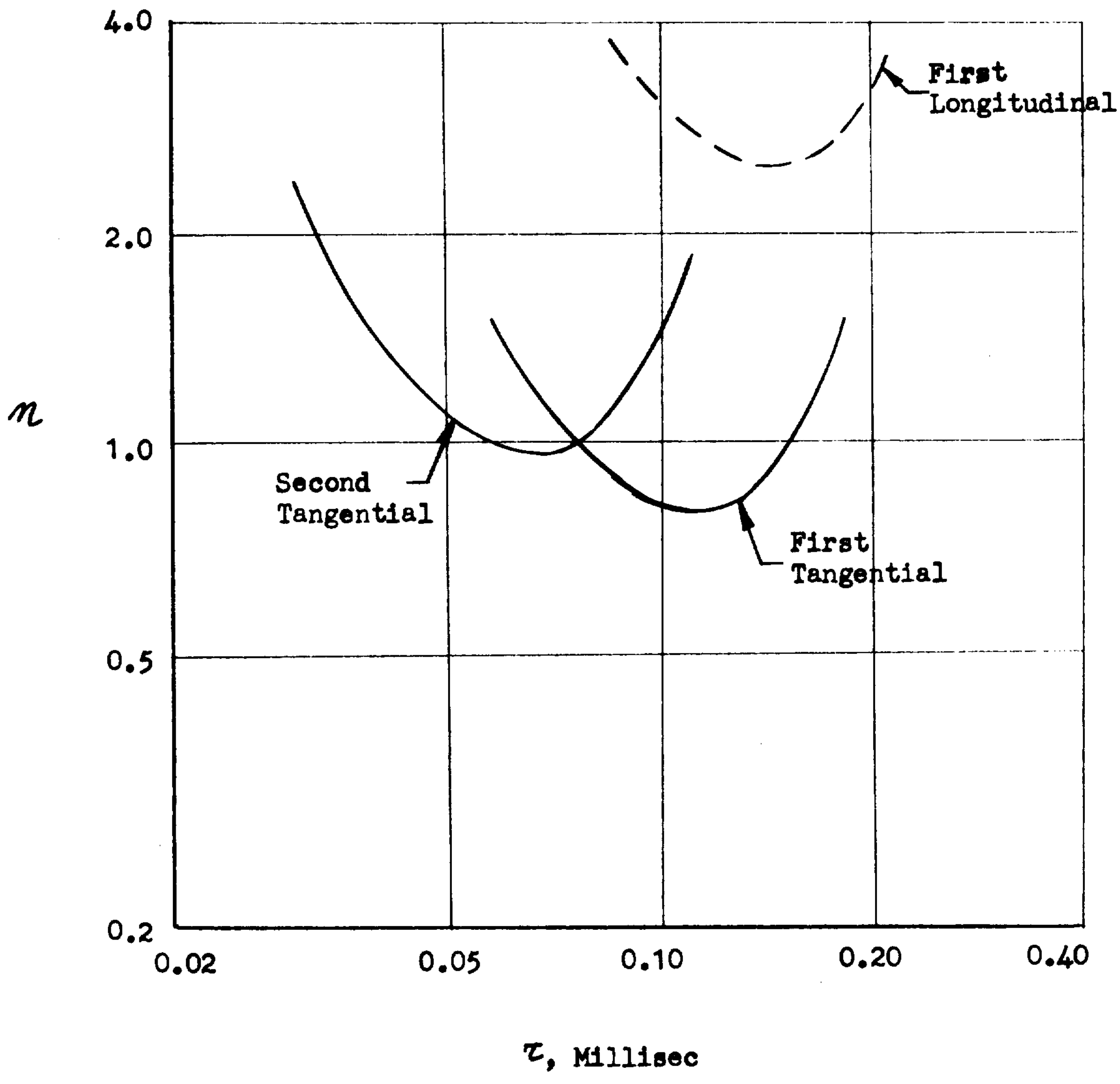

Figure V-4

PULSE CALIBRATION IN 8" X 6.5' CHAMBER: AMPLITUDE VS TIME

FOR 20 GRAIN PULSE, 1500 PSI

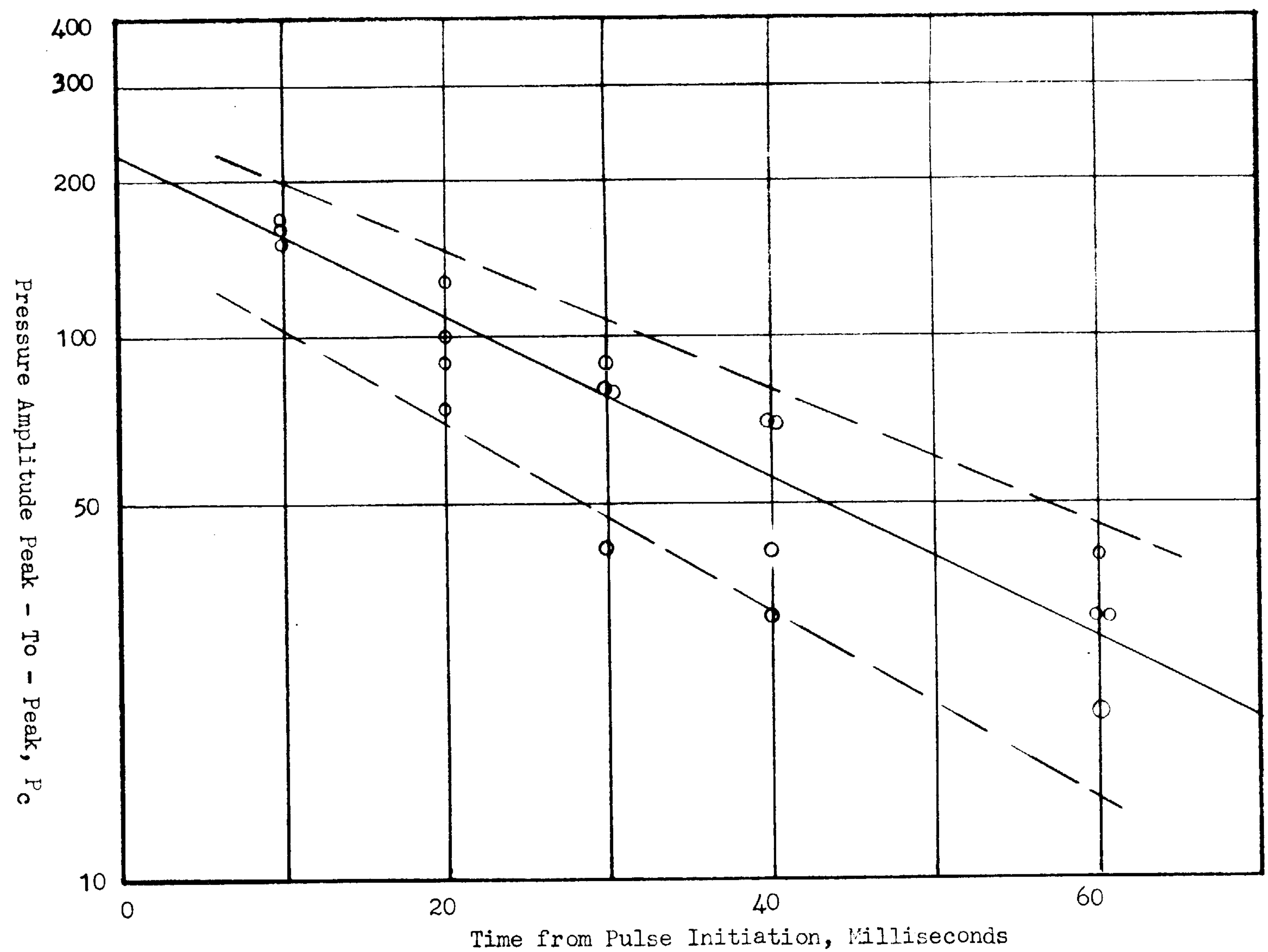

Figure V-5

PULSE CALIBRATION IN 8"x6" CHAMBER

INITIAL PULSE AMPLITUDE, P vs CHARGE SIZE

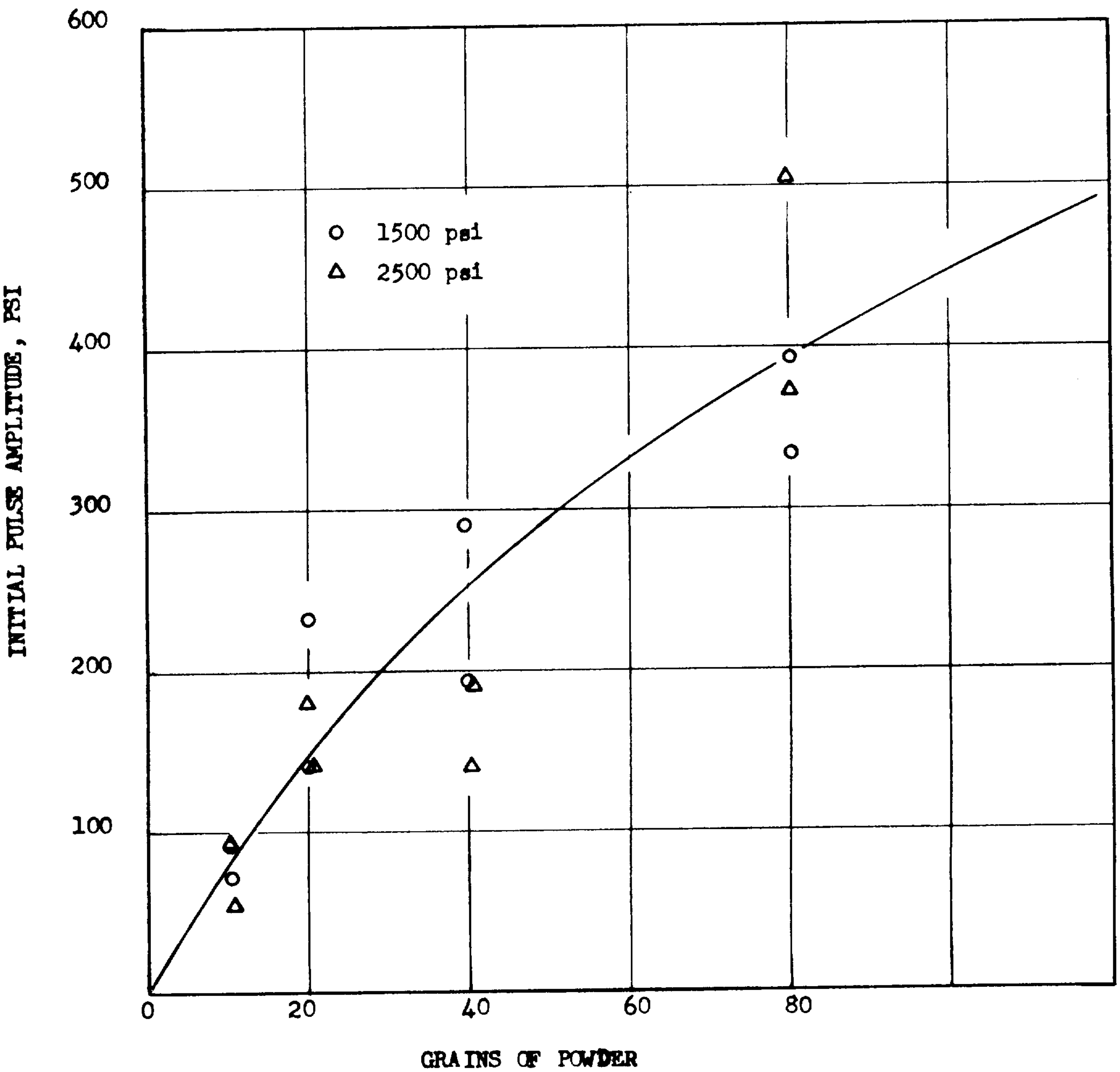

Figure V-6

PULSE CALIBRATION IN 8" x 6" CHAMBER

DAMPING FACTOR, δ

VS

CHARGE SIZE

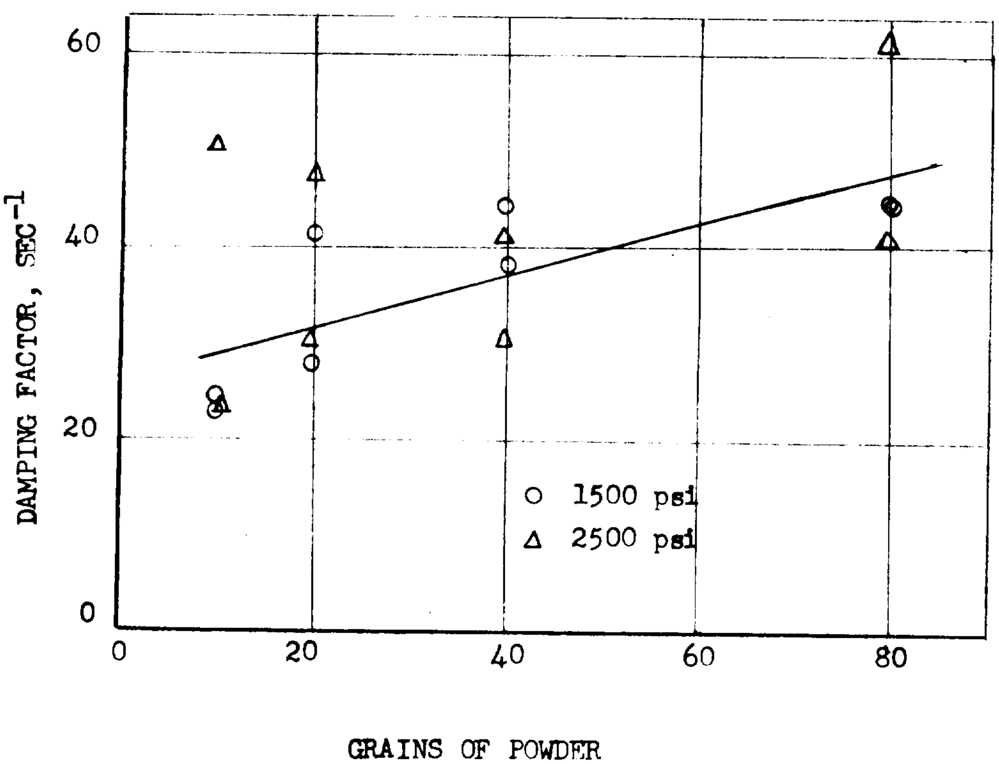

Figure V-7

HIGH PRESSURE CRYOGENIC SYSTEM

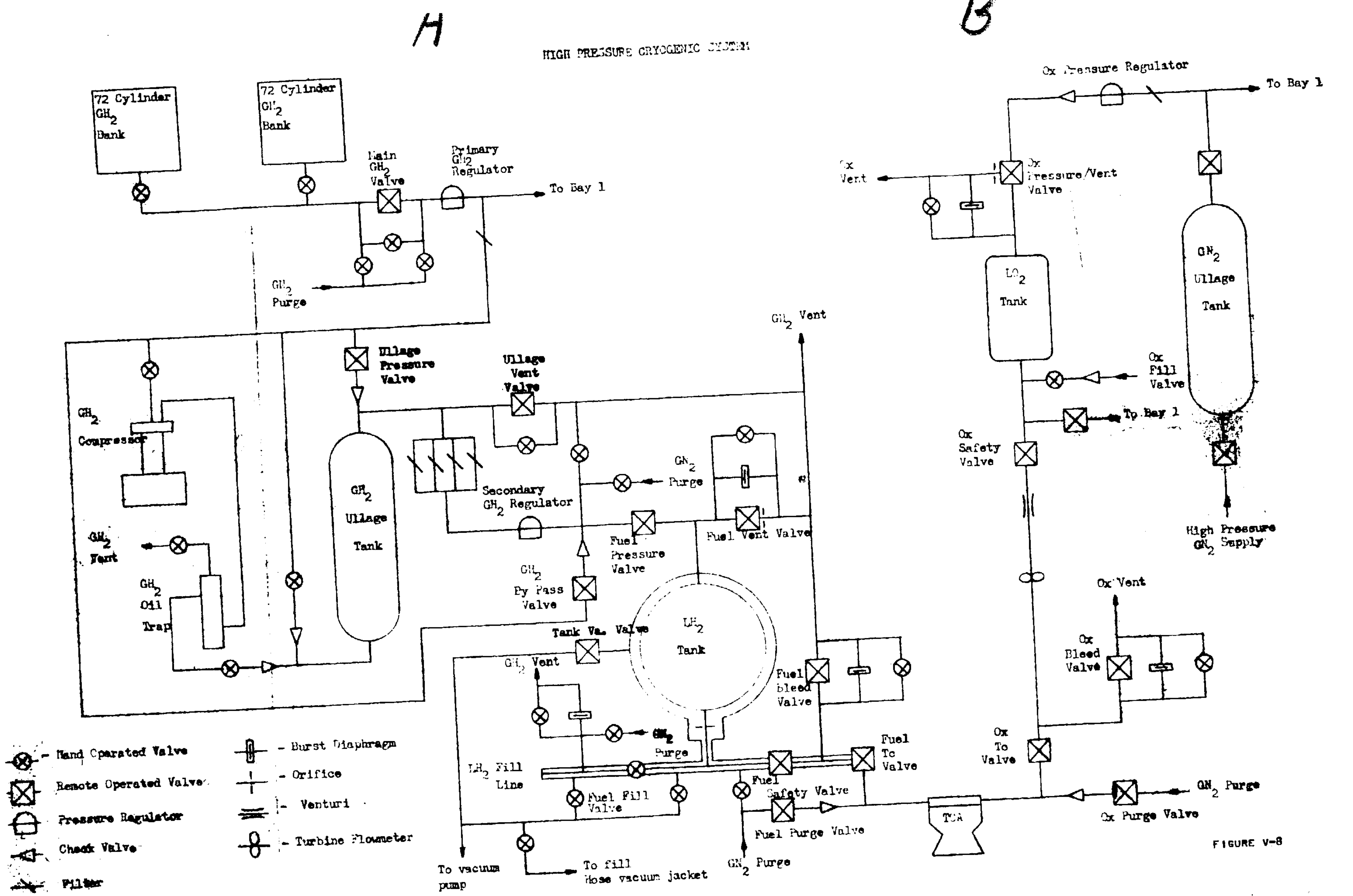

FIGURE V-8

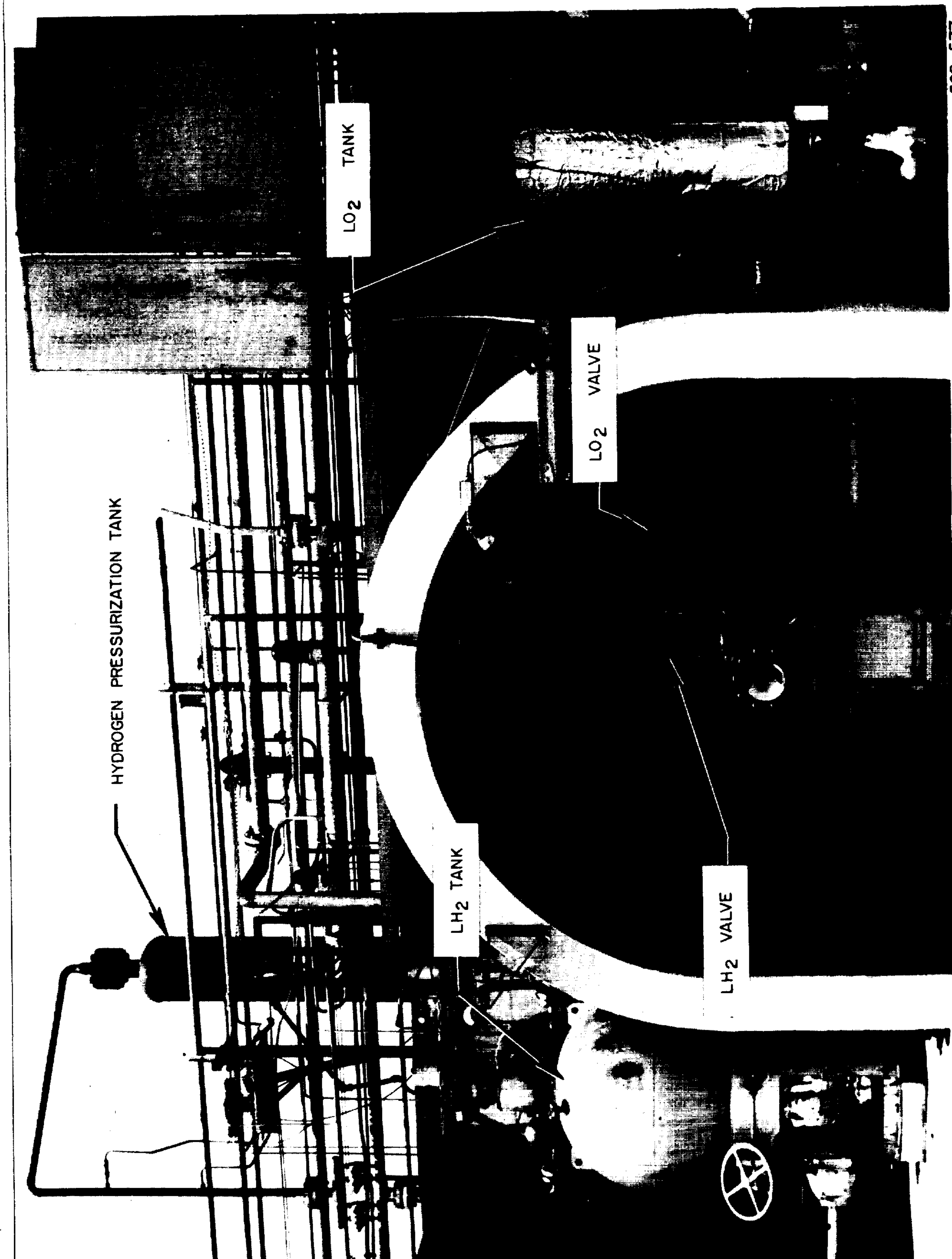

HIGH PRESSURE LO_2/LH_2 TEST STAND

Figure V-9

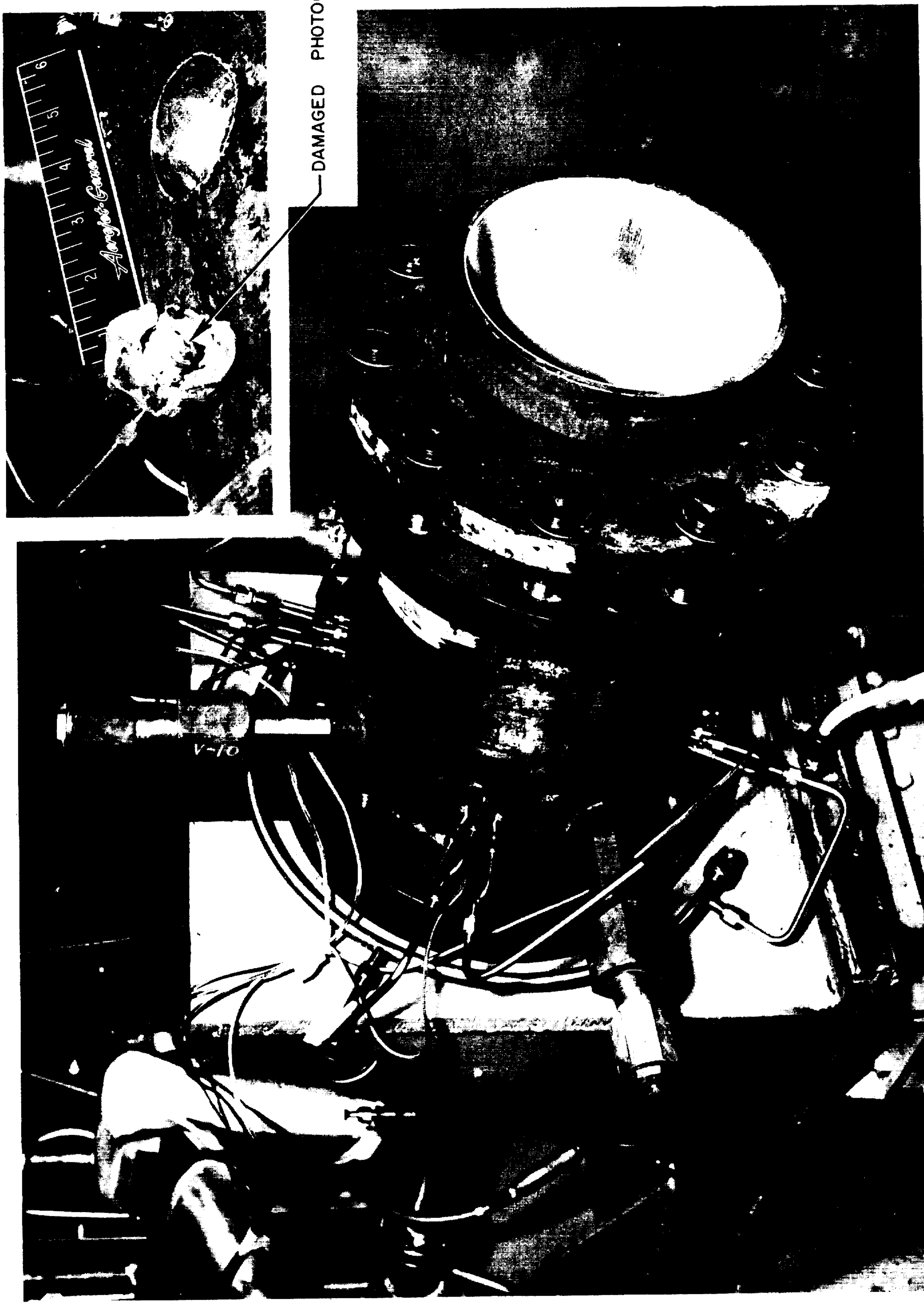

762-743

POST FIRE - TEST NO. 1

Figure V-10

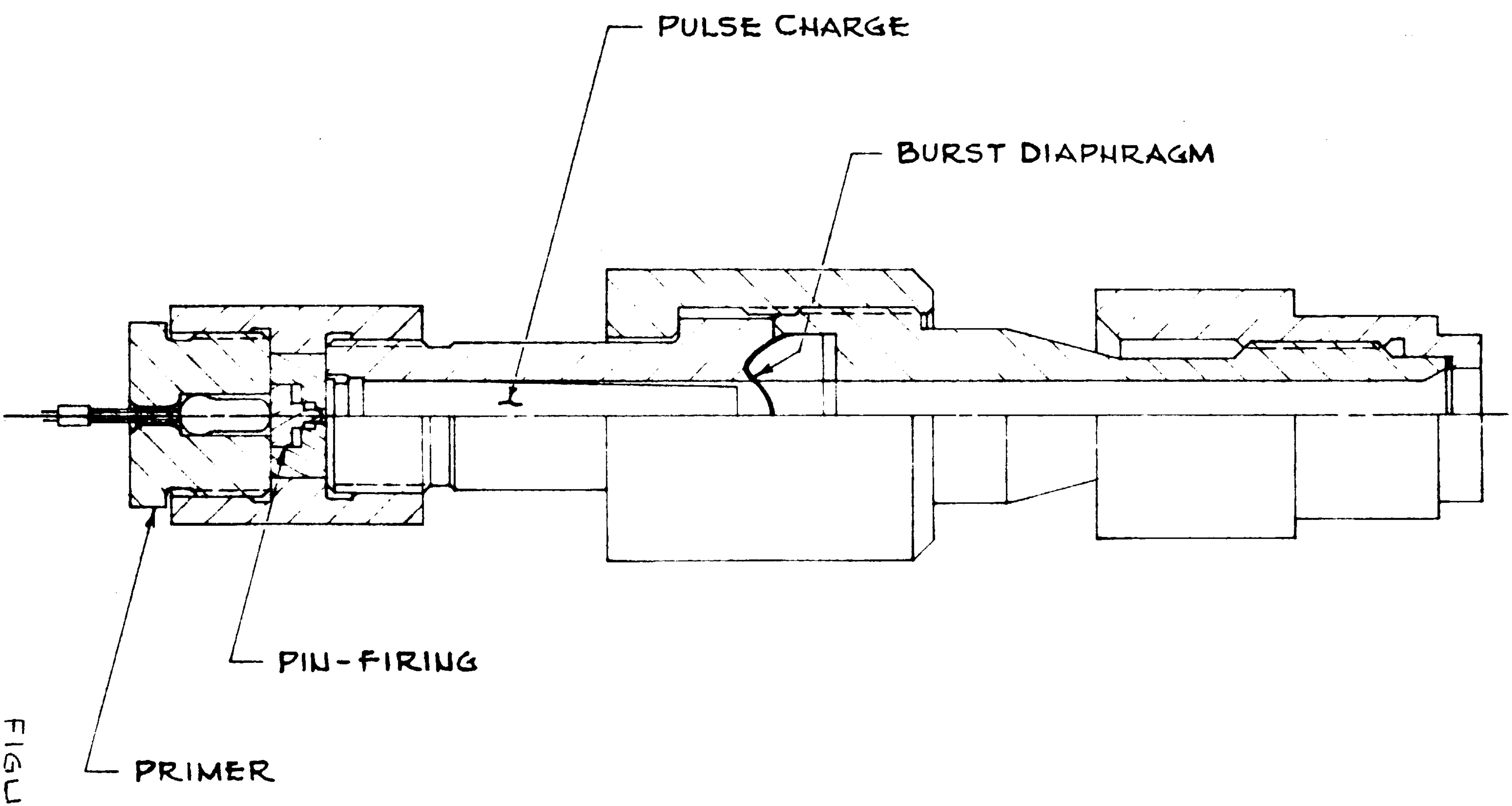

PULSE GUN

FIGURE V-11

—SYMBOLS—

1. Q_{c1} = THRUST CHAMBER CALORIMETER -1
2. Q_{c2} = " " " -2
3. P_cP_1 = CHAMBER PRESSURE PHOTOCON -1
4. P_cP_2 = " " " -2
5. P_cP_3 = " " " -3
6. P_cP_4 = " " " -4
7. GUN 1 = 10 GRAIN CHARGE
8. GUN 2 = 20 " "
9. GUN 3 = 40 " "
10. GUN 4 = 80 " "

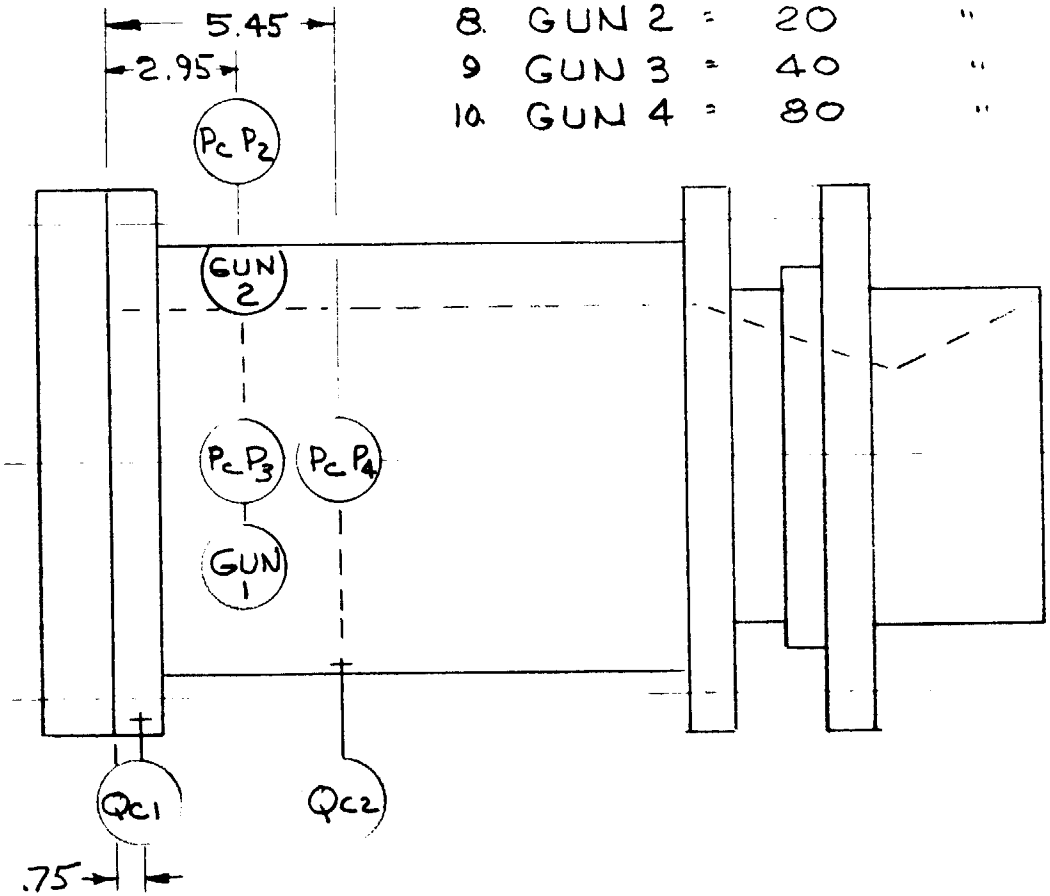

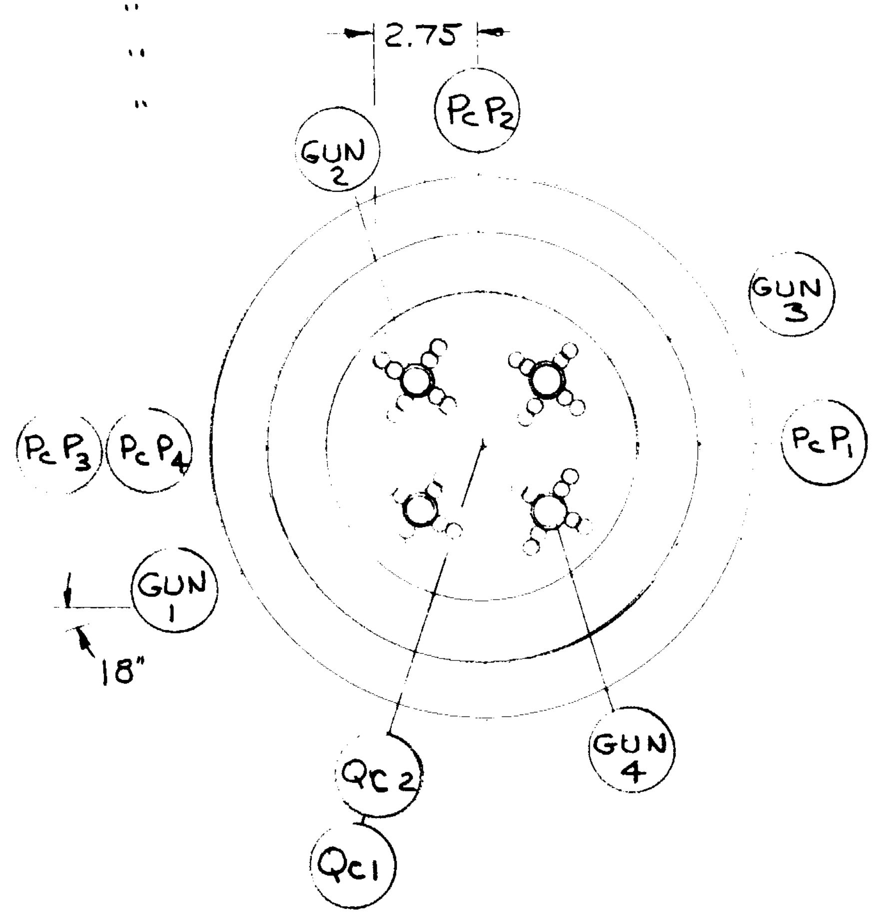

FIGURE V-12

INSTRUMENTATION LOCATION

FIGURE V-12

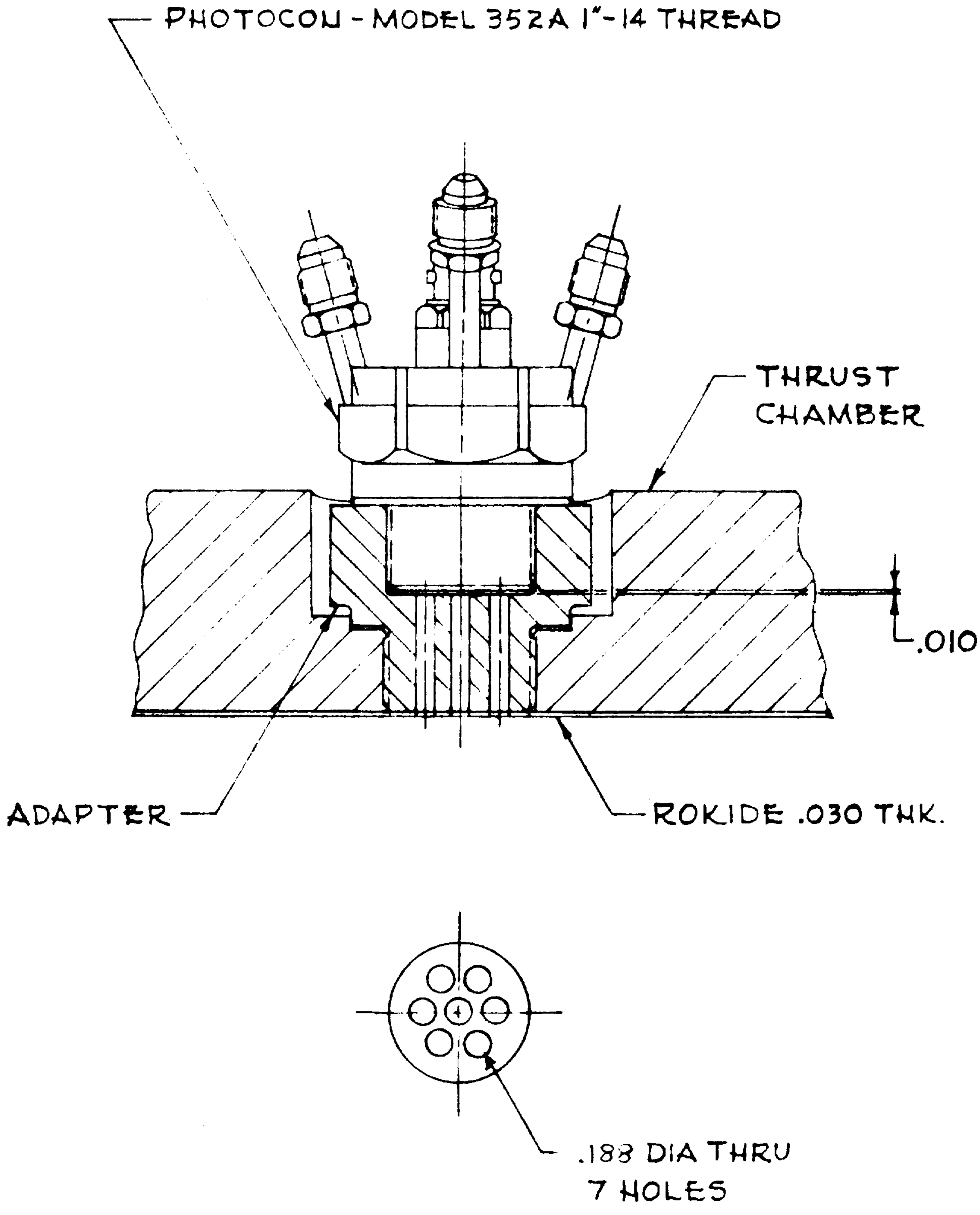

RECESSED PHOTOCON INSTALLATION

FIGURE V-13

562-576

8-IN. DIAMETER PULSE MOTOR

Figure V-14

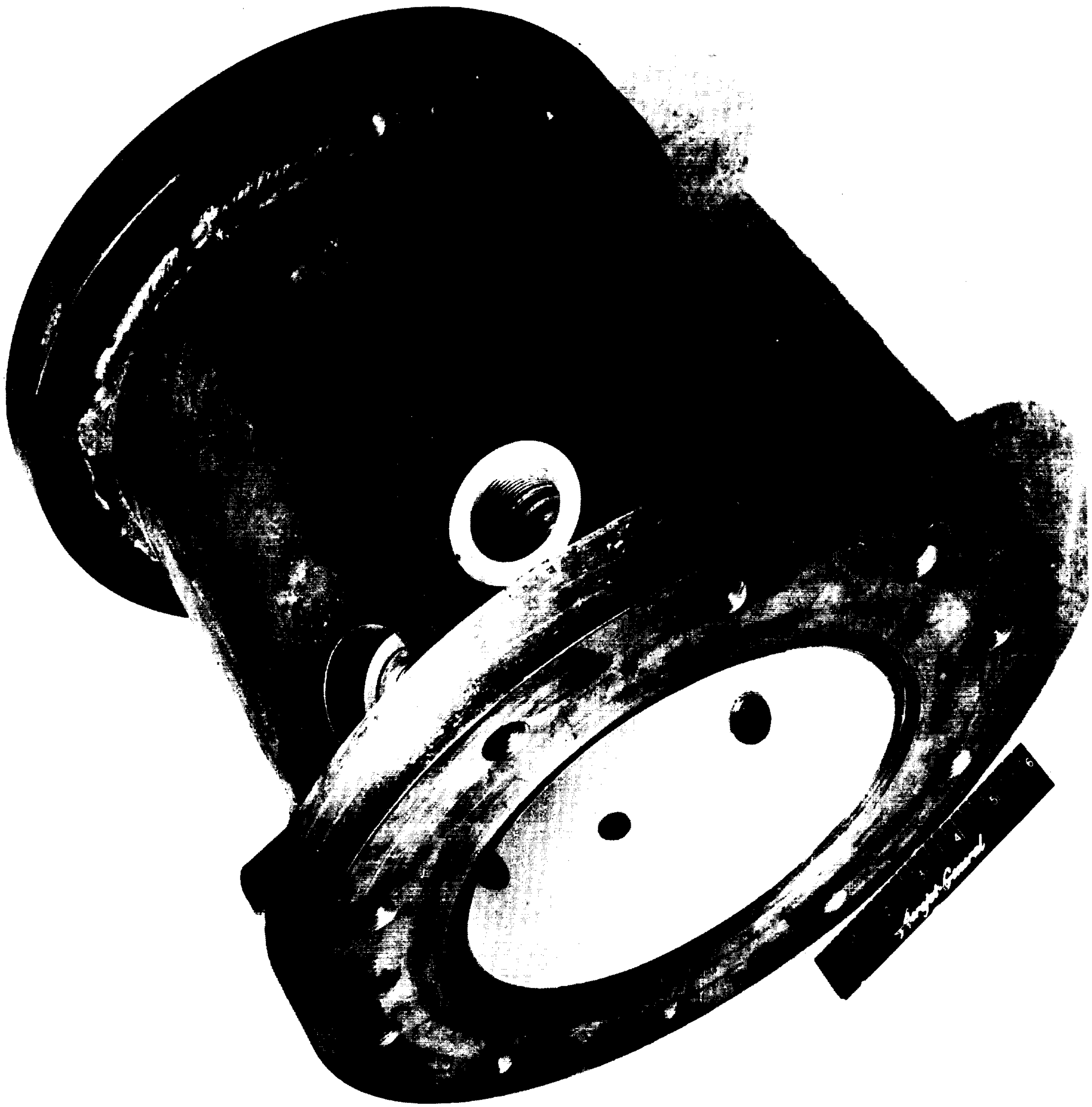

Figure V-15

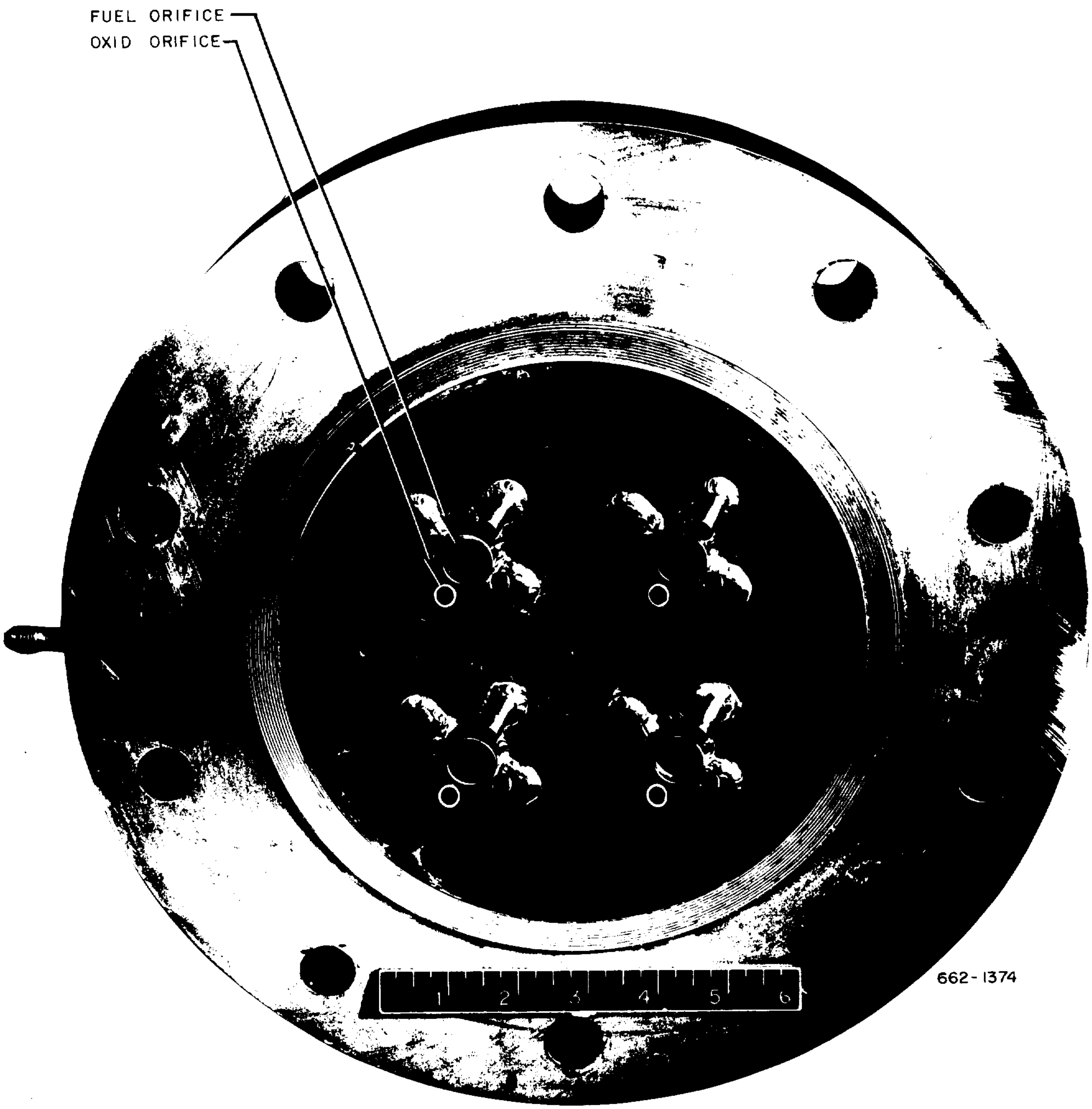

4-5K PENTAD INJECTOR

Figure V-16

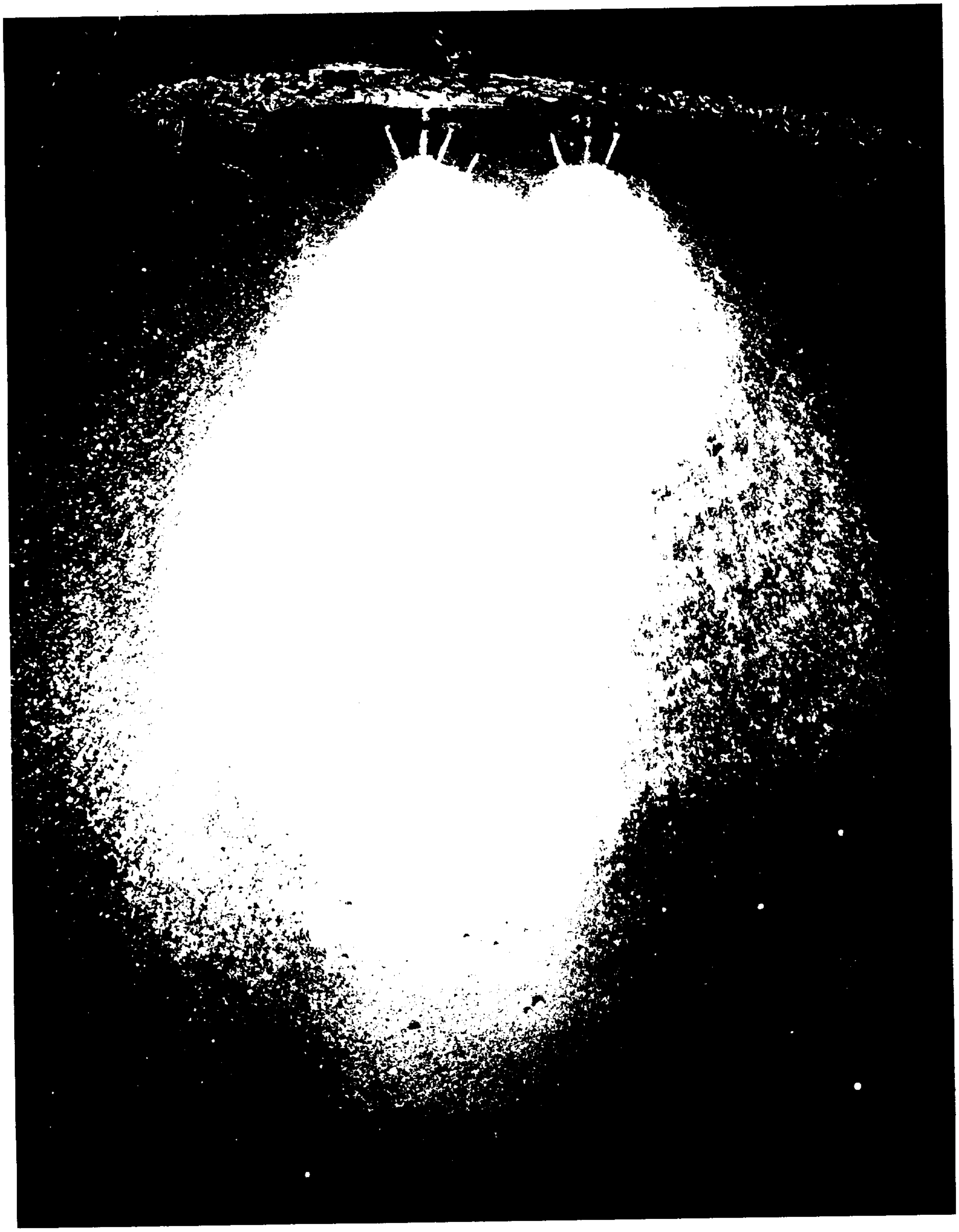

WATER FLOW TEST - 4-5 K PENTAD INJECTOR - $\frac{1}{2}$ FLOW

Figure V-17

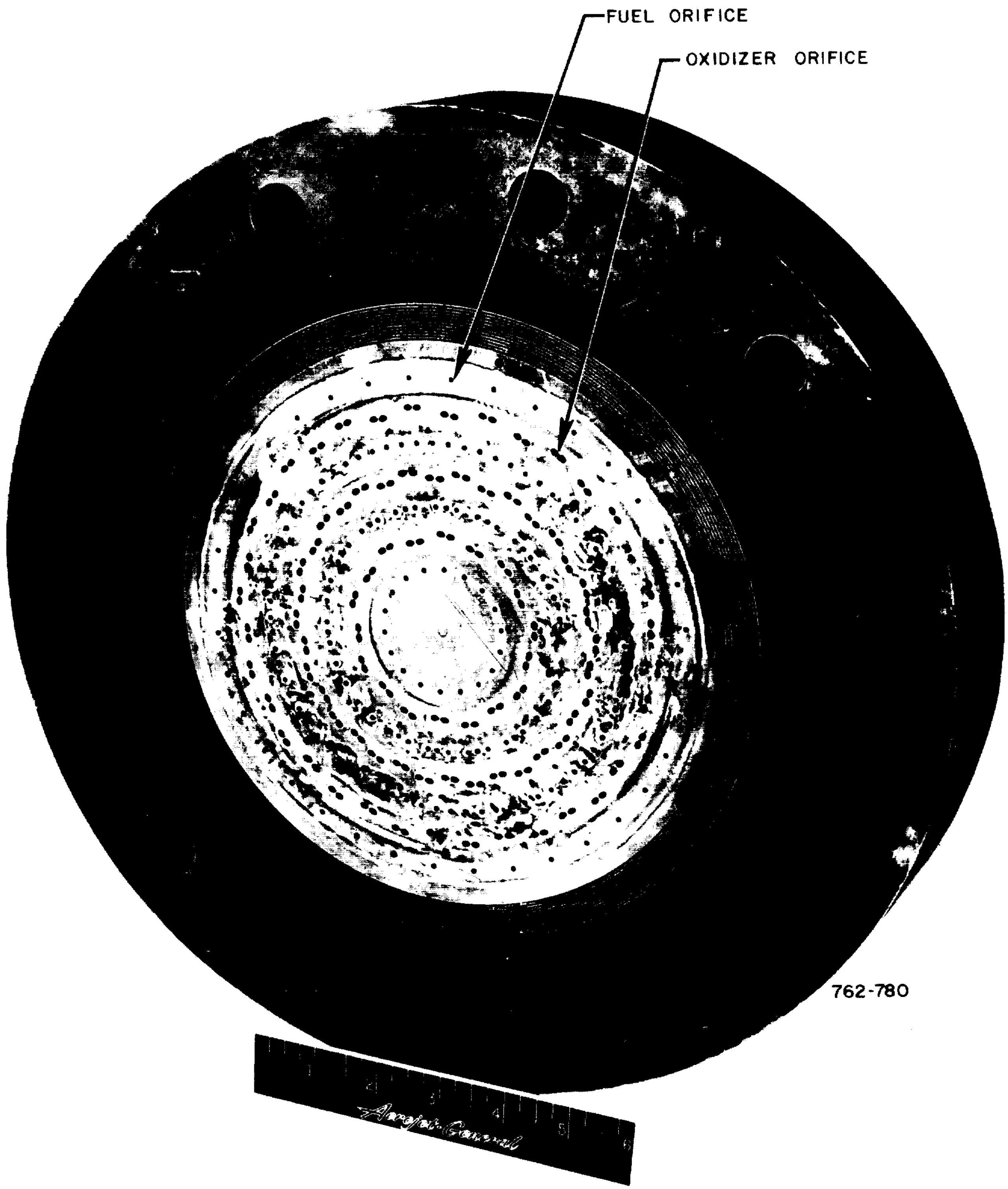

CONCENTRIC PATTERN INJECTOR

Figure V-18

762-781

WATER FLOW TEST - CONVENTIONAL PATTERN INJECTOR - $\frac{1}{2}$ FLOW

Figure V-19

SHOCK TUBE TEST SETUP

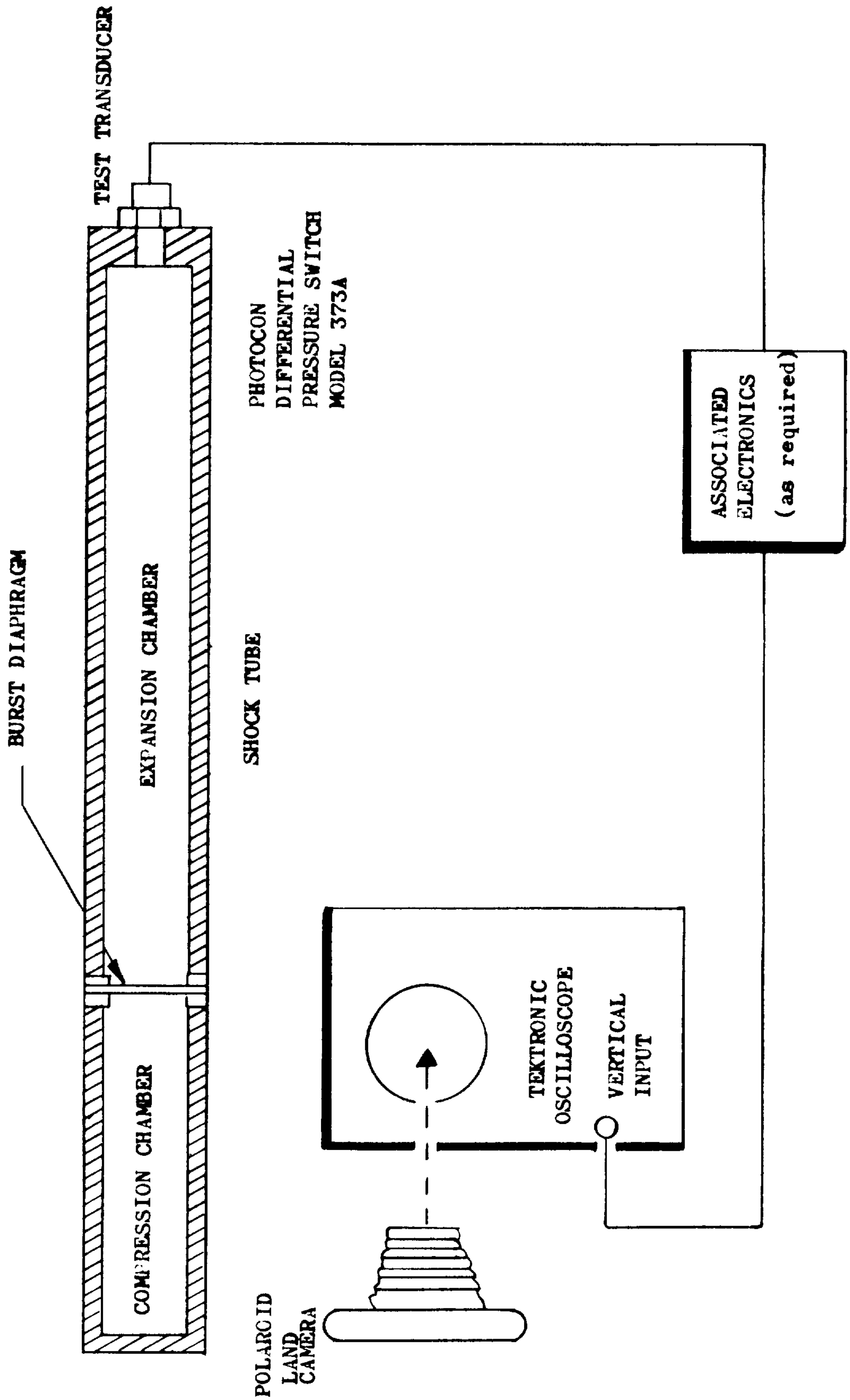

Figure V-20

RESPONSE CHARACTERISTICS,
PHOTOCON MODEL 352A WITH ADAPTER

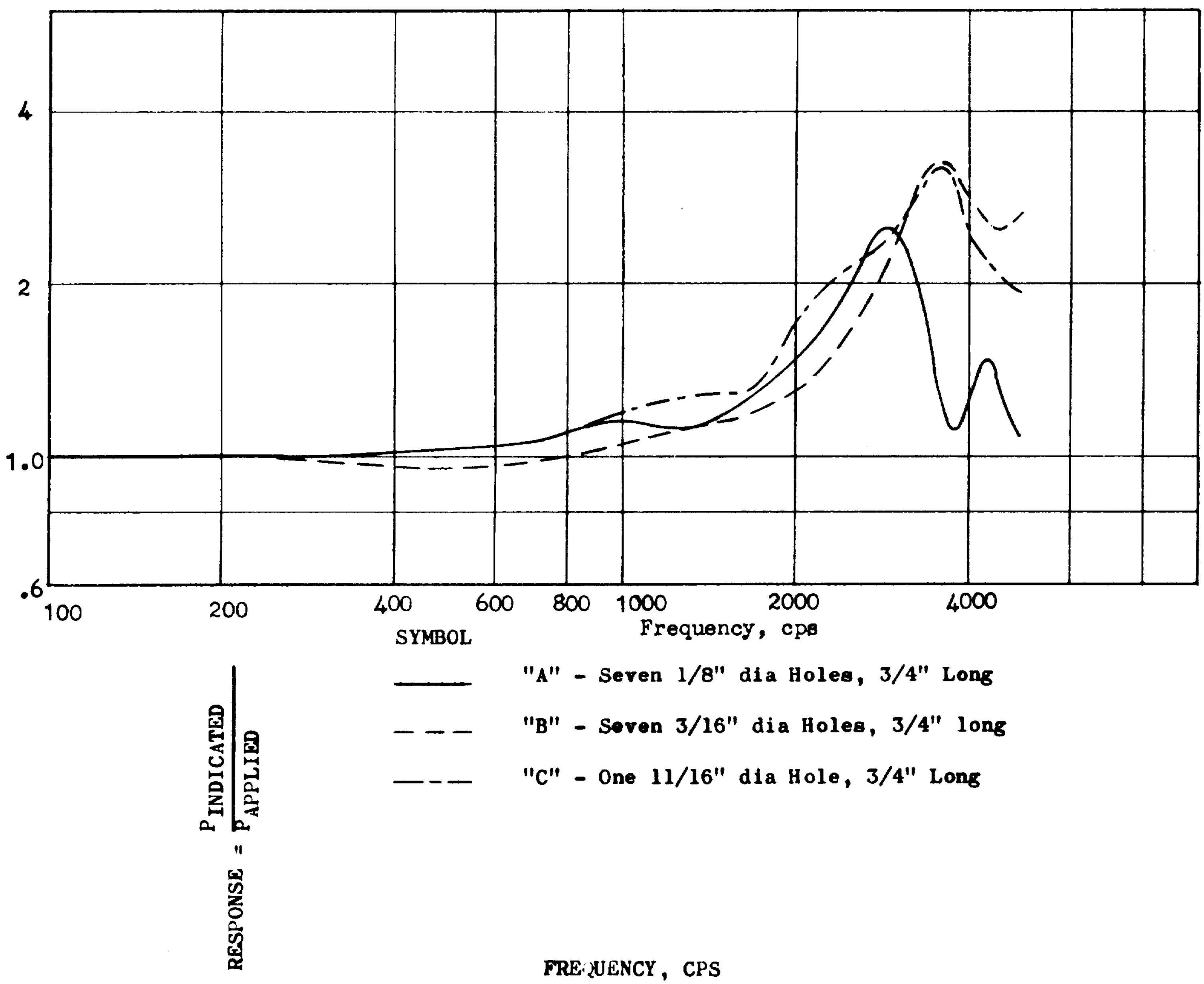

Figure V-21

AMPLITUDE OF OSCILLATION
PRODUCED BY 20 GRAIN CHARGE
IN 8 DIA x 12.75 LG CHAMBER
$P_c = 1500$ PSI
MR = 6.22
O_2/H_2

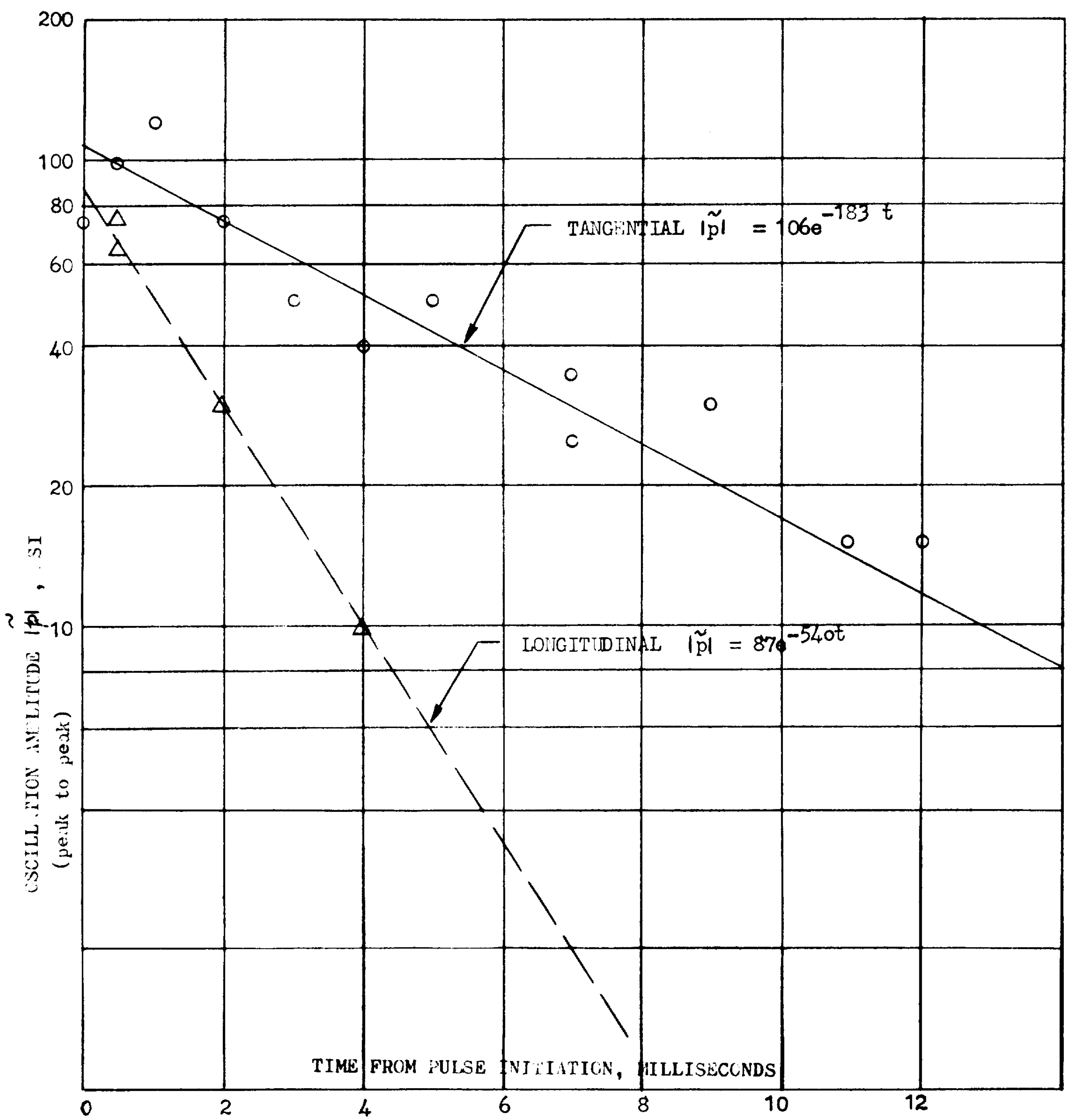

Figure V-22

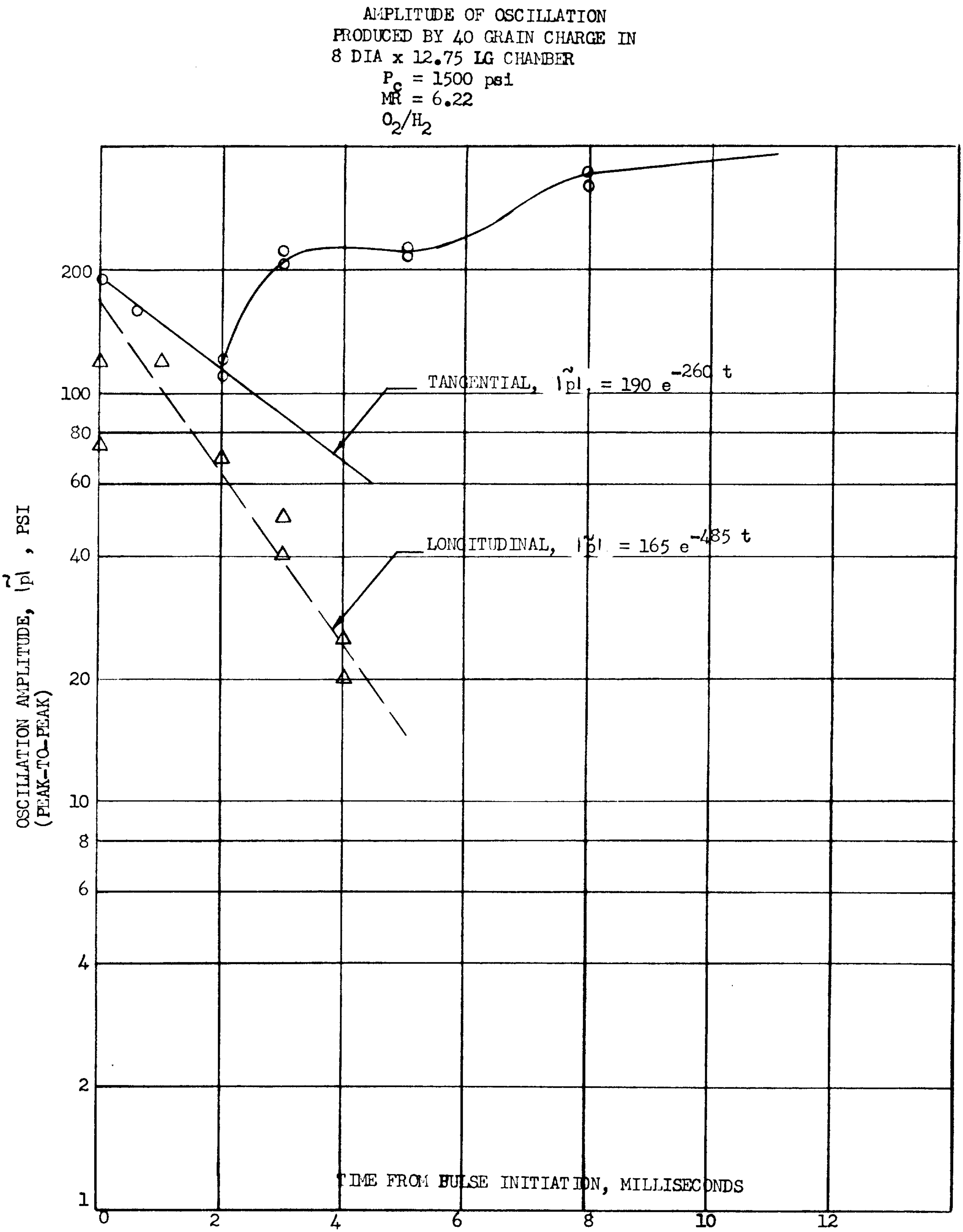
AMPLITUDE OF OSCILLATION
PRODUCED BY 40 GRAIN CHARGE IN
8 DIA x 12.75 LG CHAMBER
P_c = 1500 psi
MR = 6.22
O_2/H_2
TANGENTIAL, $|\tilde{p}| = 190\ e^{-260\ t}$
LONGITUDINAL, $|\tilde{p}| = 165\ e^{-485\ t}$
OSCILLATION AMPLITUDE, $|\tilde{p}|$, PSI
(PEAK-TO-PEAK)
TIME FROM PULSE INITIATION, MILLISECONDS
200
100
80
60
40
20
10
8
6
4
2
1
0
2
4
6
8
10
12

Figure V-23

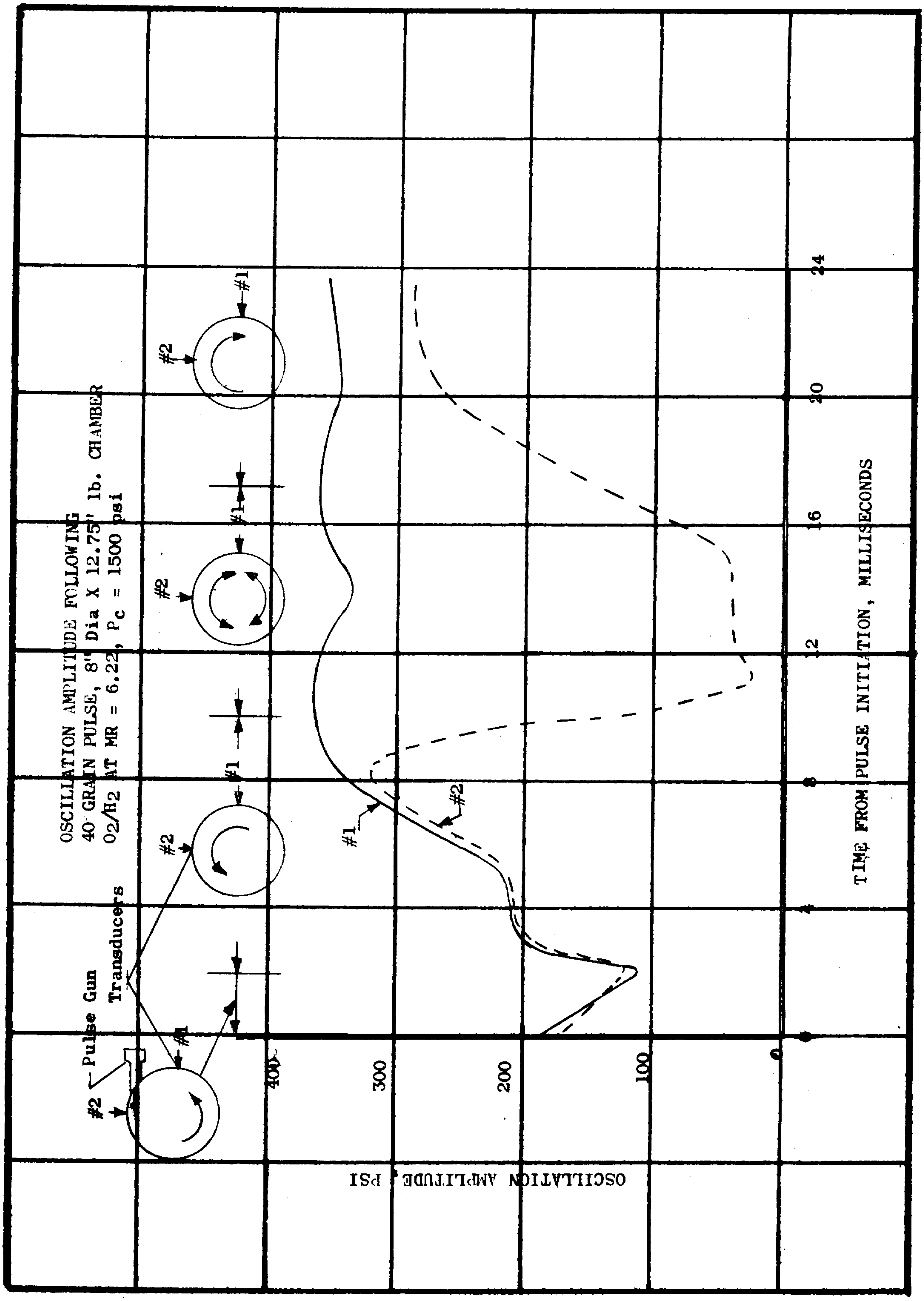
OSCILLATION AMPLITUDE FOLLOWING
40 GRAIN PULSE, 8" Dia X 12.75" lb. CHAMBER
O_2/H_2 AT MR = 6.22, P_c = 1500 psi
Pulse Gun
Transducers
#1
#2
OSCILLATION AMPLITUDE, PSI
0
100
200
300
400
TIME FROM PULSE INITIATION, MILLISECONDS
0
4
8
12
16
20
24

Figure V-24

EFFECT OF ELEMENT SIZE

ON INTERACTION INDEX

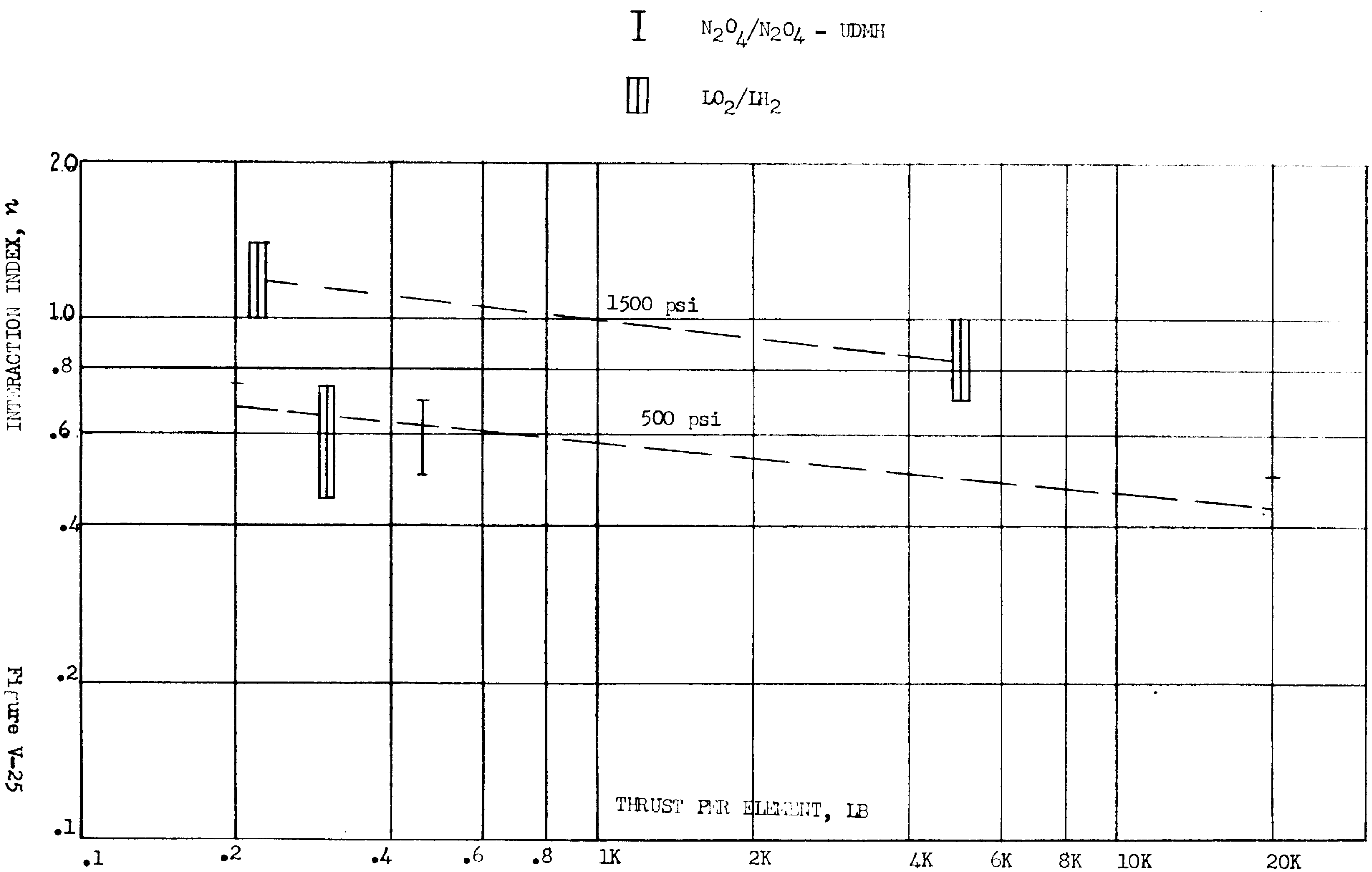

Figure V-25

EFFECT OF ELEMENT SIZE

ON SENSITIVE TIME LAG

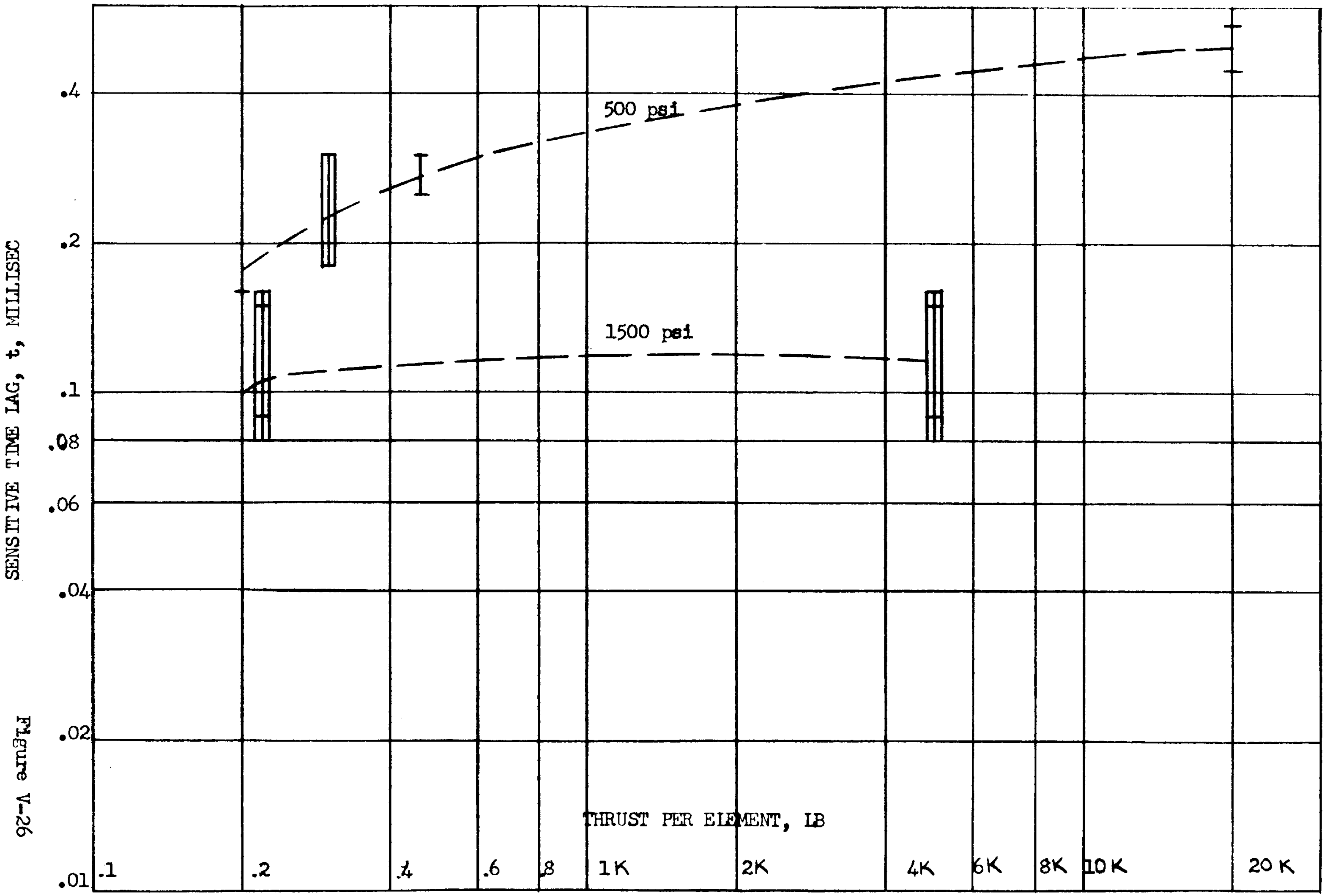

Figure V-26

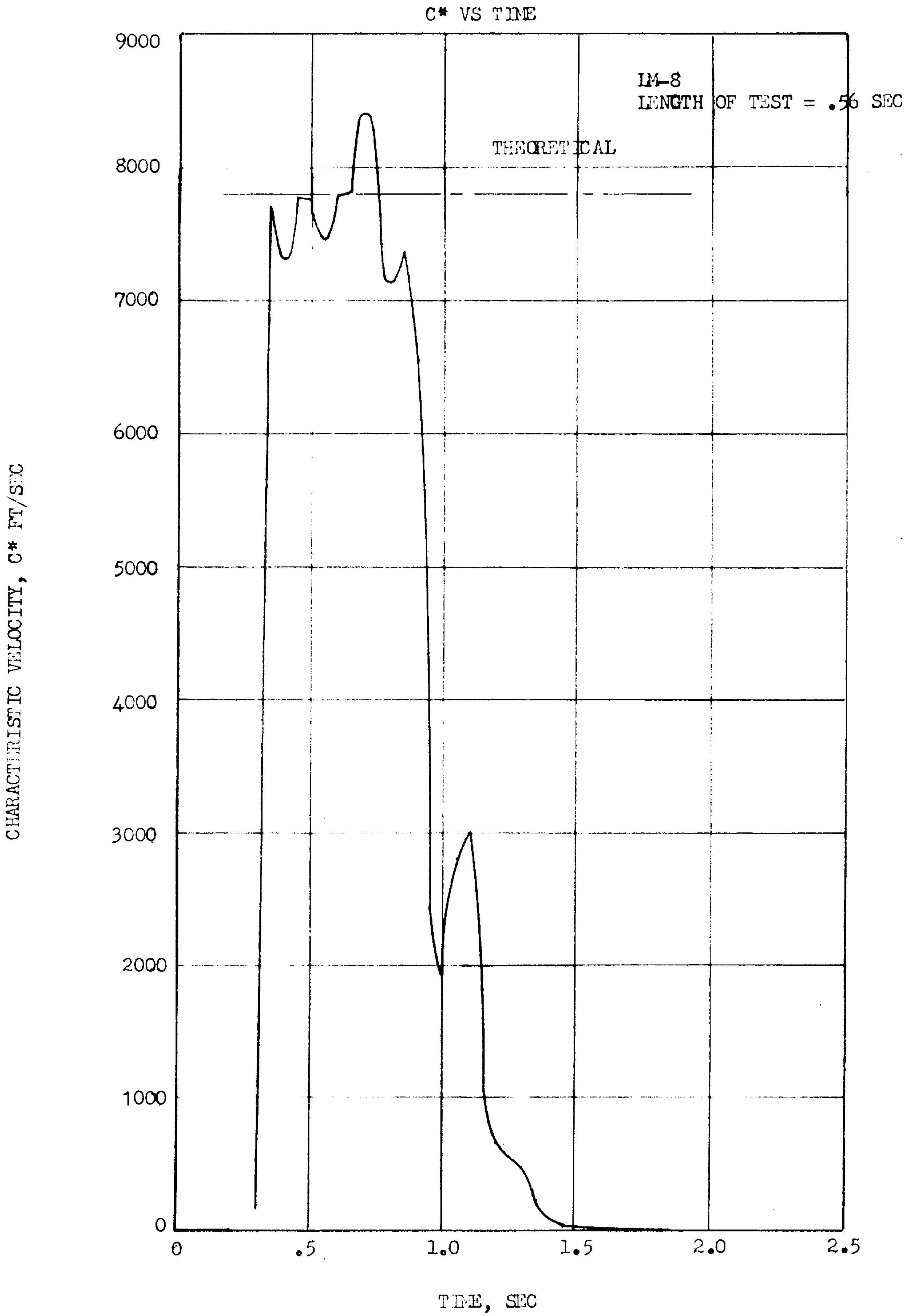
C* VS TIME
LM-8
LENGTH OF TEST = .56 SEC
THEORETICAL
CHARACTERISTIC VELOCITY, C* FT/SEC
9000
8000
7000
6000
5000
4000
3000
2000
1000
0
0
.5
1.0
1.5
2.0
2.5
TIME, SEC

Figure V-27

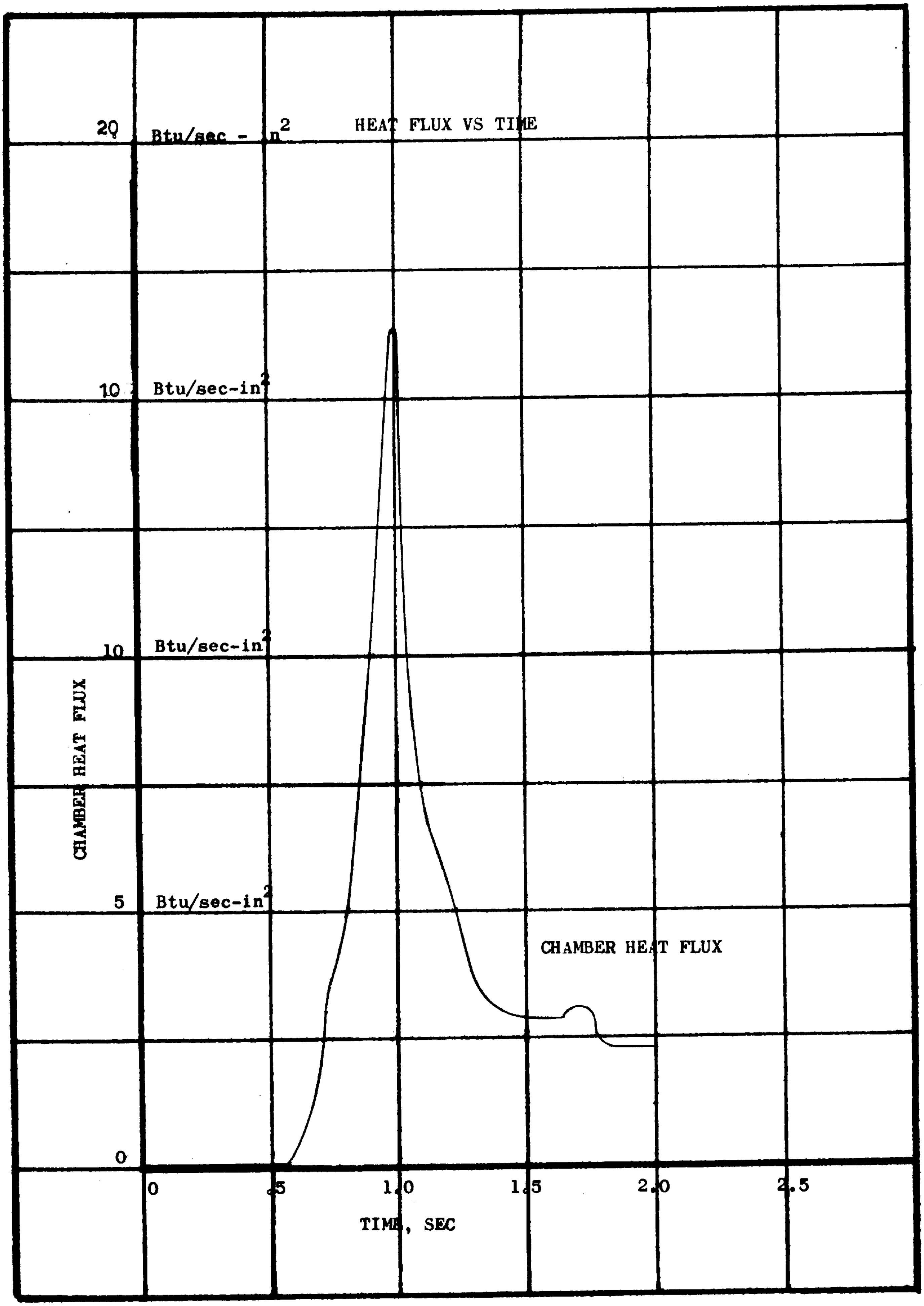

HEAT FLUX VS TIME
20 Btu/sec - in2
10 Btu/sec-in2
10 Btu/sec-in2
5 Btu/sec-in2
0
CHAMBER HEAT FLUX
CHAMBER HEAT FLUX
0
.5
1.0
1.5
2.0
2.5
TIME, SEC

Figure V-28

VI. FUTURE RESEARCH

A. INTRODUCTION

The present research program has been directed toward defining possible combustion dynamics problem areas encountered in the high chamber pressure operation of liquid rocket engines. The limited experimental results obtained in this exploratory effort indicate that the occurrence of high frequency combustion instability, with its associated severe hardware damage, is governed largely by the thrust chamber operating conditions and the design of the injector pattern. Although some preliminary trends have been defined, these areas require further investigation.

Recent development programs have indicated the desirability of the staged combustion cycle, in which the fuel rich combustion products from the gas generator (or primary combustor), after passing through the turbopump turbine which drives the pumps, are injected into the thrust chamber (secondary combustor) and burned with the remaining liquid oxidizer. This cycle introduces certain new factors into the combustion dynamics behavior of the rocket engine system which need to be considered in the near future.

In addition, much fundamental work is needed in the areas of theoretical combustion dynamic analysis and stability rating techniques. These problem areas are discussed further in the following sections.

B. OPERATING CONDITIONS

The experimental data obtained in the present program indicate that high chamber pressure operation may lead to severe combustion stability problems. However, only a small step has been taken toward chamber pressure values which will be desirable for optimizing vehicle performance. Testing should be undertaken over the entire range from 500 to 5000 psia, with a sufficient number of intermediate points to define the pressure effects clearly. It is necessary that such experimental work should be done in a systematic fashion, so that valid results can be obtained. At the present level of understanding of the combustion process, any investigation will have to consider simultaneously the factors of pressure, mixture ratio, injector pattern, and cooling techniques. The effects of chamber pressure on combustion stability must be investigated as a function of mixture ratio, and for different types of injectors. Only from such a comprehensive investigation can a proper understanding of the general problems be achieved.

Two general regimes of mixture ratio are of particular interest, namely, very low (0.77) ratios corresponding to gas generator operation, and high (6.0) ratios used in optimizing thrust chamber performance. The present program has demonstrated that the mixture ratio can exert a significant influence on the stability of thrust chamber combustion. In addition to the overall mixture ratio, consideration should be given to the distribution of both mixture ratio, and mass flow, particularly in the transverse directions. Such factors as the location and orientation of injection elements, and the use of film cooling on combustion chamber walls, are likely to exert a significant influence on combustion stability, through the parameters of mass and mixture ratio distribution.

Evidence is accumulating which shows that the temperature of the propellants prior to injection can be of importance in determining the stability of a liquid rocket engine. This effect is particularly apparent in the liquid oxygen/liquid hydrogen propellant combination. Several investigations have reported combustion instability problems for hydrogen temperatures below a certain critical value, which appears to be a function of injector type. In order to obtain the maximum benefit from the LO_2/LH_2 system, the temperature effect must be explored.

C. INJECTOR DESIGN

The effect of injector element size on combustion stability was demonstrated in the present exploratory program. The results of other investigations appear to confirm this conclusion. However, the application of these results in the design of stable injector patterns requires more systematic and quantitative data. Testing should cover the range from 100 to 100,000 lb-per-element, using each of several different types of injectors non-impinging, like-impinging, and one or more kinds of unlike-impinging, over the whole range. In addition, fundamental analytical and experimental work should be undertaken to obtain a clear understanding of the controlling parameters.

The importance of element location and orientation has been mentioned above in connection with mass and mixture ratio distribution. There are other considerations, too, involving the interaction of adjacent elements, and the transverse velocity sensitivity of individual elements and groups of elements. These influences are just begining to be appreciated, and much basic work needs to be done on them. Finally, associated with the trend to higher operating chamber pressure is the use of high injectiondensity (i.e., total flow rate divided by total injector area) in order to achieve a compact thrust chamber. The preliminary indications are that the tendency to combustion instability may be increased by the use of high injection densities. Most stability testing, including the present program, has been done with rather low values of injectiondensity. A systematic exploration of injection density effects is, therefore, clearly necessary.

D. STAGED-COMBUSTION CYCLE

The use of fuel-rich gaseous combustion products as one of the propellants in the thrust chamber of the staged combustion cycle opens a new area of combustion dynamics research. It does not appear likely that stability data from liquid/liquid injector systems can be extrapolated directly to gas/liquid systems. The nature of the propellant dispersion and mixing will have strong effects on the characteristic combustion times and sensitivity to combustion chamber conditions. In addition, new types of injector patterns required for the gas/liquid system must be investigated with regard to pressure and mixture ratio effects on combustion stability.

A second novel feature of the staged-combustion cycle which must be considered carefully are the modulations introduced by the turbine into the flow of the gaseous propellant. Such disturbances can serve to initiate destructive combustion oscillations in the thrust chamber. The significance of the feed system in high-frequency combustion instability has only recently been appreciated. Systematic investigations of oscillatory flow in the feed system, both experimental and analytical, should be undertaken. The characteristics of the flow disturbances introduced by the turbine blades, and the transfer functions of feed system components and assemblies, should be measured as functions of system operating conditions, as well as component geometry.

Third, the interaction effects due to the close-coupling of the gas generator and thrust chamber must be studied. The effect of the coupling can be observed by first determining the combustion dynamic behavior of the gas generator and thrust chamber separately, and then connecting them, noting the behavior of the complete system. A siren should be incorporated between the two components in order to simulate the flow disturbing effect of the turbine. Initial studies, utilizing small-diameter combustors, should consist of variable length testing in order to determine the longitudinal mode stability behavior, which is, to a large extent, a measure of the stability characteristics of all modes. However, because of possible transverse velocity effects, the studies should be systematically expanded to include transverse and combined longitudinal-transverse modes.

E. FUNDAMENTAL AND THEORETICAL STUDIES

The applied combustion dynamics researches described above must be accompanied by fundamental investigations of the intermediate processes which occur in the combustion of liquid propellants in a rocket thrust chamber or gas generator. The preparation of the propellants for chemical reaction, through atomization, vaporization, and mixing, is a key factor in the combustion dynamic behavior of a rocket engine. Unfortunately, too little attention has been given to these processes. The effect of injector design and propellant properties in both steady and unsteady flow should be determined over wide ranges of operating conditions. In particular, understanding of the dispersion and mixing phenomena at supercritical conditions must be obtained and related to the dynamic behavior of the overall combustion process.

An important aspect of any combustion stability investigation is the controlled initiation of oscillatory combustion. Various stability rating techniques have been developed, including the directed pulse, the non-directed explosion, and the tangential gas flow. All of these techniques have been utilized to obtain relative measures of stability of different combustion systems, and the data produced have aided in understanding the problem of combustion instability. However, very little fundamental work has been done on any of the available techniques to determine the mechanisms by which combustion oscillations are triggered. In order to obtain maximum usefulness and for application in research programs, stability rating techniques must be studied carefully. In conjunction with the determination of the exact nature of the disturbances produced in the combustion chamber, considerable effort should be expended in obtaining reproducibility and in relating these "artificial" exciting methods to the "natural" stimuli present in an actual rocket combustion.

Finally, it is becoming increasingly clear that experimental combustion dynamics data must be interpreted carefully in the light of a well-developed theory. In the present program, successful data correlation was obtained by use of the Sensitive Time Lag Theory. However, because of the linear nature of the theory, only approximate values of the stability parameters could be obtained. It si necessary, therefore, that the Sensitive Time Lag Theory be extended to the non-linear domain. With the accumulation of more experimental information, an understanding of the physical nature of the stability parameters can be gained, enabling the prediction of stability behavior prior to actual fabrication and testing. Analytical studies of the intermediate combustion processes for both liquid/liquid and gas/liquid injection systems, and comprehensive theoretical studies of system interaction effects, must be carried out concurrently with the experimental research programs outlined above. Only through such parallel analytical and experimental efforts can a complete and quantitative understanding of the combustion dynamic behavior of liquid propellant rocket engines be achieved.